

**INFERRING BEARING CAPACITY FROM SONAR BACKSCATTER:
APPLICATION FROM A MUDDY FIELD SITE**

by

Sun Woo Park

A thesis submitted to the Faculty of the University of Delaware in partial fulfillment of the requirements for the degree of Master of Science in Oceanography

Winter 2024

© 2024 Sun Woo Park
All Rights Reserved

**INFERRING BEARING CAPACITY FROM SONAR BACKSCATTER:
APPLICATION FROM A MUDDY FIELD SITE**

by

Sun Woo Park

Approved: _____
Arthur Trembanis, Ph.D.
Professor in charge of the thesis on behalf of the Advisory Committee

Approved: _____
Katharina Billups, Ph.D.
Director of the School of Marine Science and Policy

Approved: _____
Fabrice Veron, Ph.D.
Dean of the College of Earth, Ocean, and Environment

Approved: _____
Louis F. Rossi, Ph.D.
Vice Provost for Graduate and Professional Education and
Dean of the Graduate College

ACKNOWLEDGMENTS

I could not, even if I tried, name every person that helped me along the way to make this thesis become what it is now. In this section I would like to highlight some of the people that graciously lent me their time and expertise.

First and foremost, my advisor and committee chair Dr. Art Trembanis. Thank you for accepting, believing, and supporting an undergrad from South Korea. None of this would have happened without you and I am grateful.

I would also like to thank the other members of the committee, Dr. Carter DuVal and Dr. John Madsen for their expertise and input in shaping this thesis.

My family have always supported me in all that I do. I would never be here without them; Thank you.

Special thanks goes to Freddy Falcone from Virginia Tech for lending his expertise of the Blue Drop during February field work.

For general field work efforts and my time at the lab, I would like to mention and thank the members of CSHEL lab: Now Drs. Kaite McPherran and Mark Lundine, Grant Otto, Jen Repp, and Hunter Tipton for teaching me the ins and outs of all sorts of equipment.

To all the friends I have made along the way, there's so many I would need to name. I hope y'all know who you are when I say you are family to me now, and you should call me.

Honorable mentions go to all the dogs but namely Alfred, Argos, and Wrigley.

TABLE OF CONTENTS

LIST OF TABLES	vi
LIST OF FIGURES	vii
LIST OF ABBREVIATIONS	xii
LIST OF EQUATIONS	xiv
ABSTRACT	xv
 Chapter	
1 INTRODUCTION	1
2 ACOUSTIC IMAGING	7
2.1 Background	7
2.2 Site Characteristics	7
2.3 Methods	9
2.3.1 Data Collection	9
2.3.2 Post-processing	14
2.4 Results and Discussion	17
3 GEOTECHNICAL ANALYSIS	24
3.1 Background	24
3.2 Methods	26
3.2.1 Grain Size Analysis	26
3.2.2 Drop Penetrometer	31
3.2.3 Hydrodynamics and Core Analysis	32
3.3 Results and Discussion	35
3.3.1 Grain Size Analysis	35

3.3.2	Drop Penetrometer	37
4	SEDIMENT CLASSIFICATION	48
4.1	Background	48
4.2	Methods	49
4.3	Results and Discussion	51
5	SYNTHESIS AND FUTURE WORK	58
	BIBLIOGRAPHY	61
	Appendix	
A	GEOTECHNICAL ANALYSIS RESULTS	68
B	DETAILED ANALYSIS STEPS	76
C	MATLAB CODES	88

LIST OF TABLES

2.1	Table of data collection times and methods. Multibeam collected in February is unused in this thesis due to incorrect settings.	9
2.2	Final patch values for each field work. Latency correction is not needed for integrated MBES systems and was not performed. . . .	16
3.1	Comparison of grain size analysis results from October and February. O9 and F6, O7 and F8, O8 and F9, O3 and F12. Mean values are in ϕ ($-\log_2(\text{mm})$).	36
4.1	Comparison between drop penetrometer results and the final GIS classifier of each drop location. Locations with classification mismatch (all Type I errors) are highlighted in gray.	54
A.1	Sampling latitude and longitude for sediment grabs and drop penetrometer. Only grab samples were taken in October, while both grab samples and drop penetrometer data were collected in February.	68
A.2	Grain size analysis results from October (O1 - O9).	69
A.3	Grain size analysis results from February (F1 - F9).	70
A.4	Grain size analysis results from February (F10 - F18).	71
A.5	Slope and intercept value for the simplified QSBC profile in each location.	75
B.1	Pipetting timing for multiple sample analysis. Left: 4 samples at once. Middle: 3 samples at once. Right: 2 samples at once.	85

LIST OF FIGURES

1.1	A modified version of the classic Hjulström curve. Note the greater amount of flow (shear stress) needed to mobilize mud compared to fine sand.	2
1.2	Flow chart showing the order of data processing. Corresponding chapters discussing each aspect of the process are highlighted in red.	3
1.3	Three data collection methods used in this thesis and the depth ranges at which each method gives useful information. Instruments and depths not to scale, image created in BioRender.	4
2.1	Map showing area around the field work site and a zoomed in map with North and South box polygons displayed. Approximate area of the polygons are also shown.	8
2.2	Set of images showing how the Norbit was set up on the vessel. A - R/V Parker. B - Antenna and Portus pole mounted to the side of the vessel, the sonar head is mounted to the bottom of the Portus pole. C - Norbit's iWBMSH multibeam sonar before installation. D - Topside view of the sonar system. The silver sonar interface unit (SIU) is secured to the brace and combines data from the sonar head and antennas to send to the laptop.	10
2.3	Deepest sound speed profile cast during each fieldwork effort. . . .	11
2.4	Example predicted tide data from NOAA tide station #8579381 for the April survey. Note that tide height is referenced to MLLW not NAVD88 (MLLW = NAVD88 - 0.381 in the study area). Further tide information for this station can be accessed in https://tidesandcurrents.noaa.gov/noaatidepredictions.html?id=8579381	12

2.5	Diagram showing sonar alignment errors and patch testing lines. Patch test corrections are done in post-processing to reduce misalignment between lines. Images modified from Hypack (2013) and Hoy and Kissinger (2010)	12
2.6	Image of Iver3-3048. Left - Underside of the platform with red arrows pointing to EdgeTech's 2205 transducers. Right - Entire setup of Iver3-3048 as it undergoes navigational alignment. The magnetometer attachment is highlighted.	13
2.7	Workflow diagram for processing sonar backscatter from both multibeam and side scan systems. Detailed processing steps taken in this thesis can be found in Appendix B.	15
2.8	Compiled bathymetry of the field site exported at 0.3 m grid resolution. Depths range from 2.5 m to 12.5 m. Transect profiles of both boxes are shown on the right, units in meters.	18
2.9	Processed backscatter mosaic from all valid sonar files. Overlapping pixels are calculated and shown as average value of all overlap. Black denotes low backscatter intensity and yellow denotes high backscatter intensity.	19
2.10	Left: Histogram of depth distribution. Right: Histogram of backscatter intensity distribution from SonarWiz after post-processing.	20
2.11	Zoomed in image overlay of a single AUV mission line that best shows the striped light and dark pattern in backscatter. This striping is only seen on the sloped channel sides with depths greater than 8.5 m.	21
2.12	Backscatter intensity mapped on a gray scale. NaN values where there is no survey is plotted in black only to allow for easier perception of shade difference of the actual data.	22
2.13	Histogram of gray scale backscatter intensity. Red dotted lines denote the value of intensity of the drop penetrometer sampling points.	22
2.14	Map of pixels within 75 to 113 luminosity range colored in white. This denotes the location of the major gap in drop penetrometer sampling.	23
3.1	Map of all sampling locations. Latitude/longitude of locations can be found in appendix A.1	27

3.2	Image of instrument deployment setup on the vessel. Shown in small frames are images of a drop penetrometer and a ponar grab. Photo credit: Dr. Mark Lundine (background), Virginia Tech (drop penetrometer), Wildco (ponar grab)	28
3.3	Top view diagram of the boat and data collection location for each instrument, not to scale. Uncertainty bubble is visualized for each instrument.	29
3.4	Workflow diagram for processing sediment samples for grain size analysis. Sand is separated from mud/clay and processed differently. Detailed analysis steps can be found in Appendix B.	30
3.5	Pictures showing grain size analysis setup. Left: RO-TAP with a full stack of sieves for dry sieving. The top is hammered while the stack is shaken. Right: Wet sieving setup with a 63 μm sieve in a funnel.	31
3.6	Table from Lewis and McConchie (1994) showing pipetting time and grain size relationship in different temperatures. Temperature used is highlighted.	32
3.7	Location of each frame in relation to grab and drop penetrometer samples.	33
3.8	Burst average current velocity approximately 15cm above the bed over the frame deployment period. Current velocity was well under the critical shear velocity calculated for this location which was 0.59 m/s. Plot courtesy of Dr. DuVal.	34
3.9	Left: Picture showing a core sample taken by the dive team. Layers are preserved for future analysis. Right: Wet bulk density at each frame location by depth. Depth value of 0 m is the water-sediment interface.	35
3.10	Results of grain size analysis displayed on a ternary diagram. All samples fall under sandy silt, with some variation on sand percentage.	37
3.11	Results of grain size analysis showing D_{50} on the x axis and sand percentage on the y axis. Each point is labeled with the grab location number. Points are colored by the average RGB value of a 3 m square around the sampling location.	38

3.12	Left: Drop penetrometer profile of site F1. Changes in slope is highlighted with arrows. Right: Profile of QSBC with the tapering tail removed that is used for drop penetrometer analysis.	39
3.13	Depth average bearing capacity of each sampling location. Points with high average bearing capacity are boxed in red, and points with low average bearing capacity are boxed in blue.	40
3.14	QSBC profiles of F4 and F10. F4 is an example of a 'low' QSBC location and F10 is an example of a 'high' QSBC location.	41
3.15	Average QSBC of up to 60 cm sampling depth at each sampling location versus the D_{50} value. 95% confidence interval is marked for each average.	42
3.16	Sand percentage and average QSBC of each location. The marker color is the average backscatter intensity value of a 3 m square around the sampling location.	43
3.17	Average maximum penetration depth and average QSBC of each location. Linear regression is applied.	44
3.18	Top: Plots comparing the slope of the linear fit between Low and High QSBC sampling sites. Bottom: Table of calculated slope and R^2 value of the two sites. Note that because the y-axis is inverted to show penetration depth, the calculated slope value is in the positive and does not necessarily match up with the observable slope in the plot.	45
3.19	UXO burial prediction for an example 'low' QSBC site. Left: Predicted UXO burial depth using the F4 Drop 1 QSBC profile. Right: Predicted UXO burial depth using the linear fitted F4 QSBC profile.	46
3.20	UXO burial prediction for an example 'high' QSBC site. Left: Predicted UXO burial depth using the F16 Drop 1 QSBC profile. Right: Predicted UXO burial depth using the linear fitted F16 QSBC profile.	47
4.1	Workflow of ArcGIS Pro's classification wizard. Each step can be run using individual tools or the entire process can be run using the classification wizard depending on user preference.	48

4.2	Comparison of segmentation results with different spatial and spectral detail settings.	51
4.3	Results of segmentation tool. Area with no backscatter value (NaN) is set to cyan.	52
4.4	Final map product from classification through GIS. Note that NaN class is transparent both in the legend and in the map. Average QSBC for Low: 15.4 kPa, average QSBC for High: 21.8 kPa	53
4.5	Zoomed in images of misclassified points which are circled in yellow.	55
4.6	Table showing the drop penetrometer profile and sonar backscatter snippet of only the misclassified points.	56
4.7	Left: Confusion matrix of True class (penetrometer result) and Predicted class (classifier result). 4 out of 18 were misclassified with all errors being Type I. Right: Calculated precision, accuracy, and recall of the classifier.	56
4.8	Zoomed in image from figures 4.4 and 2.9 which highlights residual nadir effects from the initial sonar data.	57
A.1	Average RGB values of a 3 m square around sediment sampling points.	68
A.2	Penetrometer results F1 - F6.	72
A.3	Penetrometer results F7 - F12.	73
A.4	Penetrometer results F13 - F18.	74

LIST OF ABBREVIATIONS

ADCP: Acoustic Doppler Current Profiler

AUV: Autonomous Underwater Vehicle

CTD: Conductivity, Temperature, and Depth measuring instrument

D₅₀: Grain size corresponding to the cumulative frequency of 50%. Can be in mm or ϕ ($-\log_2(\text{mm})$)

DI: De-Ionized

EGN: Empirical Gain Normalization

GeoTIFF: Geo-referenced Tag Image File Format

GIS: Geographic Information System

GNSS: Global Navigation Satellite System

INS: Inertial Navigation System

MBES: Multi-Beam Echo Sounder

MLLW: Mean Low Low Water

NaN: Not a Number, empty value

NOAA: National Oceanic and Atmospheric Administration

PNG: Portable Network Graphics

PSU: Practical Salinity Unit

Q_{dyn} : Dynamic Bearing Capacity

QSBC: Quasi-Static Bearing Capacity

RGB: Red, Green, Blue

RTK: Real Time Kinematic

SERDP: Strategic Environmental Research and Development Program

SIU: Sonar Interface Unit

SSS: Side Scan Sonar

SVP: Sound Velocity Profile

UGC: User-defined Gain Normalization

UXO: Unexploded Ordnance

LIST OF EQUATIONS

$$2.1 \quad TL = 20\log(R + 1) + \alpha(R) + b$$

$$3.1 \quad F = m * a$$

$$3.2 \quad q = F/A$$

$$3.3 \quad QSBC = Q_{dyn}/Fac$$

$$3.4 \quad Fac = 1 + K\log_{10}(v/v_0)$$

$$3.5 \quad Size \ (\mu m) = F * \sqrt{\frac{Depth \ of \ Sampling \ (cm)}{Time \ (min)}}$$

$$3.6 \quad \phi = -\log_2(Diameter \ (mm))$$

$$3.7 \quad Bulk \ Density = \frac{Sample \ Weight}{Sample \ Volume}$$

$$4.1 \quad e_s = l_s^{1/\gamma}$$

ABSTRACT

This study expands on the application of sediment classification using acoustic backscatter and combine it with drop penetrometer data to test if the bearing capacity of the sediment layer can be related to the backscatter intensity. Total area of 5.14 km² was surveyed using a vessel mounted multibeam sonar and AUV mounted side scan sonar on the Potomac river near Indian Head, Maryland. 9 sediment grabs were taken during October 2022 field work, and 18 contemporaneous grab samples and drop penetrometer measurements were taken during February 2023. Backscatter mosaic with the geotechnical data was used to train a supervised classification algorithm in ArcGIS Pro. Applying the data interpretation techniques developed so far to cohesive fluvial environment has shown good agreement between backscatter intensity and bearing capacity (precision: 0.75, accuracy: 0.78). This could have practical applications in coastal and riverine construction in muddy environments, allowing for fast and cost effective analysis of bearing capacity of a large site. Unexploded ordnance (UXO) in munition test sites could also be managed using sonar surveys since ordnance mobility and burial could have improved prediction with bed bearing capacity data ([Trembanis and DuVal, 2021](#)). This coordinated geoacoustic and geotechnical survey approach would reduce the risk of UXO site management since minimal contact with the bottom is necessary.

Chapter 1

INTRODUCTION

Coastal regions are characterized by dynamic sedimentary processes and intensive anthropogenic impacts. Cohesive sediment is commonly found in low energy coastal environments as well as deep abyssal plains (Dutkiewicz et al., 2015). In the East coast of the continental United States, cohesive sediment is widely found in the rivers, bays, estuaries, and in the continental margins. The finer grain size leads to interesting physical qualities that impact how the grains of sediment interact with its surrounding environment. Cohesion is an interesting aspect of finer grained sediments that come from clay minerals having ionic charges on the surface. Dyer (1986) describes clay minerals as formed with layers of silica tetrahedra and aluminum hydroxide, with varying number of layers between the different clay mineral types. The clay mineral structure can exchange ions in the water with ions in the clay structure depending on the concentration of ions in the water column. The ion exchange can alter how clay minerals interact with each other, as the cohesive ionic charges on the clay surface overpower gravitational forces on the grain leading to flocculation (clumping of particles in suspension). Unlike sands and other non-cohesive sediments, cohesive sediments do not follow a linear trend with shear stress when being mobilized, as described in the Hjulström curve shown in figure 1.1 (Hjulström, 1935).

Due to the unique qualities of cohesive sediments, the geoacoustic and geotechnical properties of these sediments tend to be different from non-cohesive sediments. Cohesive sediment typically scatter less and absorb more sound compared to cohesive sediment due to their smaller grain size, leading to lower backscatter intensity when observed through a sonar (Lurton et al., 2015). Bearing capacity can be described as

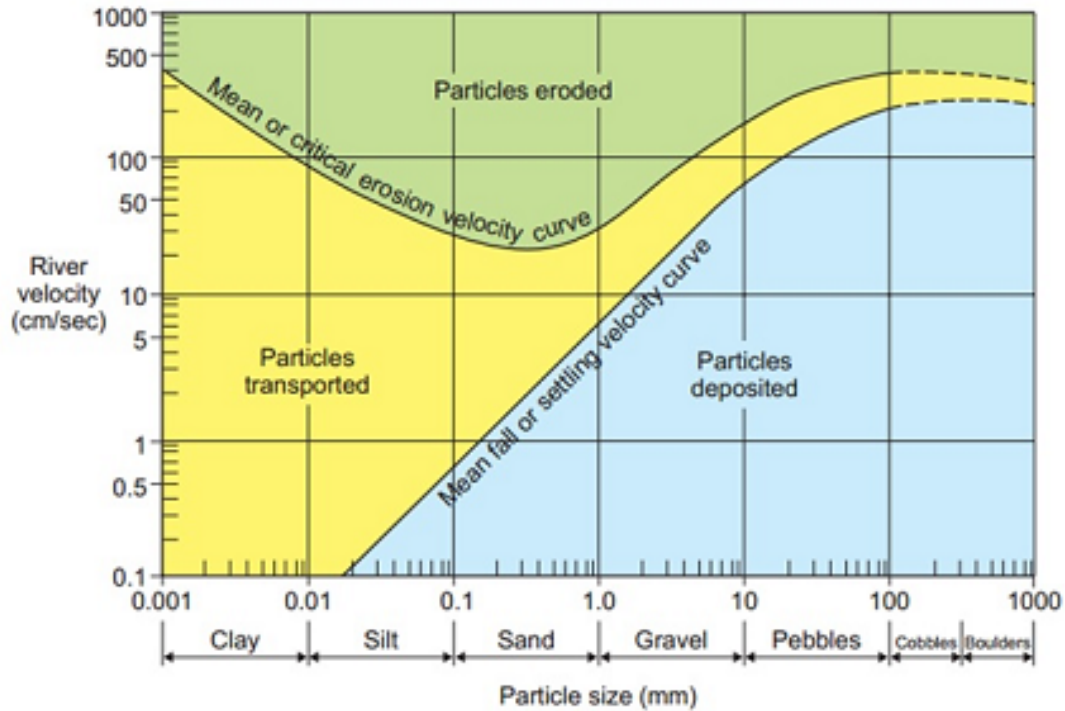


Figure 1.1: A modified version of the classic Hjulström curve. Note the greater amount of flow (shear stress) needed to mobilize mud compared to fine sand.

the amount of force the bed can withstand before deformation occurs, and can depend on factors such as sediment type, sediment density, and biological activity within the bed (Plachý et al., 2016). Bearing capacity of cohesive sediment is lesser than that of non-cohesive sediment due to smaller grain size and lower compaction of the sediment. Considering the reason of lower backscatter intensity and lower bearing capacity is based in grain size,

This study aims to analyze the sonar backscatter intensity and if bearing capacity can be inferred from backscatter in exclusively cohesive sediments (see figure 1.2). Chapter 2 will discuss the acquisition and processing of sonar backscatter data from both an AUV system and a manned surface vessel, along with a description of the study location. Combining sonar data with other instruments has been used in many studies. For example, Sahin et al. (2012) used a combination of acoustic doppler

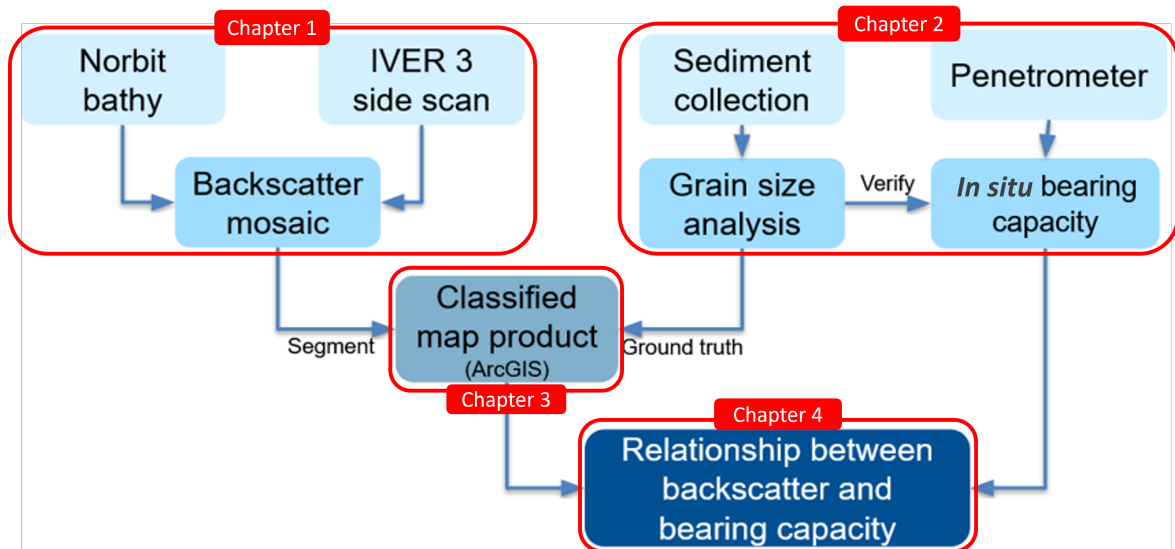


Figure 1.2: Flow chart showing the order of data processing. Corresponding chapters discussing each aspect of the process are highlighted in red.

current profilers (ADCPs), CTDs, wave measurements, and optical backscatter sensors (OBS) to observe and understand how the cohesive bed transforms with wave action. The location choice for this study was informed by geologic information from previous studies (Draut et al., 2005). Studies like Stark et al. (2012) and Stark et al. (2017) have related sonar backscatter with *in situ* bearing capacity from drop penetrometers in sandy continental shelves and mixed sediment Arctic coasts with promising results. Although sampling locations in Stark et al. (2017) did include large pockets of cohesive sediments, the focus of the study was not in differentiating between firmer or softer cohesive beds.

The geophysical sampling is discussed in chapter 3, which includes the grab sampling results and the drop penetrometer results. Both data sets are considered in relation to each other, as they give information on different depths (see figure 1.3). The ability to accurately assess the bearing capacity of the seabed is an important factor in constructing coastal structures. Understanding the unique physical characteristics of mud becomes vital in areas where underwater construction is being planned, as cohesive sediments behave differently from sand and may deform and compact under

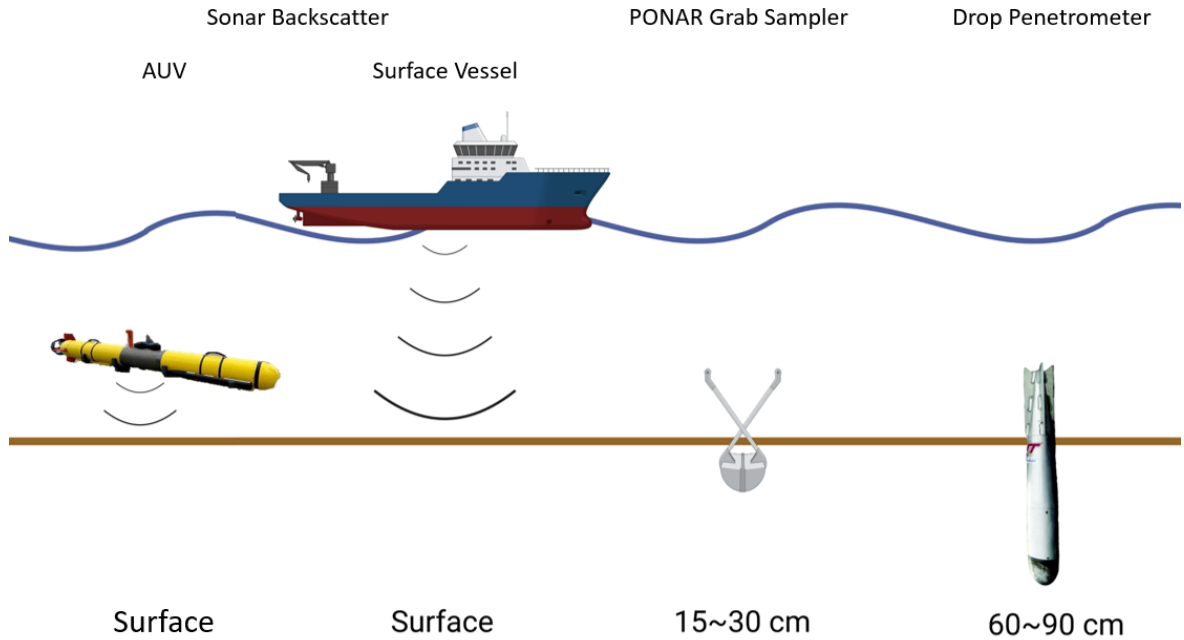


Figure 1.3: Three data collection methods used in this thesis and the depth ranges at which each method gives useful information. Instruments and depths not to scale, image created in BioRender.

load. The mechanism of a foundation interacting with a sediment bed has been explored traditionally by civil engineers (Hettler and Gudehus, 1988; Leach, 1994; Mitchell and Hull, 1974). The amount of force a unit area of cohesive sediment can withstand may vary greatly with the composition of the grains, compaction, slope of the bed, and many other factors (Valent et al., 1988). This force that needs to be exerted onto the sediment for deformation is called bearing capacity. It is an important metric in underwater construction projects like bridge construction and offshore wind farms. Analysis of bearing capacity on land is typically done by geotechnical sampling *in situ* using shear vanes and portable drop penetrometers (Leach, 1994). In submerged sediments vane shear tests and cone penetration tests are traditionally used (Guo et al., 2023). These *in situ* testing methods produces a single point of data per drop.

UXO research supported by SERDP has been interested in bearing capacity

of submerged sediments in relation to munition mobility. Traditionally, the focus has been on non-cohesive sediment beds (Traykovski and Austin, 2016; Wilson et al., 2008). Traykovski and Austin (2016) discusses hydrodynamic forcing on the munitions and bedform migration as major environmental factors in UXO mobility. Once the munition is more than 50% buried, the munition is considered no longer mobile. For non-cohesive environments burial occurs through scour around the munition and bedform migration.

As discussed above, cohesive sediments pose a distinct challenge compared to non-cohesive sediments. Trembanis and DuVal (2020) looked at munition mobility and burial in relation to storm events in the Delaware bay (estuarine, cohesive). Acoustic backscatter and penetrometer data were collected in this study. The study site was split into two subsections, with site 1 having over 60% sand overall and site 2 having over 60% silt. Two distinct groups of sediment were identified using sand percentage and max penetration depth. Areas with higher sand percentage had higher QSBC and shallower penetration depths and the reverse was true for higher mud percentage areas. Authors noted sediment bearing capacity as an important factor in predicting UXO burial. Trembanis and DuVal (2021) looked further into the same study site for connection between the geophysical properties (shallow surface) and sonar backscatter (surface) and found a strong connection. The authors noted that rheology of cohesive sediments play a big role in UXO burial in cohesive sediment beds. This thesis is an extension of the previously mentioned SERDP studies. Geoacoustic and geotechnical sampling methods used in Trembanis and DuVal (2020) and Trembanis and DuVal (2021) are used to test how the combined sampling approach holds up in an entirely cohesive fluvial environment.

In chapter 4 the acoustic backscatter from chapter 2 and the drop penetrometer results from chapter 3 are brought into GIS software to reach a classified bearing capacity map of the whole survey area. Geographic information system (GIS) is a vast field of research in its own right. GIS analysis tools can be used in ecological zone mapping, anthropogenic zoning, watershed analysis, and so much more (Marulli and

[Mallarach, 2005](#); [Salem, 2003](#); [Sonti, 2015](#); [Strager et al., 2010](#)). In this study, GIS is used not only to visualize the data that has been collected, but also as an analytic tool with segmentation and classification features. Classification using bearing capacity measurements and sonar backscatter within a small grain size range specifically within cohesive sediments is a novel application of GIS classification tools.

Chapter 5 brings everything together to assess the viability of the classification method proposed in the previous chapters. Discussion of possible future research is also included in chapter 5.

Chapter 2

ACOUSTIC IMAGING

2.1 Background

Acoustic remote sensing methods like side scan sonar (SSS) and multibeam echo sounder (MBES) are well-established tools for underwater surveying and are applied in a broad range of marine studies (Brown and Blondel, 2009; Fonseca et al., 2005; Raineault et al., 2011). A sonar system works by sending sound waves through the water column and receiving reflections of those waves. Using water column sound speed profiles from CTD measurements on site, one can calculate the distance from the sound source to the reflector. Additionally, it is possible to collect information on the sediment properties using backscatter intensity (Yu et al., 2021; Zakariya et al., 2018). The signal from this backscatter is affected by sediment grain size and incident angle of the beam (Fonseca and Mayer, 2007; Schimel et al., 2018). Acoustic imaging provides an indirect method of collecting data. By ground-truthing the backscatter using sediment grab samples or drop penetrometers, it is possible to calibrate and verify sediment classification algorithms run on backscatter data collected using sonars (Anderson et al., 2008; Parnum et al., 2007; Yu et al., 2021; Zhou et al., 2020). This has been traditionally applied to habitat mapping projects, where the goal was to determine how much area with the optimal sediment type was available for certain species (Hughes Clarke et al., 1996; Trembanis and Gutsche, 2019).

2.2 Site Characteristics

The Potomac river is located between Maryland and Virginia on the East coast of the continental United States. It flows through the District of Columbia into the

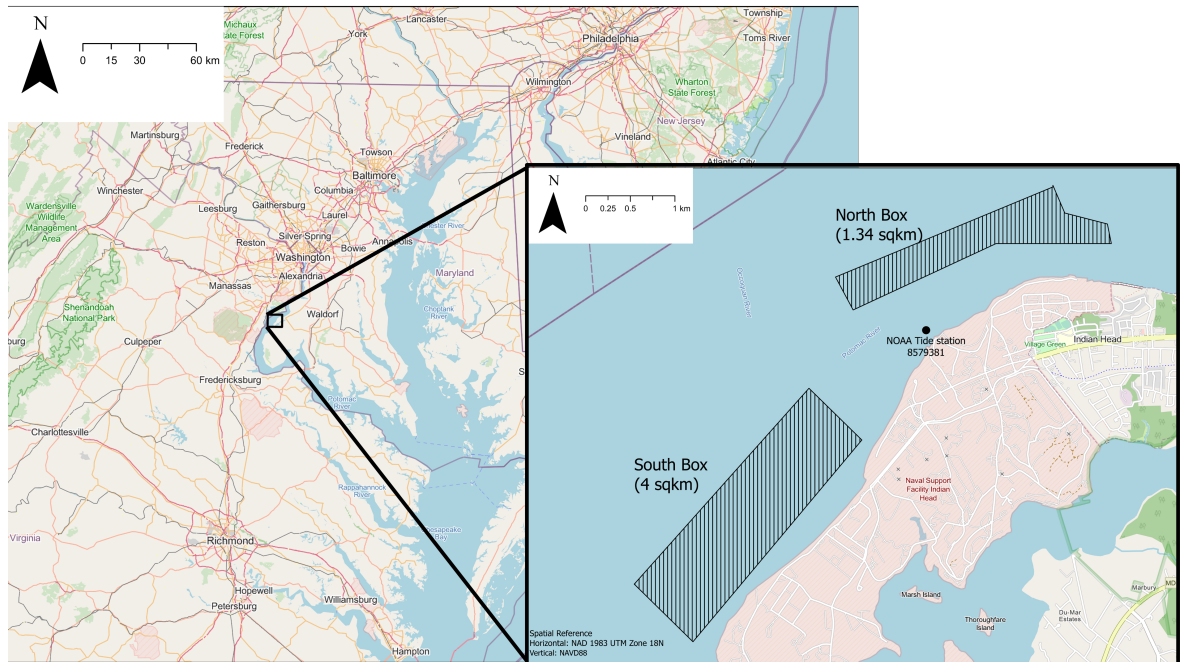


Figure 2.1: Map showing area around the field work site and a zoomed in map with North and South box polygons displayed. Approximate area of the polygons are also shown.

Chesapeake Bay (see figure 2.1). It has been and still is strategically important in military operations, with over 10 military bases currently in operation in the vicinity of the river. Data collection was done in the vicinity of Indian Head, MD. The location is home to the Naval Surface Warfare Center, Indian Head Division. Measured salinity on site was 0.02 PSU, tide ranges from 0.1 m to 1 m, depths range from 1.5 m to 15 m with the deepest area being the Mattawoman Bar channel. The channel was last commissioned to be dredged in 1999 by the Army Corp of Engineers (Shields, 1999). At the deepest part of the study site the depth is 16.9 m.

Two main sites within the larger field area were chosen to reflect the needs for the SERDP project. The North box was approximately 3,000 m by 500 m. The study site included parts of the channel while being just outside of the channel markers. The South box was approximately 4,500 m by 900 m. The area was between the main channel and a smaller side channel, and mostly flat and shallow (measured depth range

1.1 m - 8.7 m) compared to the North box (measured depth range 1.1 m - 16.9 m). Fieldwork was conducted in October 2022, February 2023, and April 2023 (see below 2.1).

	2022	2023	
	Oct	Feb	Apr
Bathymetry	X	X	X
Multibeam Backscatter	X	X	X
AUV Side Scan back	X	X	X
Grab Sample	X	X	
Drop Penetrometer		X	

Table 2.1: Table of data collection times and methods. Multibeam collected in February is unused in this thesis due to incorrect settings.

2.3 Methods

2.3.1 Data Collection

Acoustic imaging in this thesis was conducted using NORBIT Subsea’s iWBMSH multibeam sonar mounted to R/V Parker, a 23 foot Parker vessel (see figure 2.2), and EdgeTech’s 2205 dual frequency side scan mounted to University of Delaware’s Iver3-3048 platform (see figure 2.6).

The iWBMSH multibeam sonar can record between 200 and 700 kHz, with nominal frequency being 400 kHz. For bathymetry systems, sound speed profiles are needed to correct for sound speed change in the water column. CTD casts were taken at least every 2 hours or when tides changed to account for this change of sound speed in the field (figure 2.3). The nearest tide station to the survey area is NOAA station #8579381 shown in figure 2.1. Tides are microtidal in this area, ranging from 40 cm at neap tide to 70 cm at spring tide. Patch test lines were also recorded for use in post-processing corrections. Patch testing for an MBES system is important



Figure 2.2: Set of images showing how the Norbit was set up on the vessel. A - R/V Parker. B - Antenna and Portus pole mounted to the side of the vessel, the sonar head is mounted to the bottom of the Portus pole. C - Norbit's iWBMSH multibeam sonar before installation. D - Topside view of the sonar system. The silver sonar interface unit (SIU) is secured to the brace and combines data from the sonar head and antennas to send to the laptop.

because navigation, attitude, and sonar sensors need to be calibrated to each other to record accurate bathymetry (see figure 2.5). Real-time kinematic global navigation satellite system (RTK GNSS) was used to improve horizontal and vertical accuracy

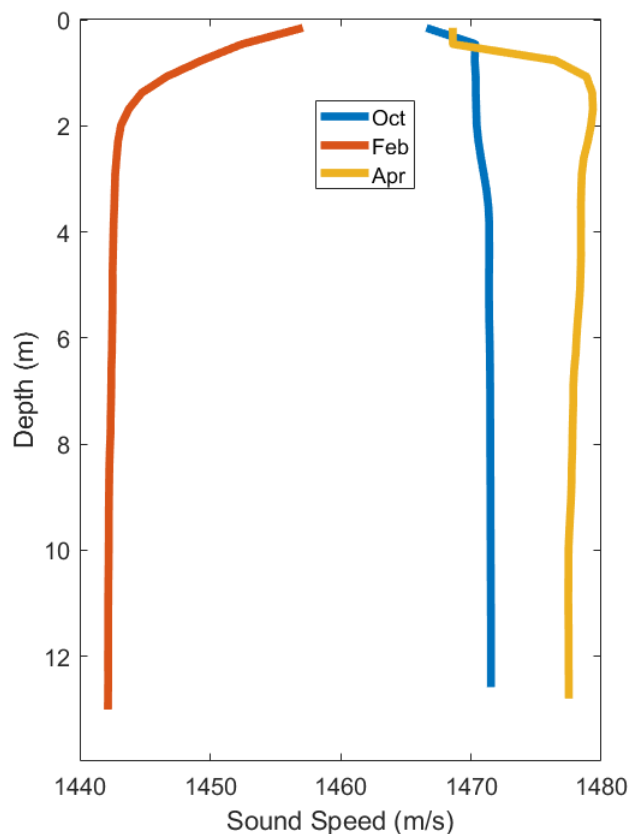


Figure 2.3: Deepest sound speed profile cast during each fieldwork effort.

of the survey. Horizontal uncertainty was under 0.03 m and vertical uncertainty was under 0.05 m using the integrated RTK GNSS. October survey was conducted covering the largest area for initial site characterization. The survey area covered both the North and South boxes. February survey was completed for part of the North box, but backscatter from this survey could not be used due to recording errors. The acquisition setting did not impact bathymetry data. April Norbit survey was done for sections in the North box, and filled out some of the South box that were not mapped in the previous surveys. Areas where geotechnical samples were taken in February were also re-mapped to see if there were any changes in backscatter over time and to ensure coverage.

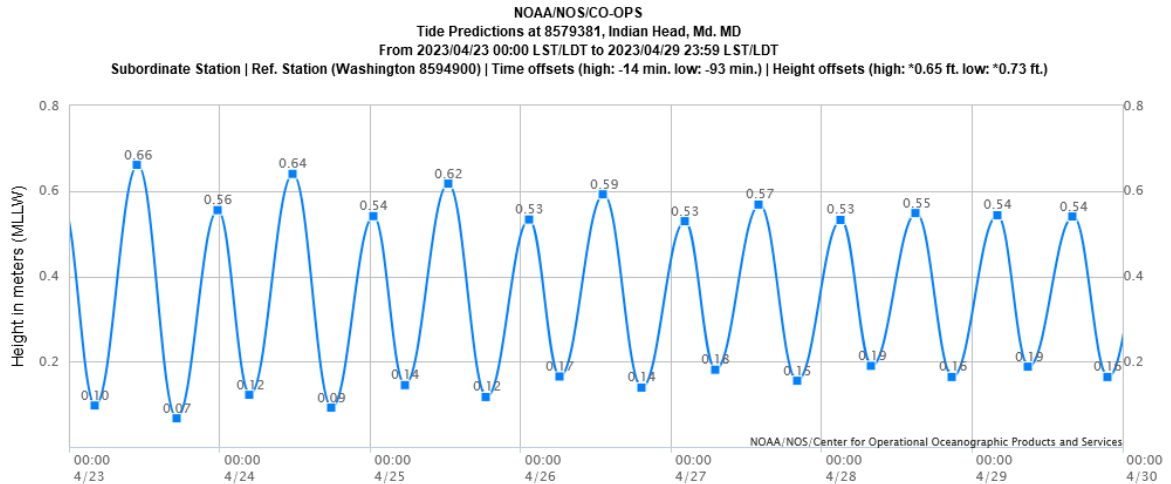


Figure 2.4: Example predicted tide data from NOAA tide station #8579381 for the April survey. Note that tide height is referenced to MLLW not NAVD88 (MLLW = NAVD88 - 0.381 in the study area). Further tide information for this station can be accessed in <https://tidesandcurrents.noaa.gov/noaatidepredictions.html?id=8579381>.

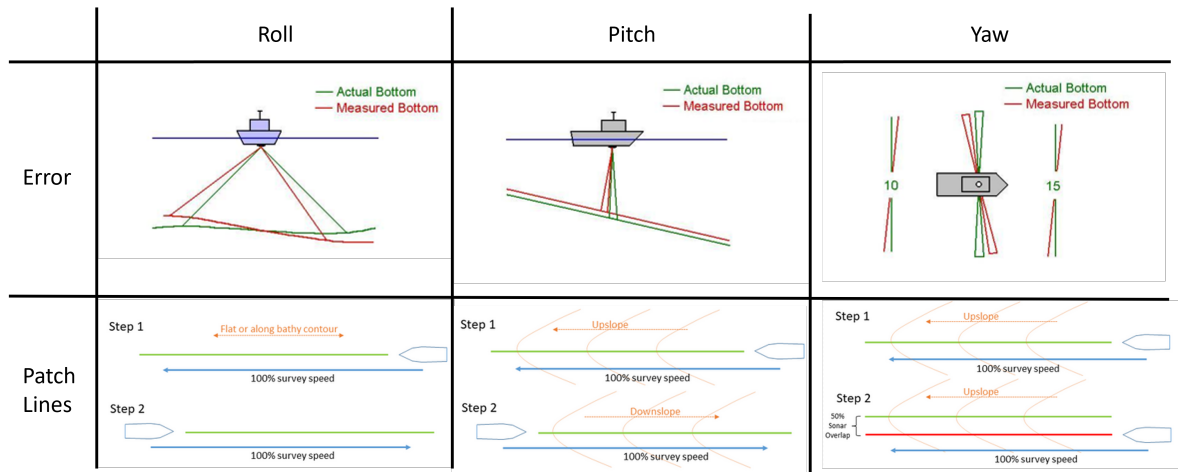


Figure 2.5: Diagram showing sonar alignment errors and patch testing lines. Patch test corrections are done in post-processing to reduce misalignment between lines. Images modified from [Hypack \(2013\)](#) and [Hoy and Kissinger \(2010\)](#).

The Edgetech 2205 is capable of simultaneously recording in 230 kHz and 540 kHz. The lower frequency data was not used as the higher frequency data resulted in



Figure 2.6: Image of Iver3-3048. Left - Underside of the platform with red arrows pointing to EdgeTech's 2205 transducers. Right - Entire setup of Iver3-3048 as it undergoes navigational alignment. The magnetometer attachment is highlighted.

better imagery especially since we were working in shallow depths close to the bed. The higher frequency data better matches that from the Norbit system as well. Compared to the Norbit iWBMSH, the AUV platform has higher uncertainty due to limited GPS correction underwater. GPS corrections are received on the surface and once the dive is underway, it estimates the fish position through an internal inertial navigation system (INS). Iver3 uses iXBlue PHINS Compact C3 fiber-optic gyroscope for its INS which introduces 0.006% drift over its total distance traveled. The longer it travels without surface corrections, the greater the inaccuracy becomes. Missions were set up so that the AUV could come to the surface and GPS corrections could be applied at least once every 4500 m. With these settings maximum drift of 29.90 m drift over 4500 m was observed, but the overall positional uncertainty was constrained using the integrated doppler velocity log (DVL) to approximately 3 m (measured uncertainty). AUV missions were run on all three excursions, but only in select areas due to battery limitations. The subsection of the North box was where instruments were being deployed for the SERDP project and was mapped every time. The subsection in the South box was mapped only once with the Iver3 since it was initially considered to

have potential, but did not end up being chosen. This extra coverage did provide a good area to get geotechnical samples since the South box had lower Norbit coverage and no overlap between lines compared to the North box.

On site, both sonar systems were used in tandem to increase coverage and efficiency of the survey. Due to time constraints iWBMSH was used to explore the larger field area and the data was reviewed in the field to determine areas of interest. While getting 150% is considered to be the standard in typical bathymetric surveys, it was not the goal in this case. For the initial October survey 40 m line spacing with 130° beam angle survey design was used, giving approximately 20 m wide survey lines in 5 m of water. Non-overlapping single pass lines obtained with these settings were enough to get a general idea of the site and move on to more detailed survey operations. Once an area was deemed suitable for further exploration, the Iver system was deployed with Marine Magnetic's Explorer (magnetometer) towed behind it. Magnetometer data was reviewed in tandem with the side scan imagery to determine geotechnical sampling locations. This was to ensure operator's safety since the area is an active UXO management site. Qualities that were considered in choosing a location were gradient in backscatter intensity, slope of the bed, lack of magnetic signature nearby, and absence of large debris nearby. Higher coverage of the area was achieved in subsequent surveys in February and April by staggering survey lines from the initial October survey to "fill in" the gaps.

2.3.2 Post-processing

Collected data was processed in Chesapeake Technology's SonarWiz v.7.11. SonarWiz can process bathymetry, side scan, sub-bottom, and magnetometer data in one software package. In this study only its bathymetry and side scan tools were used. Different tools can be used on different file types, and Patrick Zynda from Chesapeake Technology gave expert advise on what tools would work best for my raw file and desired results (personal communications, Jun. 07. 2023, Patrick Zynda).

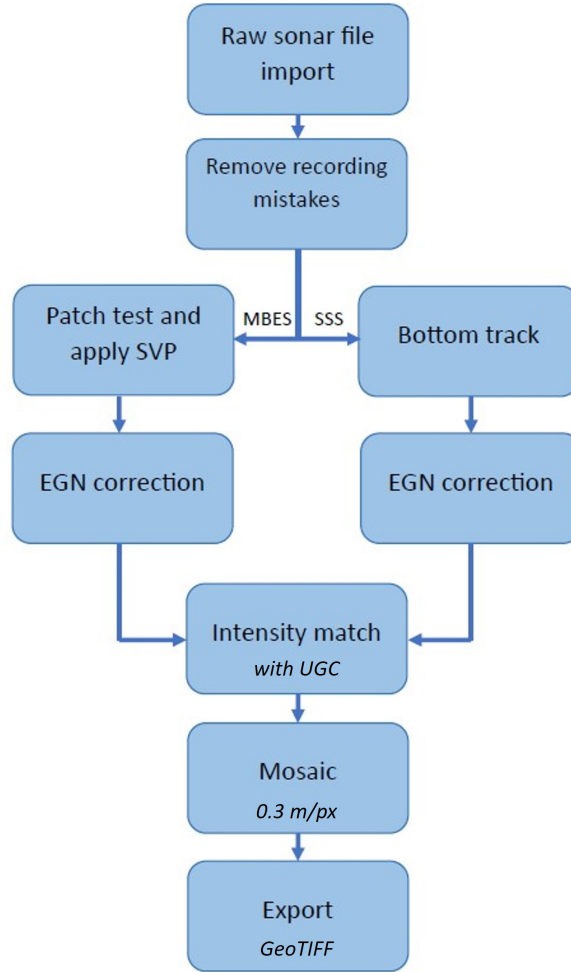


Figure 2.7: Workflow diagram for processing sonar backscatter from both multibeam and side scan systems. Detailed processing steps taken in this thesis can be found in Appendix B.

Figure 2.7 shows the workflow for post-processing backscatter from multibeam and side scan systems. For the Norbit bathymetry s7k data, sound speed profiles from the CTD were imported and used to improve ray tracing in the water column. Patch test lines were isolated and the sonar’s roll, pitch, and heading were corrected using the SonarWiz patch testing internal tool. Patch testing should be done every time the sonar is set up on the vessel, as it is correcting for small errors in mounting orientation. The corrected bathymetry was then mosaicked into a single GeoTIFF image with 0.3

m per pixel resolution and depths referenced to NAVD88.

	Roll	Pitch	Heading
Oct	0	0.5	-4
Feb	0.1	-1	-2
Apr	0.51	0.5	-2

Table 2.2: Final patch values for each field work. Latency correction is not needed for integrated MBES systems and was not performed.

Backscatter recorded from the Norbit system was processed after individual pings were corrected through the bathymetry post-processing steps described above. Although the s7k files can be imported as a side scan image file in SonarWiz, it does not allow for the level of corrections and manipulation as processing the individual pings first. Empirical gain normalization (EGN) function was applied with the entire Norbit data set to remove the effects of sonar geometry from the backscatter intensity.

Edgetech 2205’s side scan data was imported as a side scan file into SonarWiz. Bottom tracking was mostly automatic since the AUV mission is designed to fly a set distance from the seafloor, but certain sections with large logs and mid-water column noise (i.e. fish) were manually bottom tracked to obtain a clean mosaic. EGN was applied using the whole Edgetech data set. When exporting, overlapping pixels were drawn as average values of all overlap as shine through display would result in bright stripes throughout the overlapped areas. Backscatter intensity values were manually matched between the Norbit and Edgetech systems using user-defined gain corrections (UGC) by comparing overlapping areas. The UGC function uses the following equation to make corrections

$$TL = 20\log(R + 1) + \alpha(R) + b \tag{2.1}$$

where TL is transmission loss, R is range in meters, α is attenuation coefficient in dB/m, and b is static offset in dB ([Chesapeake Technology, 2023](#)). The SonarWiz dialogue allows you to modify the coefficient multiplied to the log, α , and b. In this use case, only the static offset b is modified to color match between the two sonars since

EGN corrects for attenuation and sonar geometry in the previous step. This allows data from two different systems to be used simultaneously in the classification step. Since the acquisition settings on AUV missions did not change over time and it had better overlap and backscatter data quality, backscatter from the Norbit was modified to match with Edgetech backscatter.

Data was exported with colors set to `mstlbronze`, color scale was adjusted manually to display best differentiation between higher and lower backscatter intensities using the entire backscatter dataset. Backscatter is the strength of the return sound signal received by the sonar (NOAA, 2023). SonarWiz displays the calculated backscatter strength in linear power scale by default instead of in logarithmic dB scale. Image resolution was set to 0.3 m per pixel, and color resolution was 32-bit with no image smoothing applied. While higher resolution export is possible, it was decided that it is not necessary since the margin of error on the geotechnical sampling location itself is greater than a meter. Resolution of 0.3 m per pixel gave a good balance between export efficiency and image quality.

2.4 Results and Discussion

Combined bathymetry from all three surveys can be seen in figure 2.8. The dredged channel is maintained at deeper than 10 m, while the surrounding area is typically shallower than 5 m. Most of the South Box is uniformly flat at approximately 3 m with a slightly higher mound of sediment in the middle, approximately 1 m higher than the outskirts of the box. Figure 2.10 (left) shows the distribution of depth values in the area.

Shown in figure 2.9 is the final backscatter mosaic of the entire field site. In figure 2.10 the total distribution of all intensity values is shown. The histogram is skewed towards lower intensity values, which is reasonable considering that most of the South box is uniformly low intensity. The `mstlbronze` color scheme ranges from black to yellow, with black denoting no backscatter (acoustic shadow) and bright yellow

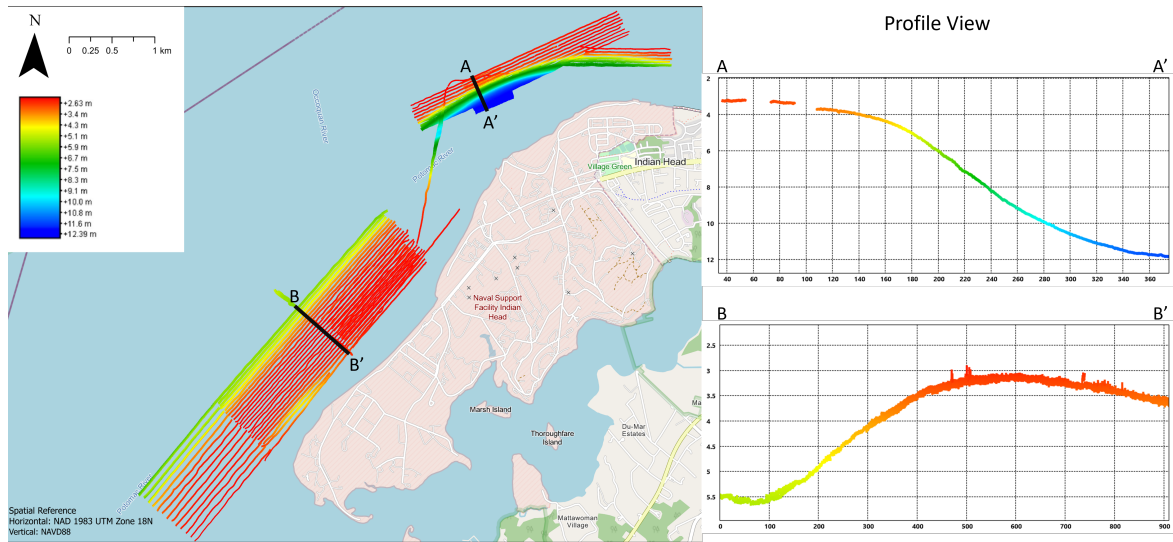


Figure 2.8: Compiled bathymetry of the field site exported at 0.3 m grid resolution. Depths range from 2.5 m to 12.5 m. Transect profiles of both boxes are shown on the right, units in meters.

denoting high backscatter. The channel can be seen as the brighter area near the bottom of the North box. Within the higher backscatter intensity channel area, 'tiger stripe' like banding of brighter and darker sections can be seen (see figure 2.11). The striping was initially thought to be ripples in the sediment or deposits of coarser grain. With the collected sediment samples, the brighter areas were actually determined to be areas with high bivalve density. Although outside the scope of this thesis, it is interesting that higher bivalve concentrations are observed on the channel slope as opposed to any other location in the area.

Impact of biological factors in sonar backscatter datasets cannot be understated. Studies like Gutsche (2011), Keller (2011), and Trembanis et al. (2017) have focused on deriving potential biological signals from backscatter. To determine the reason for high or low backscatter compared to the background, direct observation is necessary because of the possibility of environmental factors other than sediment type impacting backscatter intensity. By its very nature, substrate-dwelling organisms can change the surrounding sediment texture and hydrological environment and the hydrological



Figure 2.9: Processed backscatter mosaic from all valid sonar files. Overlapping pixels are calculated and shown as average value of all overlap. Black denotes low backscatter intensity and yellow denotes high backscatter intensity.

environment provides a niche for different organisms, demonstrated in [Pilditch et al. \(1997\)](#). The main takeaway here is that several environmental factors can impact sonar backscatter intensity. Direct observation and sampling should always accompany sonar surveys when attempting to infer sediment qualities from backscatter.

For easier comparison of backscatter intensity to other values, the final RGB image of figure 2.9 was also converted to a gray scale luminosity image using MATLAB `rgb2gray` function (figure 2.12). The resulting image maps the brightness of the pixel on a 0 to 255 scale that gives a single intensity value. Distribution of the intensity values are plotted in figure 2.13 which also shows where each drop penetrometer sampling

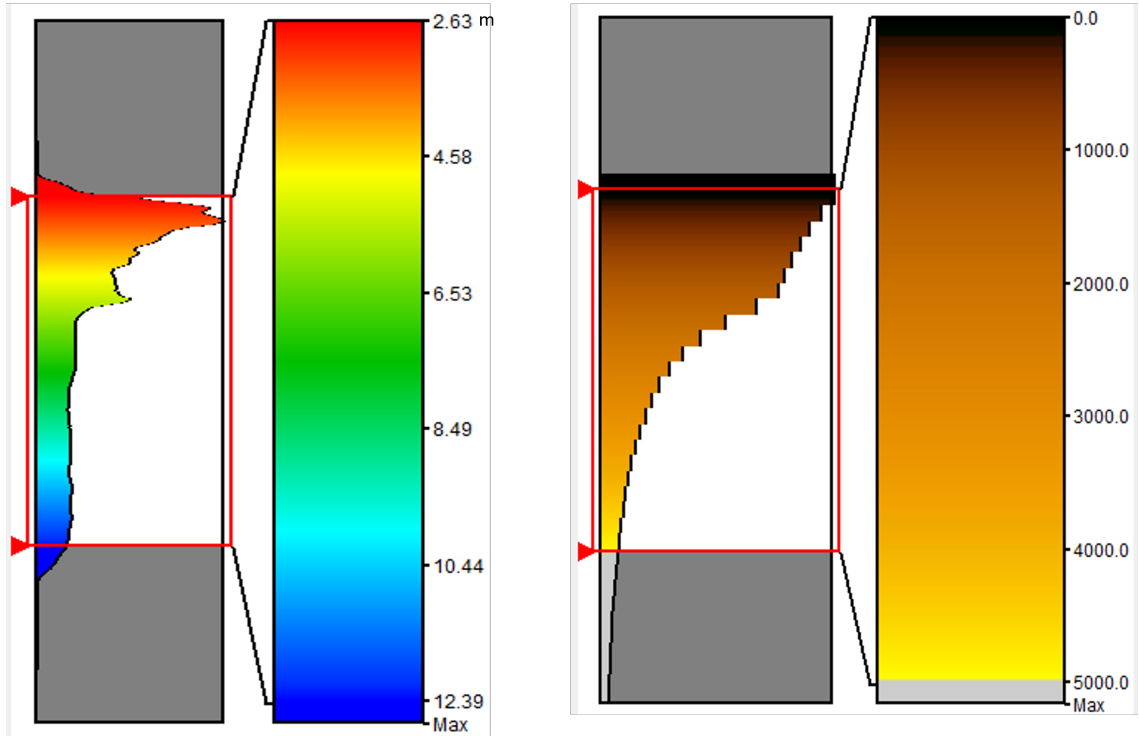


Figure 2.10: Left: Histogram of depth distribution. Right: Histogram of backscatter intensity distribution from SonarWiz after post-processing.

point places on the histogram. Note that sampling was done to represent a wide range of luminosity, but a notable gap in the 75 to 113 luminosity range exists. Location of pixels within this luminosity range is shown in figure 2.14. A large portion of the North box was in this range despite most of the sampling efforts being focused in this area. Due to the more extreme gradient of backscatter displayed in the channel walls, a major portion of the gradient in backscatter was not captured in this study. This may have contributed to classification issues in chapter 4.

Figure 2.13 also can demonstrate the limitations of using two different sonar systems to get backscatter. The Norbit system was used to get greater coverage while the AUV got greater resolution data. This is shown in figure 2.13, the Norbit system shows a greater range of distribution from 0 to 150, with a peak at approximately 40. The AUV on the other hand contributes to the peak around 70 and tapers down to

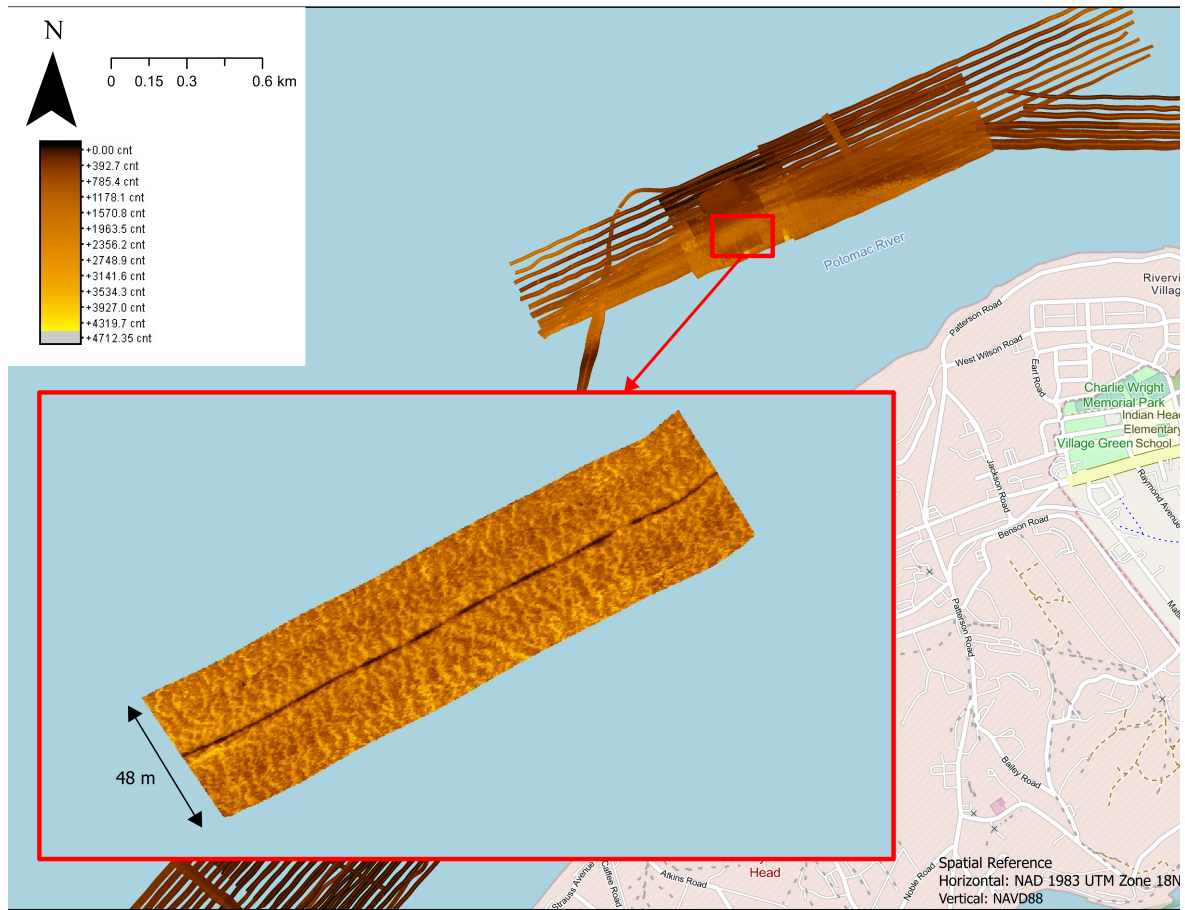


Figure 2.11: Zoomed in image overlay of a single AUV mission line that best shows the striped light and dark pattern in backscatter. This striping is only seen on the sloped channel sides with depths greater than 8.5 m.

150. While UGC was used to match the values as seamless as possible, the luminosity distribution still clearly shows differences in spectral quality. Using a single sonar system is recommended to get the best possible results in classification.

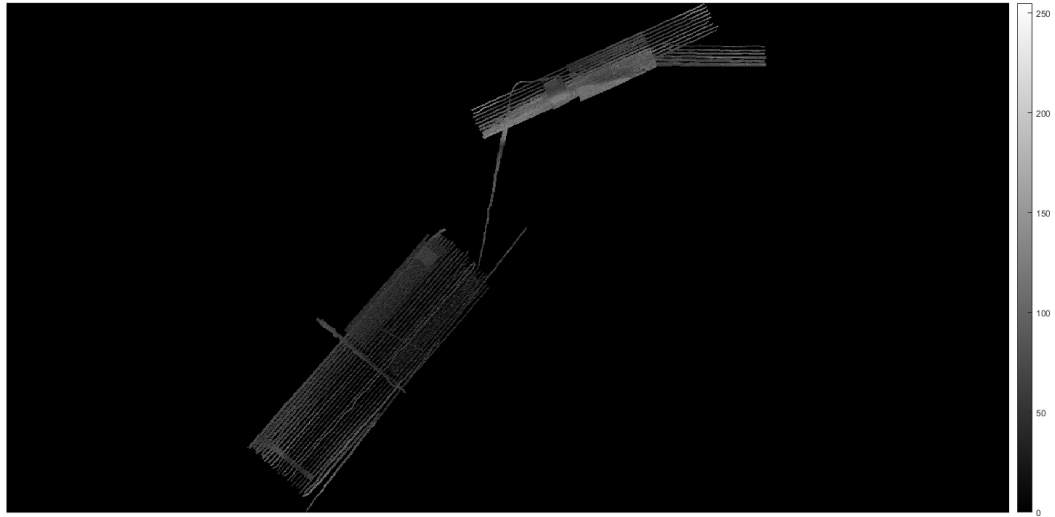


Figure 2.12: Backscatter intensity mapped on a gray scale. NaN values where there is no survey is plotted in black only to allow for easier perception of shade difference of the actual data.

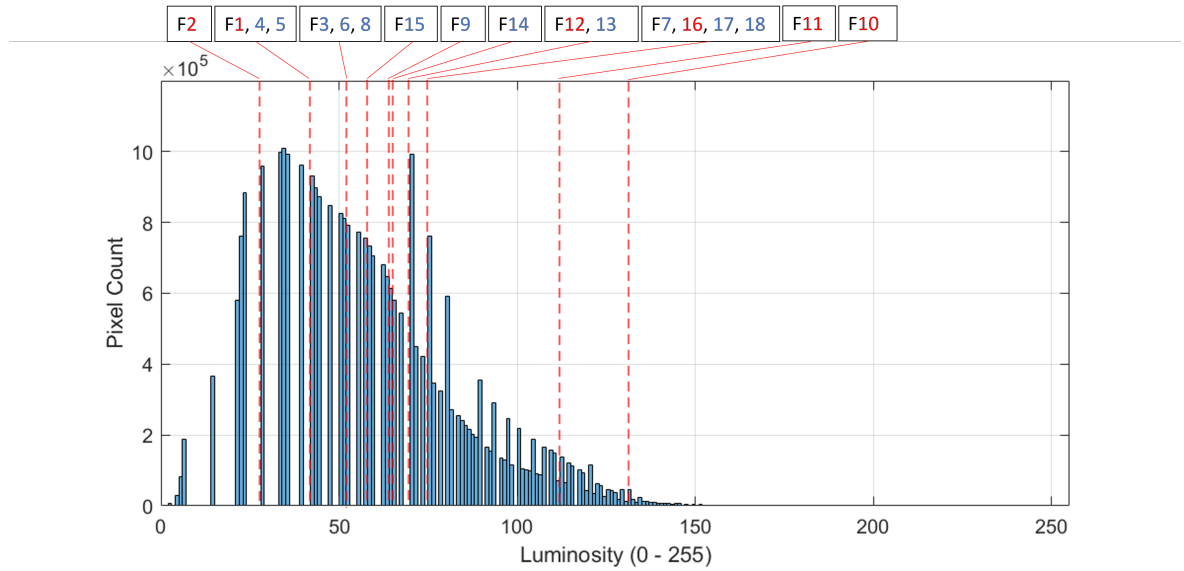


Figure 2.13: Histogram of gray scale backscatter intensity. Red dotted lines denote the value of intensity of the drop penetrometer sampling points.

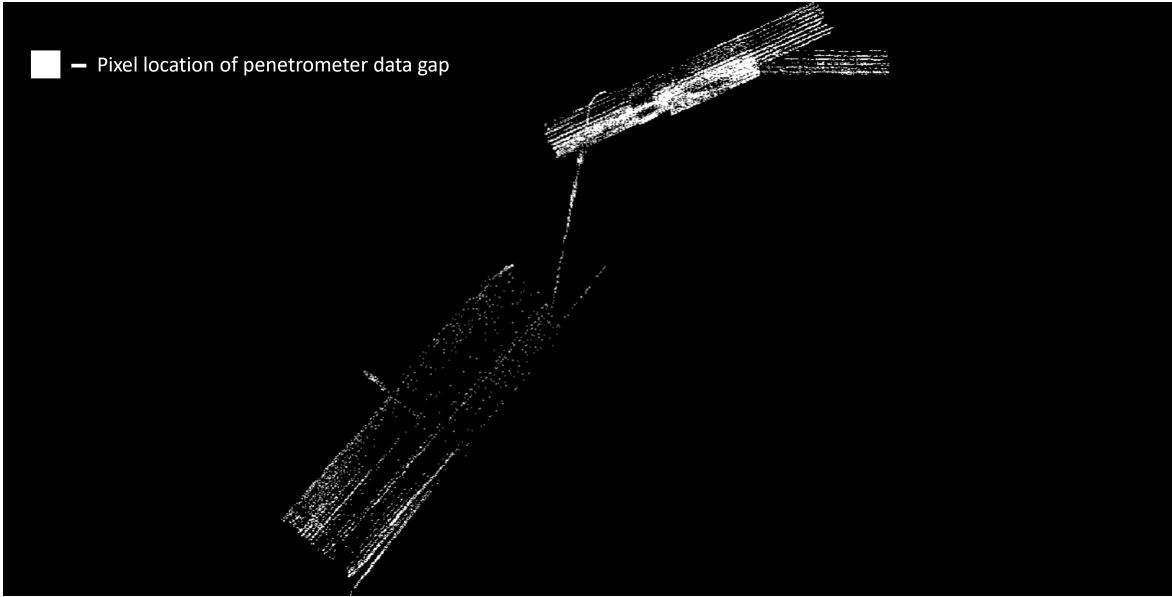


Figure 2.14: Map of pixels within 75 to 113 luminosity range colored in white. This denotes the location of the major gap in drop penetrometer sampling.

Chapter 3

GEOTECHNICAL ANALYSIS

3.1 Background

Acoustic imaging provides an indirect measurement of the seabed morphology and texture through sound wave reflections. To make a more concrete statement on the physical properties of the sediment, direct measurement and observation are needed. The geotechnical property of interest in this study is bearing capacity. Bearing capacity has been traditionally measured by taking sediment cores from the site of interest and measuring the force needed to deform the cored sediment (Leach, 1994). This process can be challenging for multiple reasons. 1. Taking a good core can be expensive or difficult. Penetration depth of a gravity corer can vary, resulting in uneven data collection. 2. Transporting cores without disturbing stratigraphy or compaction is difficult and expensive. Space may also be a limiting factor if you are operating from a small boat. Vibration can cause the sediment layers to shift and impact analysis results. 3. Core storage can be an issue. If the area of interest is high in organic matter, you will need cold storage to keep the samples from decaying. The core also needs to be stored upright, and can take up more space than expected. 4. Interacting with the sediment impacts consolidation and its physical properties, especially when the core is lifted from the bed. Instruments like a drop penetrometer mitigate these problems by taking *in situ* measurements of bearing capacity (Stark et al., 2012, 2017). The drop penetrometer has a known weight, known contact surface area in the shape of a cone, and an accelerometer inside the device. Using Newton's Second Law of Motion the user can arrive at a dynamic bearing capacity or Q_{dyn} (see equations below, F -

Force, m - mass, a - acceleration, q - bearing capacity, A - area). The raw data is stored within the device for post-operations download and processing.

$$F = m * a \quad (3.1)$$

$$Q_{dyn} = F/A \quad (3.2)$$

Dynamic bearing capacity measures bearing capacity as the drop penetrometer is moving through the sediment. Since the UXO are typically considered and managed as a stationary object, a conversion to quasi-static bearing capacity (QSBC) is necessary.

$$QSBC = Q_{dyn}/Fac \quad (3.3)$$

where

$$Fac = 1 + K \log_{10}(v/v_0) \quad (3.4)$$

K is an empirical constant dependent on soil type and behavior, v is penetration velocity, and v_0 is reference velocity of 2 m/s (Stark et al., 2017). Specifically determining the value of K of the sediment in the field site was outside the scope of this thesis. To arrive at a reasonable QSBC, the calculated QSBC of the Potomac site using various K values was compared to a typical QSBC range of muds outlined in Stark et al. (2017). In this study K value of 0.2 was chosen to reach a reasonable match of QSBC with Stark et al. (2017) and Trembanis and DuVal (2021).

Accompanying drop penetrometer sampling is the standard grain size analysis from sediment grabs. Folk (1974) outlines the importance of grain size analysis in discussing sediment characteristics like porosity, permeability, and firmness. Each sediment sample is divided into two major categories: cohesive and non-cohesive. The non-cohesive grains are dry sieved, meaning that the grains are dried and sorted with a sieve stack. The cohesive grains are too small to be sieved effectively, so they are wet

sieved and pipetted. Wet sieving involves washing the sample through a 63 μm sieve to select only the smaller grains for pipetting. Pipetting method, or the Andreason pipette technique, calculates grain size using Stokes Law. [Dyer \(1986\)](#) describes it as

$$Size (\mu\text{m}) = F * \sqrt{\frac{Depth\ of\ Sampling\ (cm)}{Time\ (min)}} \quad (3.5)$$

where F is a constant dependent on temperature. Andreason pipette technique is applicable to grains between 0.5 μm and 63 μm as below 0.5 μm brownian motion impacts particle settling. Details of the grain size analysis process is detailed in the following section. Grain size is typically displayed either in μm or ϕ . ϕ can be calculated using the following formula:

$$\phi = -\log_2(Diameter\ (mm)) \quad (3.6)$$

3.2 Methods

3.2.1 Grain Size Analysis

Sediment samples were taken at 27 locations to provide a more comprehensive site characterization. Of the 27, 9 were taken in October 2022, and 18 were taken in February 2023 (see [table A.1](#) and [figure 3.1](#)). Locations for sampling were chosen to reflect the widest range of backscatter intensity possible in the study site, and effort was made to collect samples only in areas with backscatter data.

Instrument deployment setup on site can be seen in [figure 3.2](#). The drop penetrometer and ponar grab was separated by approximately 2 m to give the operators enough room to keep the lines from tangling. An important point to note is the positional accuracy of the sampling locations (see [figure 3.3](#)). Unlike the sonar equipment which requires accurate positioning, horizontal and vertical accuracy of the GPS used in recording the sediment sampling locations are consumer grade. The horizontal accuracy of the SIMRAD Chart Plotter is 3 m. Additional uncertainty occurs due to

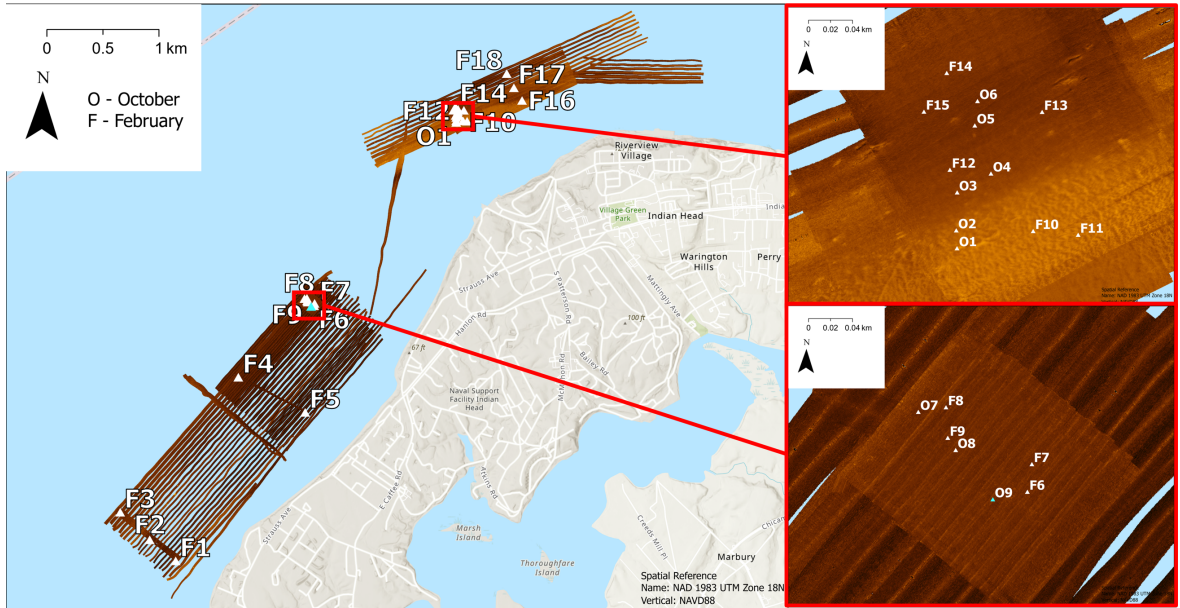


Figure 3.1: Map of all sampling locations. Latitude/longitude of locations can be found in appendix A.1.

variations in deployment location on the boat. The instrument does not go down orthogonal to the water surface due to currents and boat drift. The drop penetrometer and ponar grab locations are considered as a single dot when in reality they are deployed at least 2 m apart. This all adds to the positional uncertainty of sampling, which should be taken into account when pairing the results of the geotechnical samples with the more positionally accurate sonar backscatter.

Grabs were taken using Wildco’s Petite PONAR. Due to its relative small size (15 cm width, 15 cm height, 10.9 kg), it is easy to transport and use. The maximum volume of sample that can be taken is 2400 mL. It was lowered and retrieved by hand with a 50 feet rope. Once the ponar hit bottom, the latitude and longitude of the location was recorded along with a site number. This location is the same location used for the drop penetrometer results. Sample bags were labeled with the site number for identification later. Two samples bags were taken from each ponar grab, one from each wing of the grab. One bag was used for grain size analysis, and the other bag was frozen and stored until the end of the experiment. To transport the sample bags

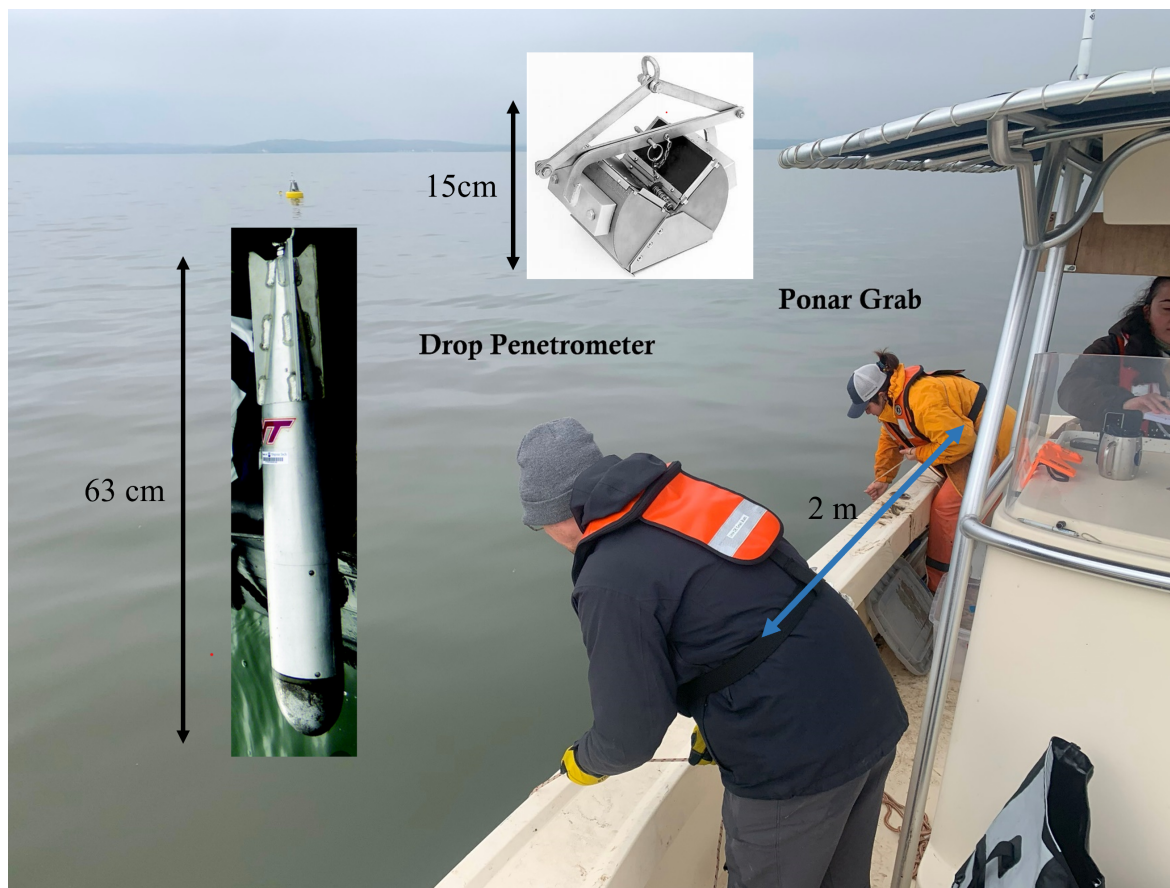


Figure 3.2: Image of instrument deployment setup on the vessel. Shown in small frames are images of a drop penetrometer and a ponar grab. Photo credit: Dr. Mark Lundine (background), Virginia Tech (drop penetrometer), Wildco (ponar grab)

from the field site to the lab, large cooler boxes filled with ice were used to slow down decay. No significant decay was noticed after transport. The samples were then put in a 4 °C environmental room until sub-samples were taken from the bags.

Grain size analysis of the samples were done following [Folk \(1974\)](#), and a workflow diagram can be seen in figure [3.4](#). The samples in the bag were mixed well before a 30 g sub-sample was taken. Folk notes that one should take samples of 50 g or more for sandy sediments, but for very muddy samples only 15 to 30 g are enough to get sufficient results ([Folk, 1974](#)). Wide mouth mason jars were labelled with the

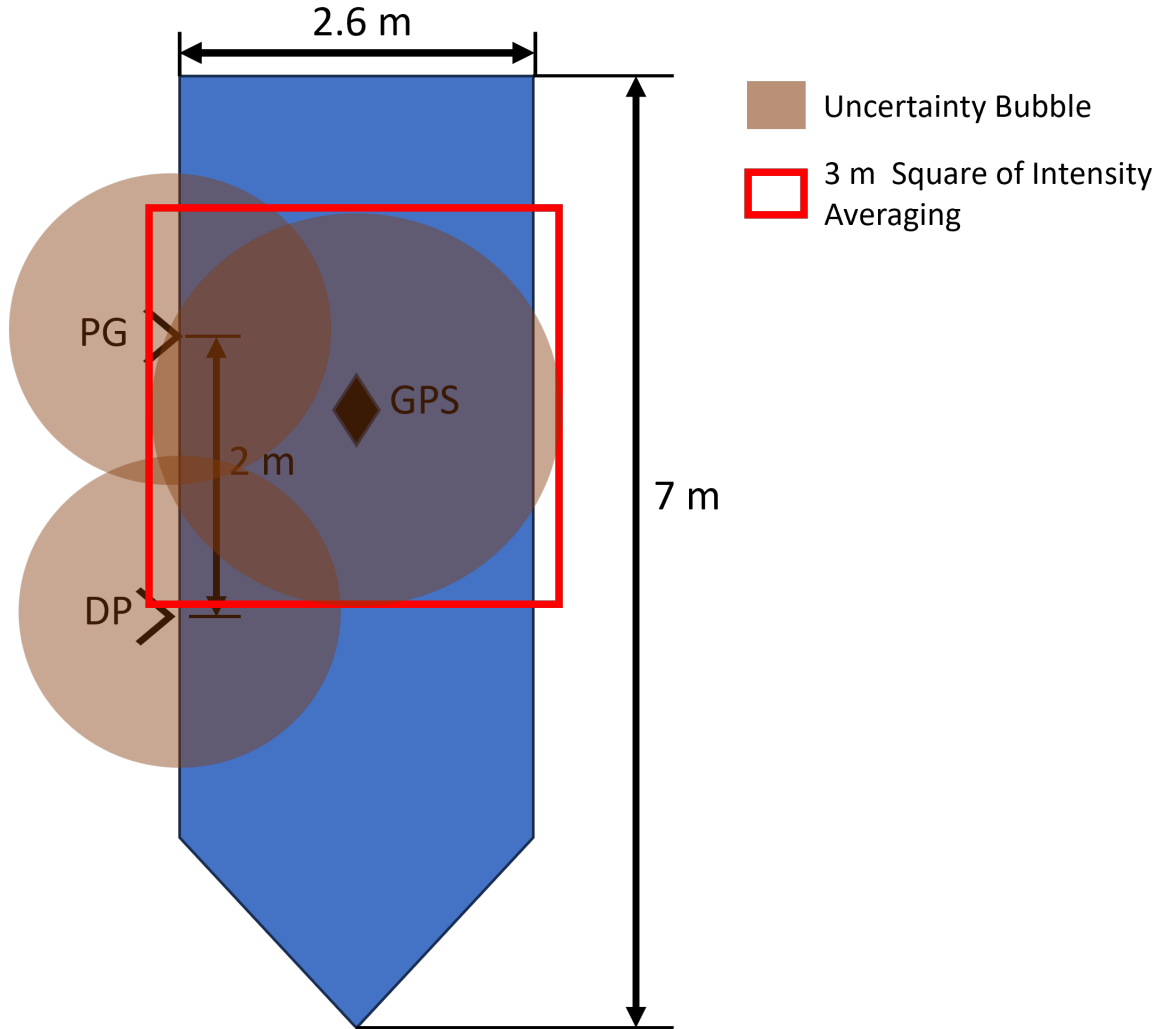


Figure 3.3: Top view diagram of the boat and data collection location for each instrument, not to scale. Uncertainty bubble is visualized for each instrument.

location number. Sample weight, location number, and latitude and longitude of the sample was recorded in a separate log sheet. Organic matter was removed by adding 30% hydrogen peroxide to the sample jar in small batches until no more CO₂ bubbles formed. Once the organic digestion process was complete, the whole mixture was wet sieved through a 63 μm sieve with de-ionized water to separate the sand fraction from the mud and silt fraction (see figure 3.5, right). The sand fraction was then put in a 60 °C oven to completely dry in preparation for dry sieving. The mud and silt fraction

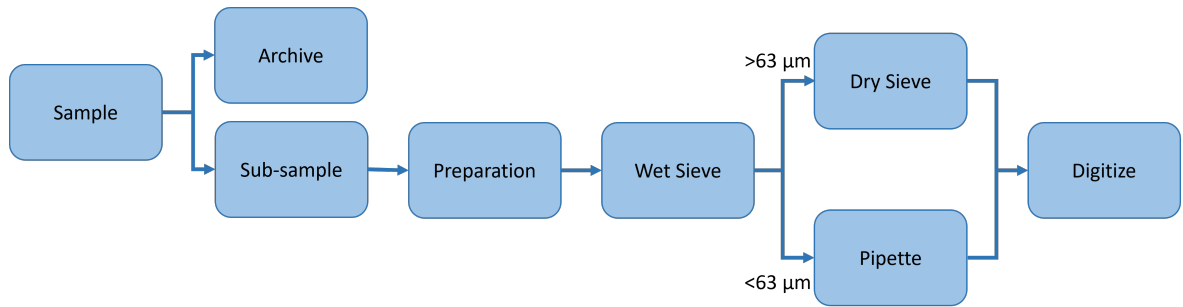


Figure 3.4: Workflow diagram for processing sediment samples for grain size analysis. Sand is separated from mud/clay and processed differently. Detailed analysis steps can be found in Appendix B.

were put into a 1000 mL graduated cylinder for pipetting.

For dry sieving, the total dried sand amount was weighed and recorded. It was then poured into the topmost sieve in a sieve stack. The sieve stack was comprised of 1000, 710, 500, 355, 250, 180, 125, and 63 μm sieves plus the bottom pan. Due to the smaller size of grains present in the experiment location, the 1000 μm sieve was mostly unnecessary. The whole sieve stack was placed into a W. S. Tyler’s RO-TAP RX-29 and shaken for 15 minutes (see figure 3.5, left). Individual sieves were taken apart and the weight of its contents were weighed and recorded. Any grains that fell through the 63 μm sieve were collected in the pan. Pan contents were weighed and added to the graduated cylinder.

For pipetting, each graduated cylinder was filled to the 980 mL line with the washed out sample from wet sieving and de-ionized water. After its corresponding sand fraction was dry sieved, the pan contents were added to the cylinder. Then the cylinder was filled to the 1000 mL mark with 20 mL of 1.000 g/L hexametaphosphate solution, which acts as a dispersant and stops the fine particles from floccing. With preparations done, the sample was thoroughly mixed. 20 mL sub-samples were pipetted at specific time intervals after the mixing was stopped. The corresponding time and grain size class of the sub-sample is shown in figure 3.6. Each sub-sample beaker was filled with additional 20 mL of the hexametaphosphate solution used in a previous step. The



Figure 3.5: Pictures showing grain size analysis setup. Left: RO-TAP with a full stack of sieves for dry sieving. The top is hammered while the stack is shaken. Right: Wet sieving setup with a 63 μm sieve in a funnel.

beaker was dried in a 60 °C oven and weighed. Weights of each size class was recorded on a log sheet. Measured weight was estimated back to the weight of size class in the full 1000 mL sample, minus dispersant weight. This final value was also recorded on a log sheet.

With all weights recorded, GRADISTAT (version 8; [Blott, 2010](#)) was used to calculate distribution statistics of each sample. Raw values were exported to MATLAB to compare the grain size analysis results to other data, and for visualization.

3.2.2 Drop Penetrometer

The drop penetrometer used in this study was a Bluedrop from Blue C Designs Inc. It measures approximately 63 cm in total length and weighs 7.7 kg, making it highly portable and convenient to use on field. It has been tested and used extensively in the past by Dr. Nina Stark and her research group ([Stark et al., 2012, 2017](#)) who provided assistance on the field with the deployment in February. The Bluedrop was deployed and recovered by hand, since the deepest area was approximately 15

Table 7-2. Depth (cm) of Pipette Insertion for a Given Temperature (assuming particles of S.G. = 2.65)

Temp. °C	Total Suspension 20 sec	4.5φ 44μ 2 min	5φ 31μ 4 min	5.5φ 22μ 8 min	6φ 16μ 15 min	7φ 8μ 30 min	8φ 4μ 2 hr	9φ 2μ 8 hr	10φ 1μ 32 hr
14.0	20.0	17.8	17.7	17.8	17.7	8.8	8.8	8.8	8.8
14.5	20.0	18.1	17.9	18.1	17.9	9.0	9.0	9.0	9.0
15.0	20.0	18.3	18.2	18.3	18.1	9.1	9.1	9.1	9.1
15.5	20.0	18.4	18.4	18.5	18.4	9.2	9.2	9.2	9.2
16.0	20.0	18.8	18.6	18.8	18.6	9.3	9.3	9.3	9.3
16.5	20.0	19.1	18.9	19.1	18.9	9.4	9.4	9.4	9.4
17.0	20.0	19.3	19.1	19.3	19.1	9.6	9.6	9.6	9.6
17.5	20.0	19.5	19.4	19.5	19.4	9.7	9.7	9.7	9.7
18.0	20.0	19.8	19.7	19.8	19.6	9.8	9.8	9.8	9.8
18.5	20.0	20.0	19.9	20.0	19.9	9.9	9.9	9.9	9.9
19.0	20.0	20.2	20.1	20.2	20.2	10.0	10.0	10.0	10.0
19.5	20.0	20.5	20.4	20.5	20.3	10.2	10.2	10.2	10.2
20.0	20.0	20.7	20.6	20.7	20.6	10.3	10.3	10.3	10.3
20.5	20.0	21.0	20.9	21.0	20.9	10.4	10.4	10.4	10.4
21.0	20.0	21.3	21.1	21.3	21.1	10.5	10.5	10.5	10.5
21.5	20.0	21.5	21.3	21.5	21.3	10.7	10.7	10.7	10.7
22.0	20.0	21.8	21.6	21.8	21.6	10.8	10.8	10.8	10.8
22.5	20.0	22.0	21.9	22.0	21.8	10.9	10.9	10.9	10.9
23.0	20.0	22.3	22.1	22.3	22.1	11.1	11.1	11.1	11.1
23.5	20.0	22.6	22.4	22.6	22.3	11.2	11.2	11.2	11.2
24.0	20.0	22.8	22.7	22.8	22.6	11.3	11.3	11.3	11.3
24.5	20.0	23.1	22.9	23.1	22.9	11.4	11.4	11.4	11.4
25.0	20.0	23.3	23.2	23.3	23.2	11.6	11.6	11.6	11.6
25.5	20.0	23.6	23.5	23.6	23.4	11.7	11.7	11.7	11.7
26.0	20.0	23.9	23.8	24.0	23.7	11.9	11.9	11.9	11.9
26.5	20.0	24.2	24.0	24.2	24.0	12.0	12.0	12.0	12.0
27.0	20.0	24.5	24.3	24.5	24.2	12.1	12.1	12.1	12.1
27.5	20.0	24.7	24.6	24.7	24.5	12.3	12.3	12.3	12.3

Note: *Time (min) = Depth of withdrawal (cm)/(1500 × A × d²), where A is a constant for a given water viscosity and particle density and d is the particle diameter.

Figure 3.6: Table from Lewis and McConchie (1994) showing pipetting time and grain size relationship in different temperatures. Temperature used is highlighted.

m. Deployment of the Bluedrop was coordinated with sediment sampling (see figure 3.2) to provide maximum comparison between the *in situ* bearing capacity, sediment grain size, and acoustic backscatter intensity. 18 locations were chosen (F1 - F18), and at each location the Bluedrop was deployed 5 times. Drop location's latitude and longitude is included in appendix A.1, approximated to be the same as the ponar grab locations.

3.2.3 Hydrodynamics and Core Analysis

As a part of the greater UXO mobility research, three instrument frames were deployed in the North box to collect hydrodynamic data. The location of these frames can be seen in figure 3.7. Burst average data from the Aquadopp ADCP mounted to the AquaCross is used in figure 3.8 to illustrate the overall calm conditions between February deployment and April recovery. Critical shear velocity for silty sand was calculated following equation outlined in [Fischenich \(2001\)](#) for silts and sands. D_{50} value of F13 ($0.032 \mu\text{m}$) was chosen for this calculation as it was a close sample location with similar backscatter intensity values to the AquaCross frame location. Calculated shear velocity for this grain size is 0.59 m/s , well above the maximum observed current velocity of 0.38 m/s . Calm conditions allows combining of backscatter data over longer periods of time, since it is unlikely that the sediment quality has changed over this time period.

Push cores were also taken near the frames by divers during frame recovery. The cores captured approximately 40 cm of sediment with the layers intact for laboratory analysis. The cores were sent to the Naval Research Lab for wet bulk density measurement, which can be seen in figure 3.9. Bulk density is calculated by

$$\text{Bulk Density} = \frac{\text{Sample Weight}}{\text{Sample Volume}} \quad (3.7)$$

and can describe how compacted the sediment is. Bulk density can have an impact on bearing capacity of sediments as well. A common analogy is a sponge with low bulk density deforming easily under load (low bearing capacity). Comparing the measured wet bulk density at each frame location, all profiles showed very low bulk density up to approximately 5 cm in depth. At deeper depths the bulk density plateaued and was mostly consistent throughout. The UD frame location had the greatest bulk density after the initial low density layer of 1.57 g/cm^3 . Bulk densities of the SeaSpider location and the AquaCross were 1.48 g/cm^3 and 1.37 g/cm^3 , respectively.

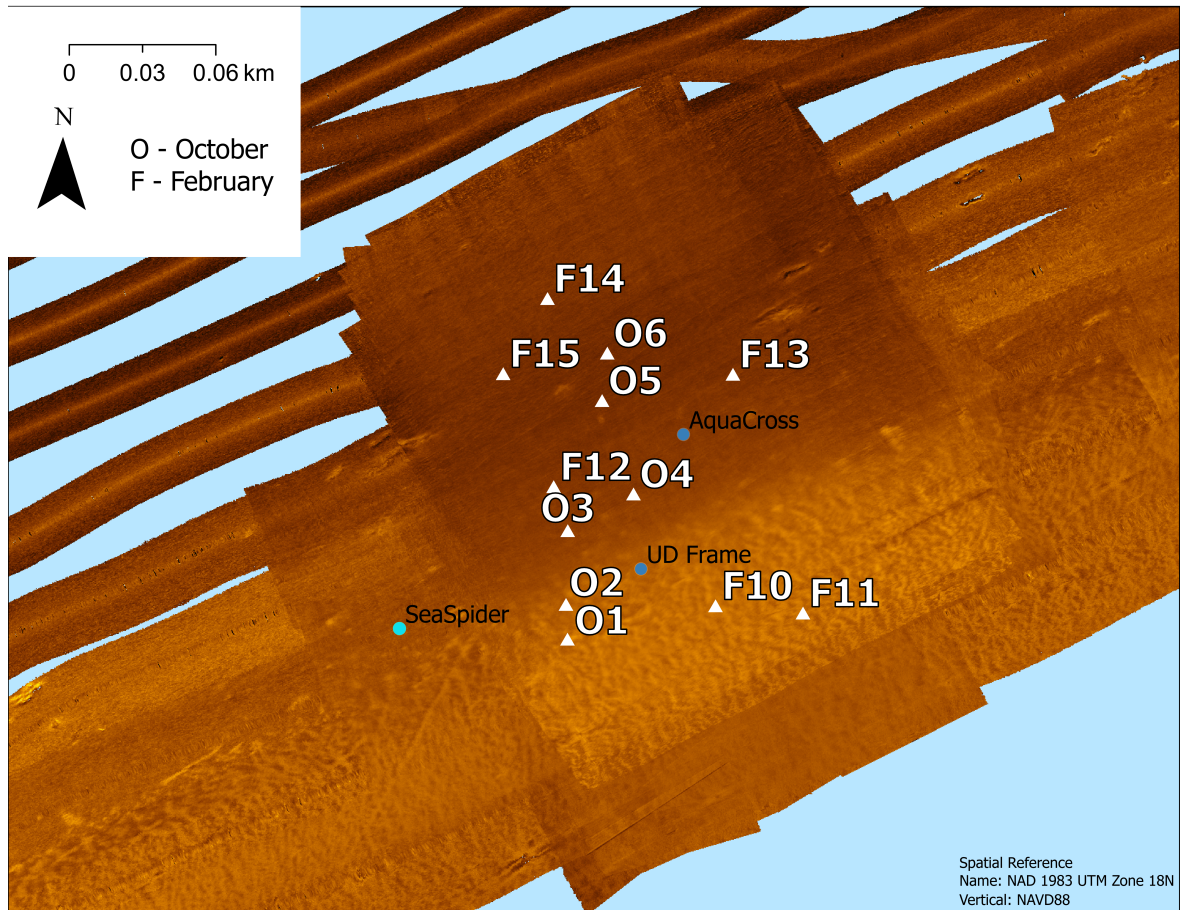


Figure 3.7: Location of each frame in relation to grab and drop penetrometer samples.

3.3 Results and Discussion

3.3.1 Grain Size Analysis

The grain size analysis results are shown in figure 3.10. Figure 3.11 displays the relationship between D_{50} in ϕ and sand percentage of each sampling location. Detailed analysis report from GRADISTAT can be found in appendix A.2, A.3, and A.4. Grabs from October and February that were near each other are compared in table 3.1. All 27 sites were sandy silt with sand percentages varying from 17% to 27.4%. The samples were moderately to poorly sorted. Sites F2, O1, and O7 had the highest sand percentages (27.4%, 25.7%, 24.2% respectively) while F10, F14, and F15 had the lowest sand percentages (17.0%, 17.7%, and 17.7% respectively). D_{50} of each location ranged

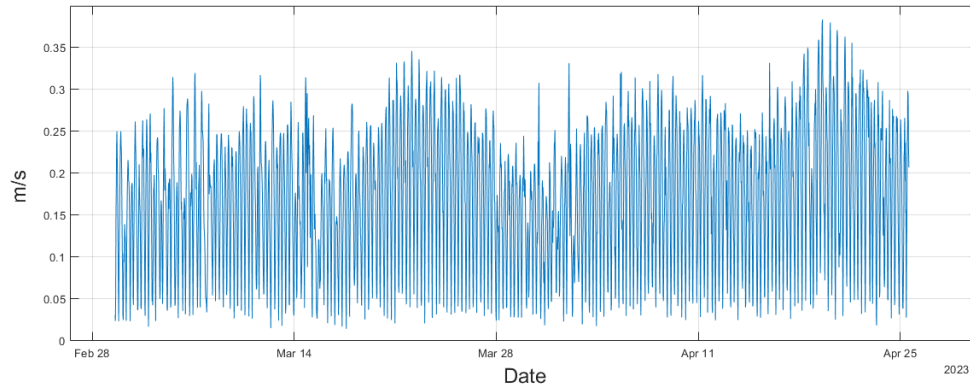


Figure 3.8: Burst average current velocity approximately 15cm above the bed over the frame deployment period. Current velocity was well under the critical shear velocity calculated for this location which was 0.59 m/s. Plot courtesy of Dr. DuVal.

from 4.54ϕ to 5.05ϕ , which was the most notable value when considered in combination with penetrometer results.

	South 1	South 2	South 3	North
	O9	O7	O8	O3
Mean	4.82	4.676	4.832	4.897
Sorting	0.913	0.772	0.937	0.942
Skewness	0.538	0.196	0.637	0.701
Kurtosis	2.698	3.034	3.271	4.034
Mean	Very Coarse Silt	Very Coarse Silt	Very Coarse Silt	Very Coarse Silt
Sorting	Moderately Sorted	Moderately Sorted	Moderately Sorted	Moderately Sorted
Skewness	Fine Skewed	Symmetrical	Fine Skewed	Symmetrical
Kurtosis	Platykurtic	Platykurtic	Platykurtic	Mesokurtic
% Gravel	0.0	0	0	0
% Sand	23.4	24.2	23.1	20.1
% Mud	76.6	75.8	76.9	79.9
	F6	F8	F9	F12
Mean	5.12	5.097	4.972	5.125
Sorting	1.326	1.324	1.15	1.258
Skewness	1.144	1.095	1.045	0.775
Kurtosis	4.097	4.064	3.878	4.376
Mean	Coarse Silt	Very Coarse Silt	Very Coarse Silt	Coarse Silt
Sorting	Poorly Sorted	Poorly Sorted	Poorly Sorted	Poorly Sorted
Skewness	Very Fine Skewed	Very Fine Skewed	Fine Skewed	Fine Skewed
Kurtosis	Mesokurtic	Mesokurtic	Mesokurtic	Mesokurtic
% Gravel	0	0	0	0
% Sand	21.5	21.9	22.5	19.4
% Mud	78.5	78.1	77.5	80.6
Distance (m)	28.2	22.4	11.5	18.9

Table 3.1: Comparison of grain size analysis results from October and February. O9 and F6, O7 and F8, O8 and F9, O3 and F12. Mean values are in ϕ ($-\log_2(\text{mm})$).

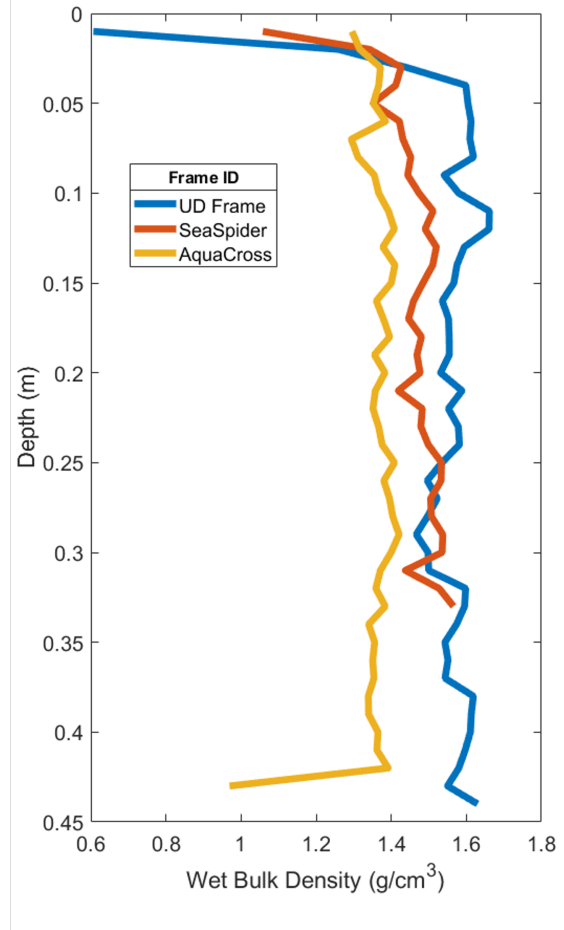


Figure 3.9: Left: Picture showing a core sample taken by the dive team. Layers are preserved for future analysis. Right: Wet bulk density at each frame location by depth. Depth value of 0 m is the water-sediment interface.

3.3.2 Drop Penetrometer

A total of 90 drops were analyzed from 18 drop sites. Data from one drop site (F1) will be shown and discussed as an example in this section, while all of the data will be included in appendix A (figures A.2, A.3, A.4). Figure 3.12 shows a scatter plot of the five drops deployed at this location, with quasi-static bearing capacity (QSBC) on the x axis and penetration depth on the y axis. This figure illustrates why multiple drops are necessary - two drops (1 and 5) have gone 10 cm more than the other three.

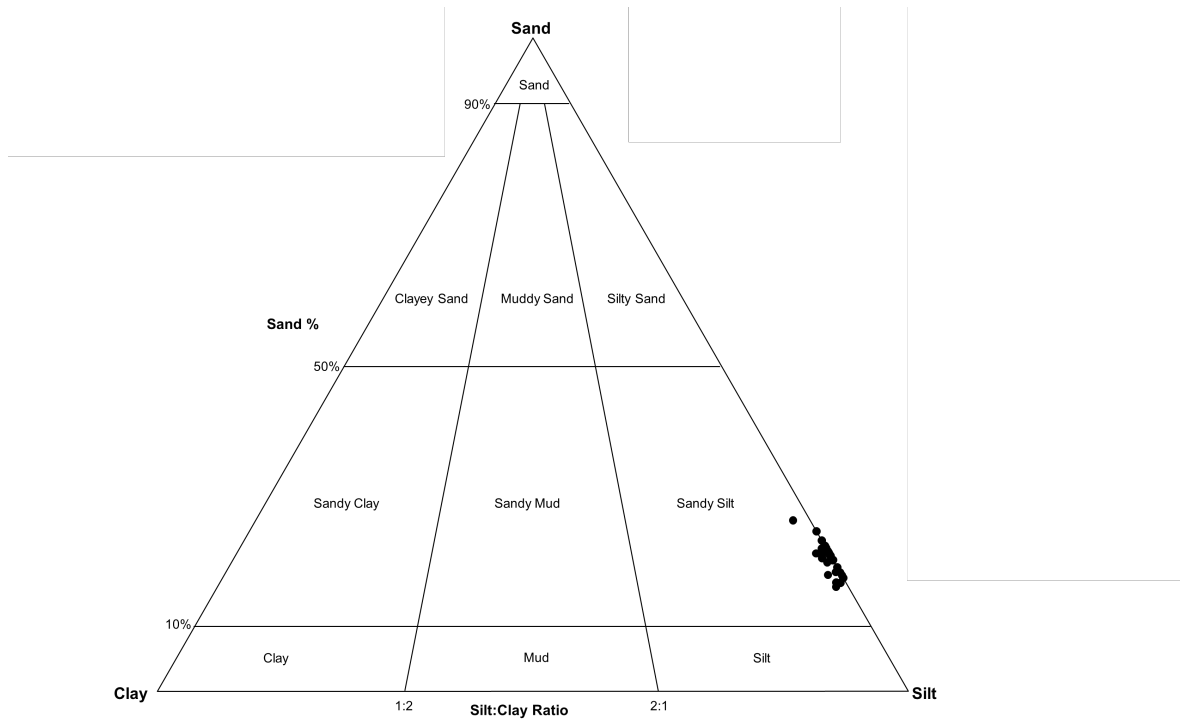


Figure 3.10: Results of grain size analysis displayed on a ternary diagram. All samples fall under sandy silt, with some variation on sand percentage.

This could be due to the penetrometer hitting an already disturbed bed, slight variation in drop angle, or the penetrometer may have hit something other than sediment on the three drops that did not sink as far. Slope and the rate of change in QSBC can be interpreted to changes in compaction. In the top 30 cm, QSBC increases with depth which makes sense with increasing weight over the layer increasing compaction. Noticeable peak in QSBC to nearly 40 kPa at 0.3 m is most likely indicates a shift in sediment layer. The tapering "tail" of QSBC when the drop penetrometer is coming to a stop is removed manually to eliminate the effects of the stop in QSBC profile analysis.

For further analysis in ArcGIS, average QSBC was plotted by drop location in MATLAB. This can be seen below in figure 3.13, with drop location by number is on the x axis and average value of QSBC is on the y axis. Drops F1, F2, F10, 11, 12, and 16 had higher averages than other drops, above 16 kPa. These 6 drop points were

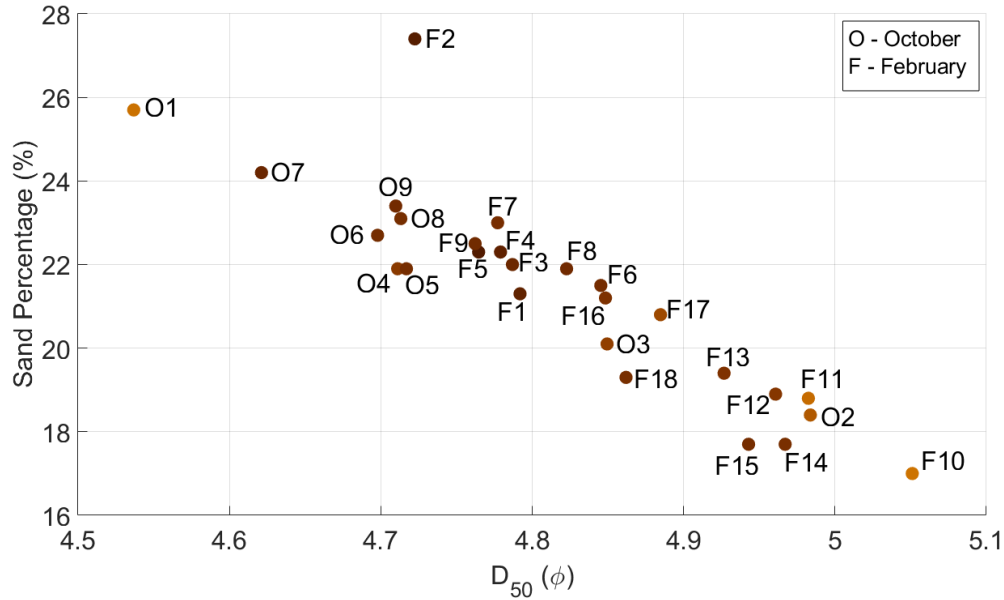


Figure 3.11: Results of grain size analysis showing D_{50} on the x axis and sand percentage on the y axis. Each point is labeled with the grab location number. Points are colored by the average RGB value of a 3 m square around the sampling location.

classified as 'high bearing capacity' for classifier training in the next step, while the other points were classified as 'low bearing capacity' (see figure 3.14 for an example drop profile of each). While there could be debate on where this divide between 'high' and 'low' QSBC should be, 16 kPa allowed for the most even number of samples per class (6 high, 12 low). This is important for the classifier to work properly in chapter 4. If there is a specific target bearing capacity value, drop penetrometer collection should be coordinated to get an even number of samples within each class.

D_{50} is plotted against average QSBC in figure 3.15. It is notable that D_{50} does not have a great correlation with average QSBC, which is interesting when in non-cohesive sediment grain size can be used to calculate bearing capacity (Jensen et al., 2020; Plachý et al., 2016). With more data points a better understanding of this relationship could be explored. In figure 3.16, each point is colored by the average backscatter intensity of a 3 m square around the sampling point. Averaging is done to

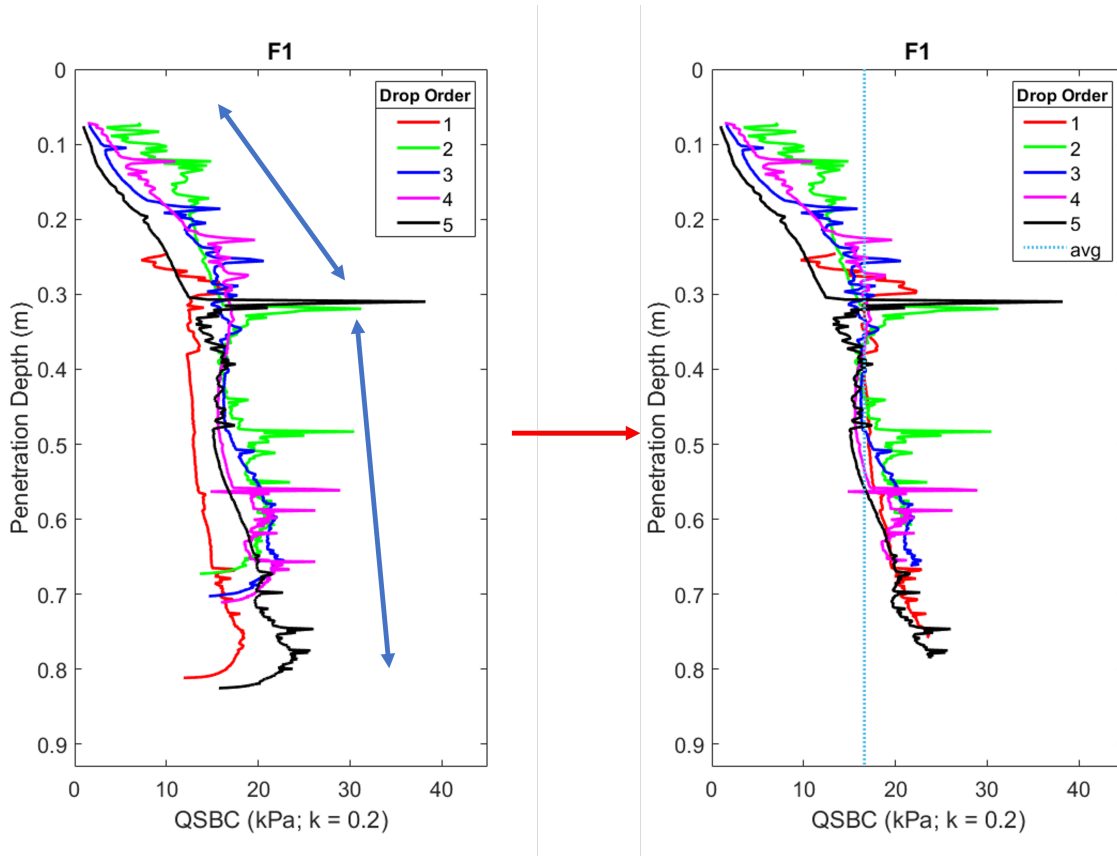


Figure 3.12: Left: Drop penetrometer profile of site F1. Changes in slope is highlighted with arrows. Right: Profile of QSBC with the tapering tail removed that is used for drop penetrometer analysis.

account for positional inaccuracy in the GPS record outlined in the methods section. The figure shows that with lower sand fractions, the average QSBC trends higher (weak correlation) and the backscatter intensity is also higher. The slight trend of higher average QSBC with low sand fraction can be explained in context of the Hjulström curve (figure 1.1). With more cohesion more force is needed to deform the undisturbed bed. The higher backscatter intensity with the lower sand fraction is odd though, as typically larger grain size is related to higher backscatter intensity. I believe this to be the result of high shell fraction and higher reflectivity on the hard shells to be the cause of this effect. Another possible cause of the mismatch may be due to stratigraphy of the sediment. Divers during field operations noted a "thin, firmer crust" below which

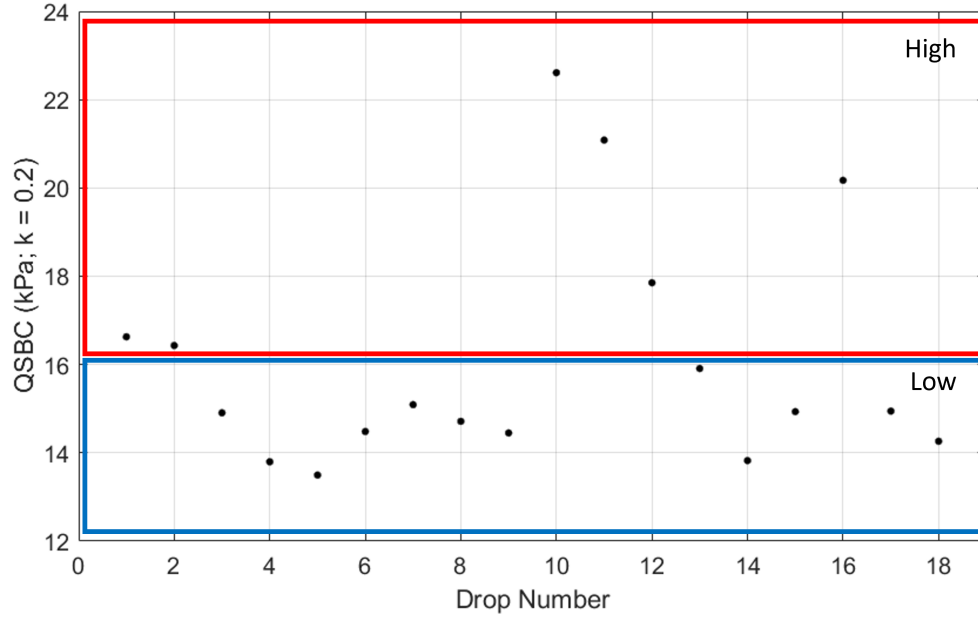


Figure 3.13: Depth average bearing capacity of each sampling location. Points with high average bearing capacity are boxed in red, and points with low average bearing capacity are boxed in blue.

lay much softer, unconsolidated mud. Since the backscatter cannot penetrate into the sediment layer, only the surficial crust is observed, leading to higher backscatter intensity in low sand samples.

If the average QSBC of a location is the value of interest, a simpler approach could be considered. In figure 3.17, the average maximum penetration depth of each sampling site is plotted with the average QSBC. Linear regression has been applied to show good match between the two ($R^2 = 0.9170$). In the field when an estimate of the average QSBC is needed, maximum penetration depth of the drop penetrometer could be used to arrive at a rough comparison between sites.

Another useful data product could be a simplified profile of the QSBC. A linear regression can be applied to the data profile of each location to produce a slope and y-intercept value, which gives a reasonable prediction of a QSBC profile. The trade-off is between data resolution and computational cost. Looking at figure 3.18, a notable

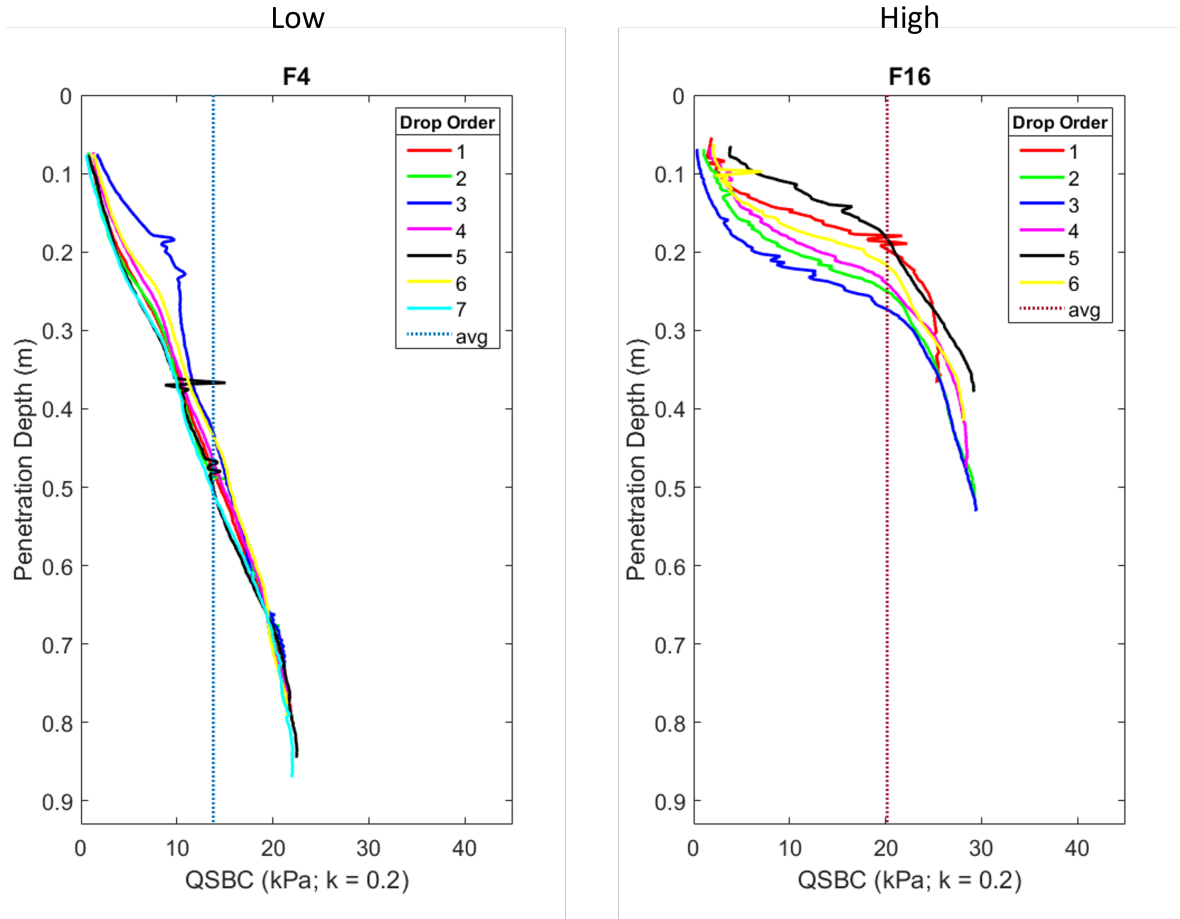


Figure 3.14: QSBC profiles of F4 and F10. F4 is an example of a 'low' QSBC location and F10 is an example of a 'high' QSBC location.

difference in slope can be observed between a representative 'low' QSBC location and 'high' QSBC location. Such a simplified profile can give an approximate burial depth of UXO while requiring minimal computational resources. Table of slope and intercept of all locations can be seen in Appendix A.5. In the case of significant change in QSBC due to stratigraphy, other models than linear regression could be applied to fit the needs of the user.

Efficacy of the simplified QSBC profile was tested by using a burial depth prediction model developed in Trembanis and DuVal (2021) and comparing the results from both the simplified and observed QSBC profiles. In figure 3.19, predicted burial

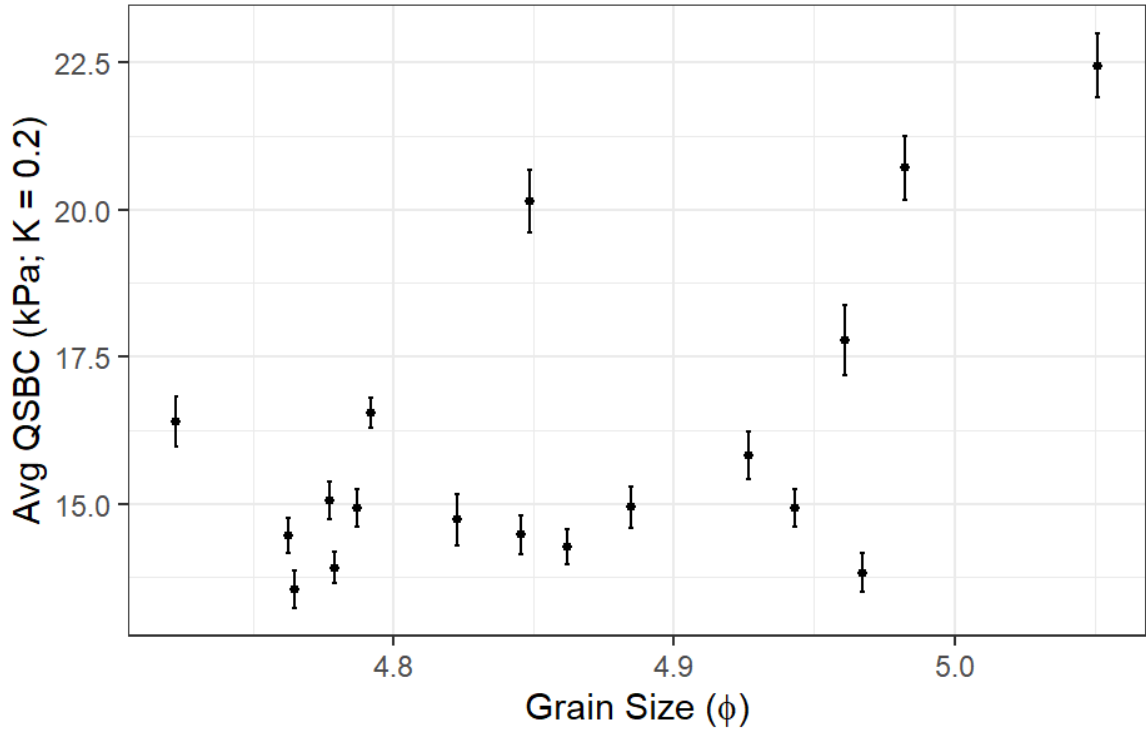


Figure 3.15: Average QSBC of up to 60 cm sampling depth at each sampling location versus the D_{50} value. 95% confidence interval is marked for each average.

depth of an UXO (weight: 55.2 kg, diameter: 0.15 m, length: 0.69 m) in an example 'low' QSBC site is shown. Using the observed profile, predicted burial depth was 0.23 m while the simplified profile predicted burial depth of 0.20 m. In figure 3.20, the same is shown an example 'high' QSBC site. The predicted burial depth for the observed profile is 0.13 m, and the predicted burial depth for the simplified profile is 0.13 m. For both 'low' and 'high' QSBC sites, the simplified profile was able to predict burial depth of the UXO similar to the observed profile.

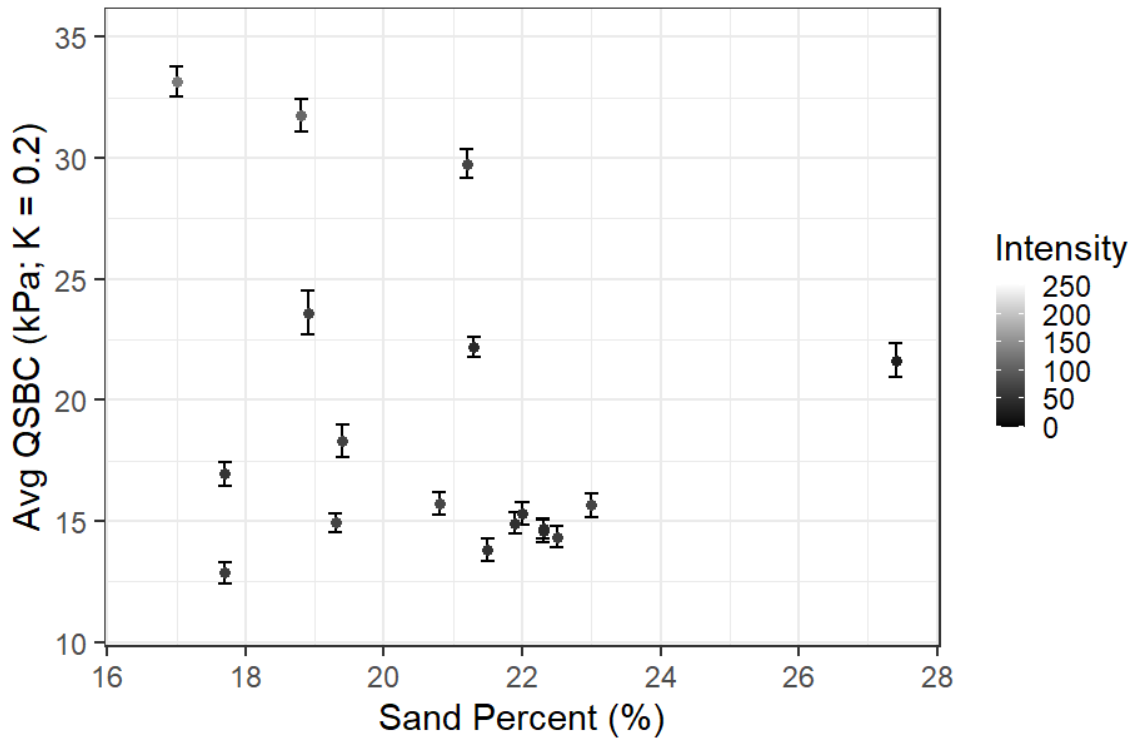


Figure 3.16: Sand percentage and average QSBC of each location. The marker color is the average backscatter intensity value of a 3 m square around the sampling location.

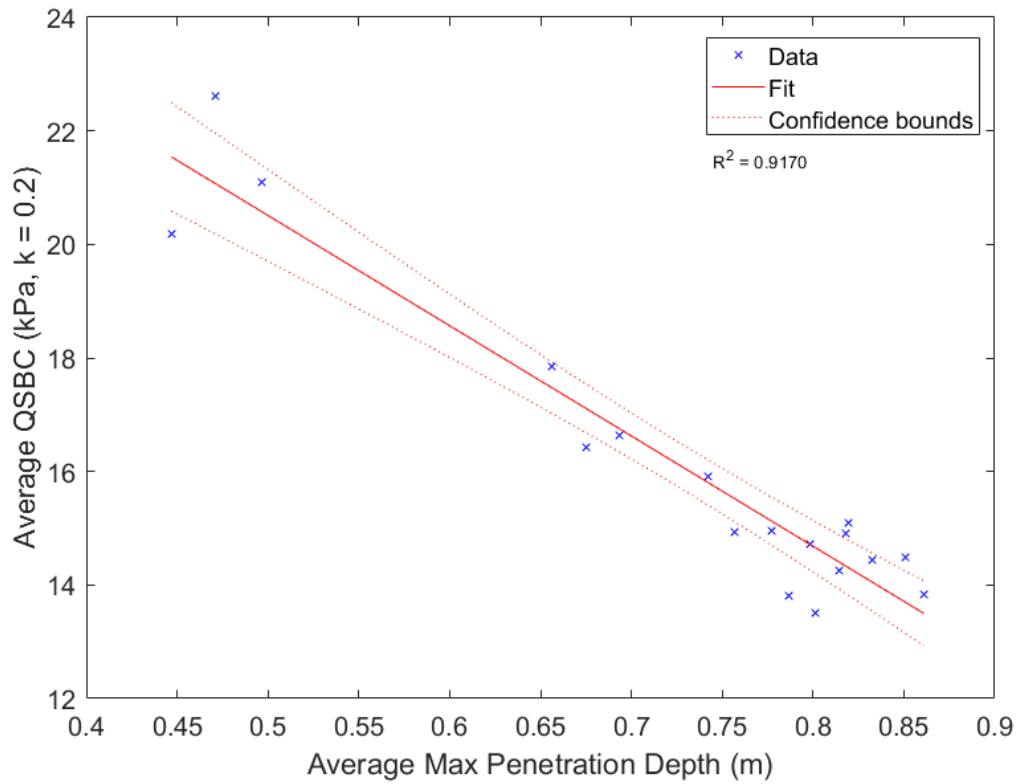
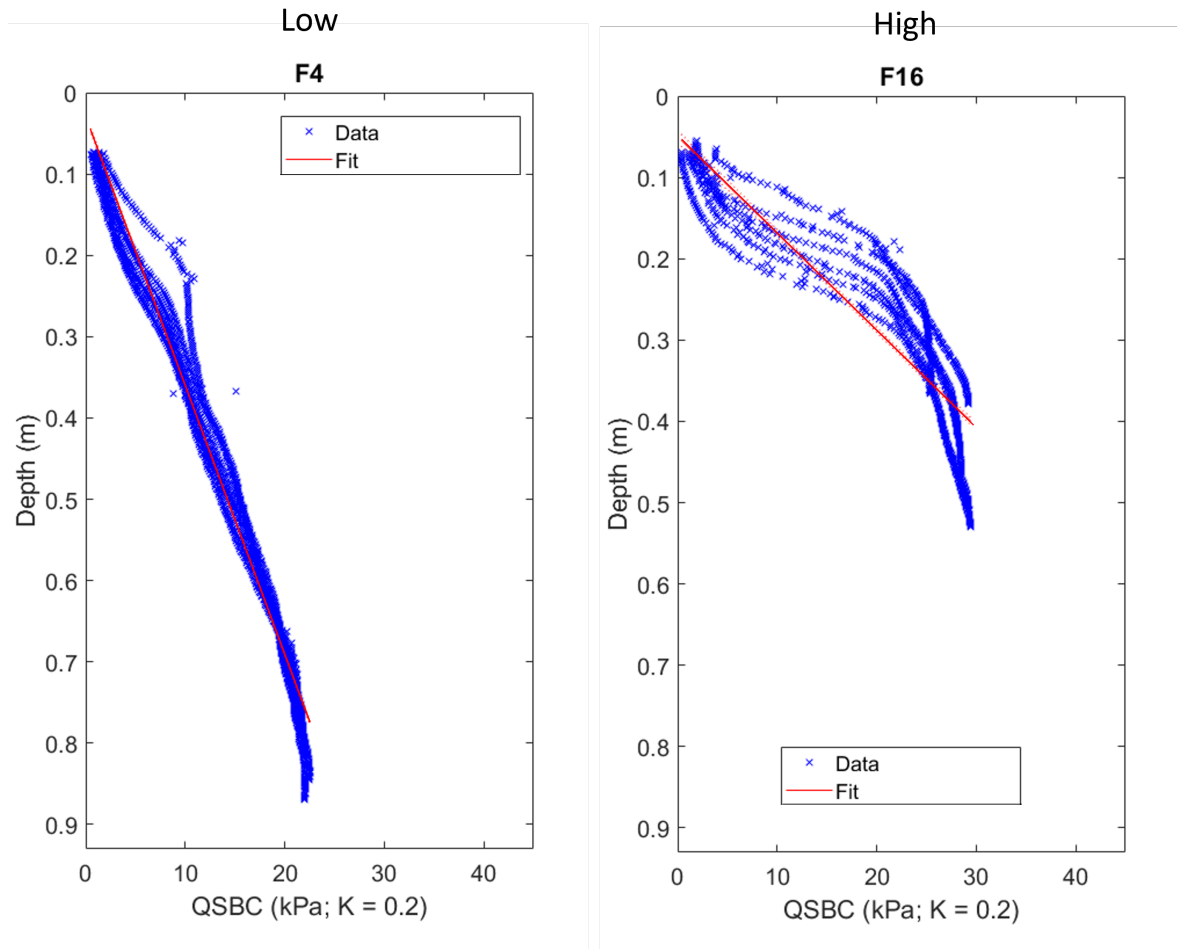


Figure 3.17: Average maximum penetration depth and average QSBC of each location. Linear regression is applied.



	F4	F16
Slope	0.0331	0.0119
R ²	0.97	0.80

Figure 3.18: Top: Plots comparing the slope of the linear fit between Low and High QSCB sampling sites. Bottom: Table of calculated slope and R² value of the two sites. Note that because the y-axis is inverted to show penetration depth, the calculated slope value is in the positive and does not necessarily match up with the observable slope in the plot.

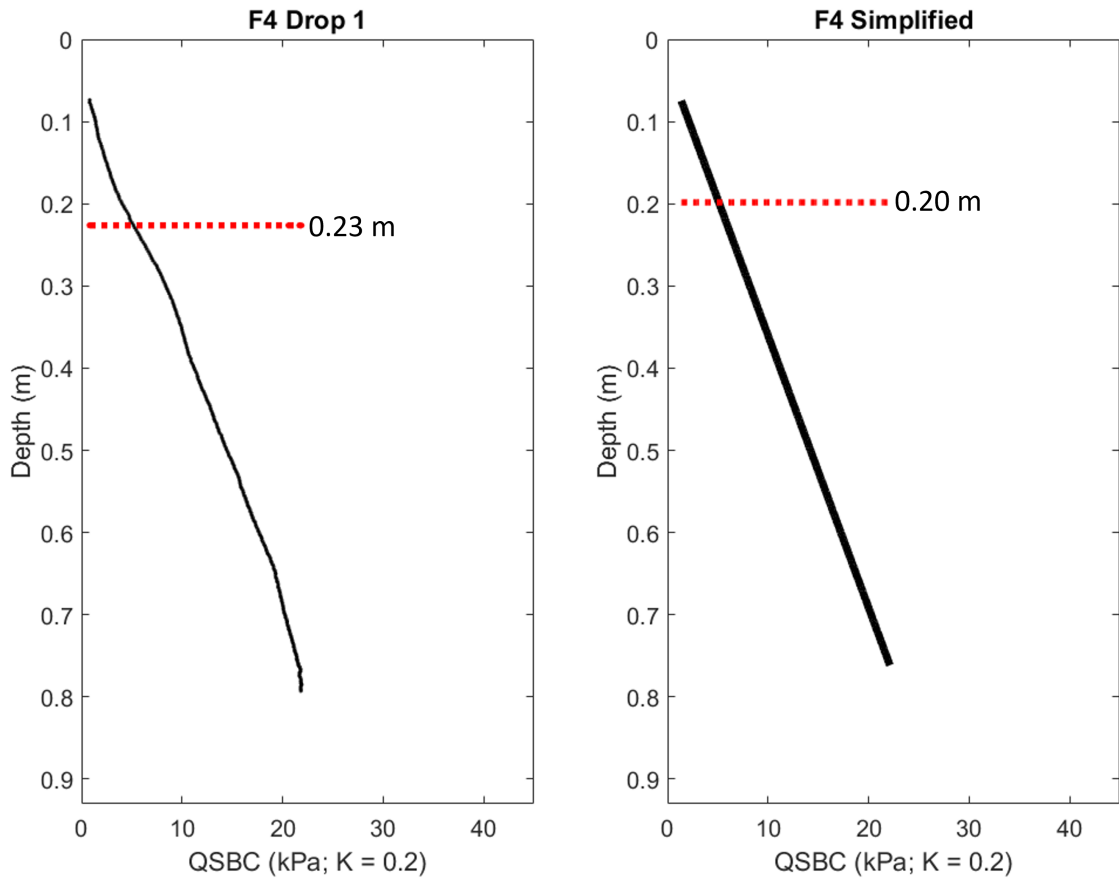


Figure 3.19: UXO burial prediction for an example 'low' QSBC site. Left: Predicted UXO burial depth using the F4 Drop 1 QSBC profile. Right: Predicted UXO burial depth using the linear fitted F4 QSBC profile.

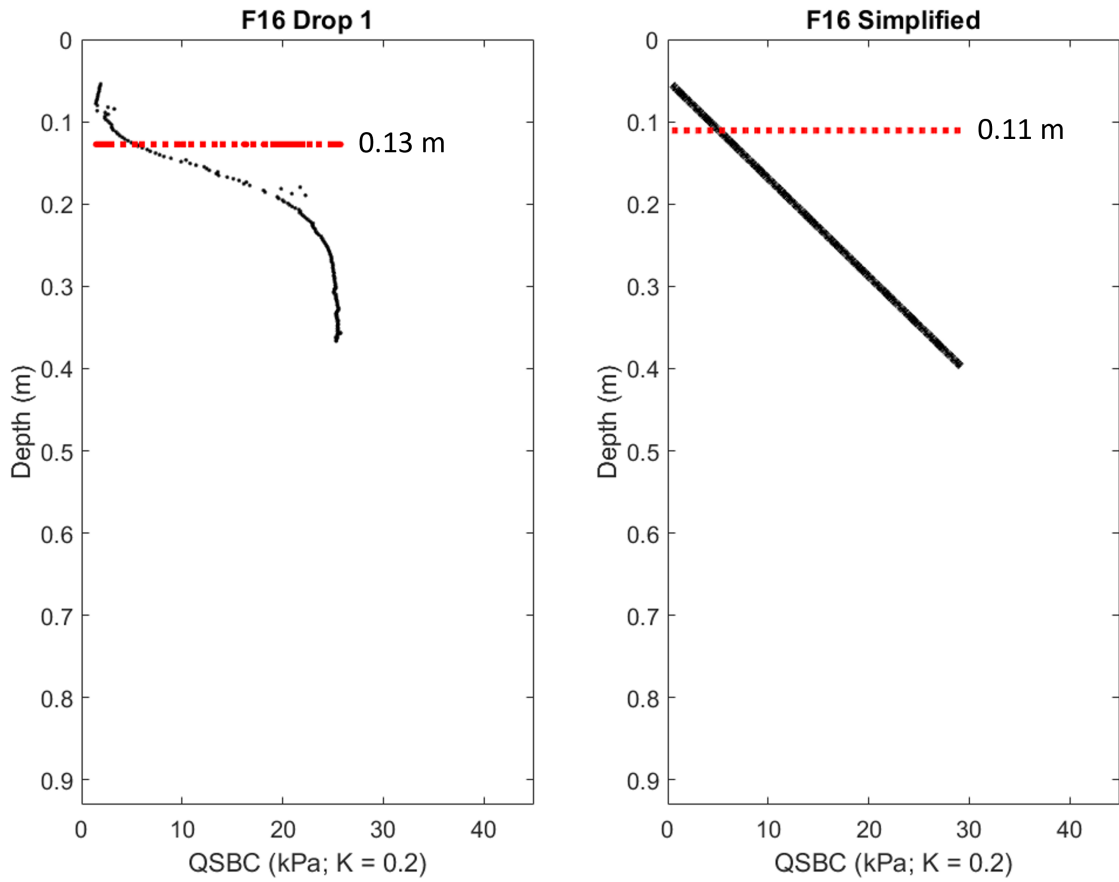


Figure 3.20: UXO burial prediction for an example 'high' QSBC site. Left: Predicted UXO burial depth using the F16 Drop 1 QSBC profile. Right: Predicted UXO burial depth using the linear fitted F16 QSBC profile.

Chapter 4

SEDIMENT CLASSIFICATION

4.1 Background

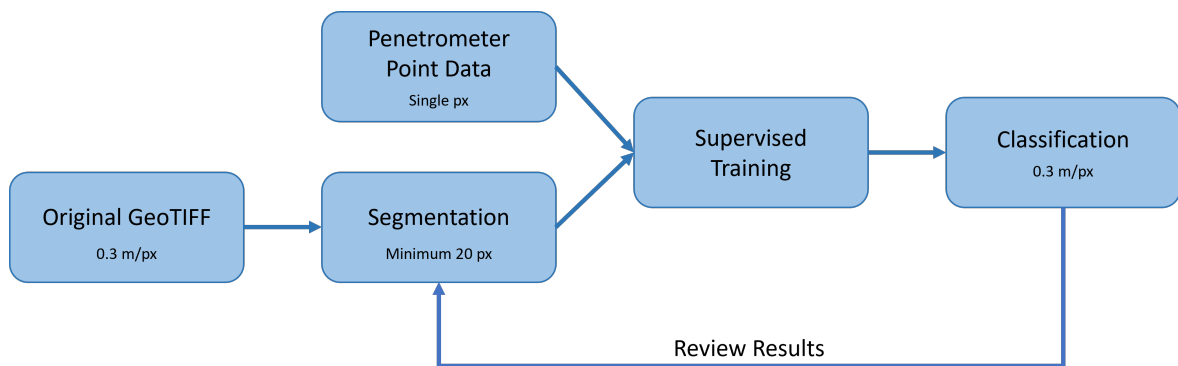


Figure 4.1: Workflow of ArcGIS Pro's classification wizard. Each step can be run using individual tools or the entire process can be run using the classification wizard depending on user preference.

In the realm of oceanography, GIS has been used to map underwater habitats (Gutsche, 2011; Raineault et al., 2011; Yang et al., 2009) and classify across a large grain size spectrum (Brown et al., 2019; Keller, 2011; Van Rein et al., 2011). Gutsche (2011) used auto-segmentation and supplementary manual segmentation where the auto-segmentation algorithm failed to identify benthic organism clusters in the Delaware bay and coastal Atlantic areas and achieved high resolution classification maps. Brown et al. (2019) on the other hand explored how different sonar frequencies can be used and combined to get a better understanding of sediment composition with depth. Depending on frequency, the backscatter image can reflect various qualities of the sediment that is being ensonified.

While the location, environment, and final goal is different for each study mentioned above, the concept of processing spectral imagery and grouping certain pixels together to achieve a reasonable separation of sediment qualities is the same. The process can be simplified as shown in figure 4.1. The goal of this chapter is to demonstrate how segmentation and classification can be achieved even when there is very little variation in sediment quality.

4.2 Methods

ESRI's ArcGIS Pro was used to process and classify backscatter image products from SonarWiz. The GeoTIFF was imported and displayed in RGB with no stretch and no percent clip to maintain the original colors. When the GeoTIFF is imported into ArcGIS, each pixel is assigned 4 values: red, green, blue, and gamma. In very simplified terms, gamma values denote the brightness (or contrast) of an image. Gamma encoding is a power-law function and is described in [Thompson et al. \(2016\)](#) as

$$e_s = l_s^{1/\gamma} \quad (4.1)$$

where e_s is encoded brightness value, l_s is the original brightness value, and γ is the scaling factor.

Gamma value for the backscatter GeoTIFF was set to 1.0 since this marginally improved segmentation results compared to 0.8 due to increased contrast between shades of brown. ArcGIS Pro offers a image classification wizard as part of their spatial analyst toolbox, which offers a streamlined work process that goes from an RGB image to a classified map product. Steps of this workflow is shown in figure 4.1.

ArcGIS takes spectral and spatial detail when segmenting and classifying an image ([ESRI, 2023](#)). Spectral detail defines how far away the RGB γ values of different pixels have to be to be put in the same segment. The value can be set from 1.0 to 20.0, and higher the value, greater the discrimination between colors. Spectral detail can be lowered to ignore noise in the backscatter data if any remain, but it should be

high enough to pick up actual changes in backscatter intensity. Spatial detail defines how small and close together distinct segments can be. Valid values range from 1 to 20 (whole numbers only), higher values allow for smaller and closer segments. Spatial detail should be set high enough that the smallest feature that you want to observe can be its own segment.

Configuration in the classification wizard does have an impact on the quality of the final results. First, a supervised classification method was selected since penetrometer data was collected on site and could be used to train the classification algorithm. Classification type was object based, which takes into account surrounding pixel information. Object based was chosen instead of pixel based because the sediment type at one pixel is likely affected by and impacting its surrounding environment. A simple low/high/NaN classification schema was set up for this classification.

For segmentation multiple configurations of settings were tested before the final spectral detail of 20.00 and spatial detail of 19 was reached. See figure 4.2 for effects of setting change and figure 4.3 for final segmentation results. Spectral detail was the value that impacted the final results more than spatial detail. Minimum segment size was set to 20 pixels which is the smallest size cluster allowed in ArcGIS. It was set to the minimum so as to not lose image resolution in the segmenting process. The 20 pixels can be arranged in any shape, allowing for anywhere between a 0.3 m * 6 m rectangle to a irregular polygon that is 20 pixels in total. There is a trade-off between resolution and computing resource availability, but the dataset used in this study was small enough that the classifier could run on a typical consumer grade laptop. If the collected backscatter data was very rough due to weather conditions or acquisition settings, this value could be set larger to smooth over residual sonar effects from the GeoTIFF.

Each drop penetrometer data point occupies a single pixel in the GeoTIFF and all drops were used to train the classifier. Accurate placement of the drop points was achieved by placing cross-hair shaped point notes of the drop penetrometer locations

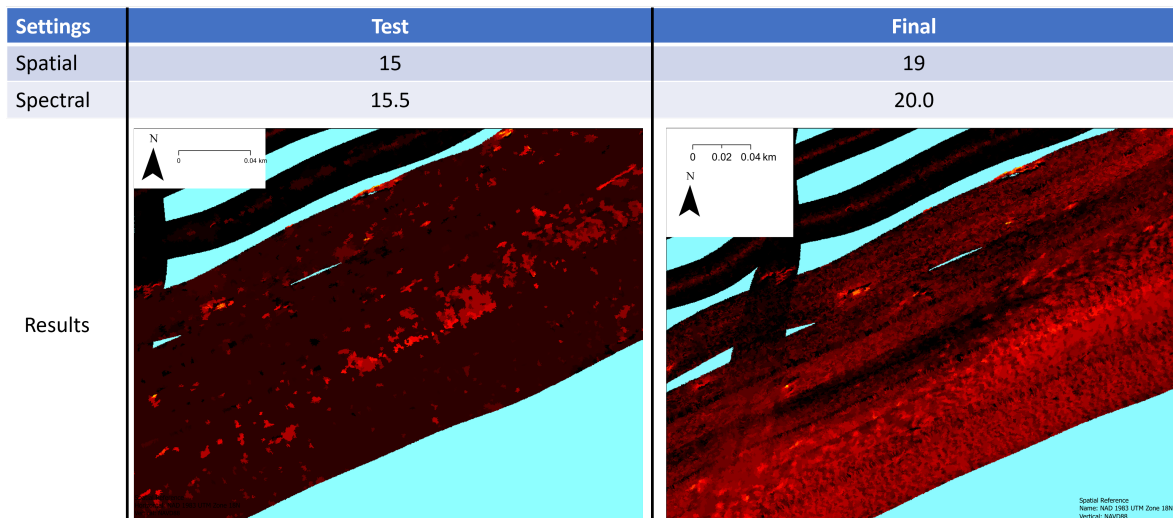


Figure 4.2: Comparison of segmentation results with different spatial and spectral detail settings.

in the base map and aligning the training sample points to the center of the cross-hairs. In total 30 training samples were given to the classifier: 6 high, 12 low, and 12 NaN. Support vector machine was used instead of k-nearest neighbor for classifying since the support vector machine classifier handles data with unbalanced training sample numbers per class. For segment attributes active chromaticity color was selected to reflect the RGB values in the original GeoTIFF. The final output was reviewed and exported as a GeoTIFF, PNG, and a map display.

4.3 Results and Discussion

Final results of the classification are shown in figure 4.4. Most of the South box is classified as 'low' in dark blue, with the south-most corner being classified as 'high'. Half of the North box is classified as 'high' in red, with all of the channel being classified as 'high'. In total, 89.55% of the surveyed area was classified as 'low' and 10.45% was classified as 'high'. Comparing the result of the classifier to the initial training points, the classifier has a tendency to underestimate bearing capacity. In table 4.1, all of the errors are colored in gray and all errors were of high penetrometer locations being

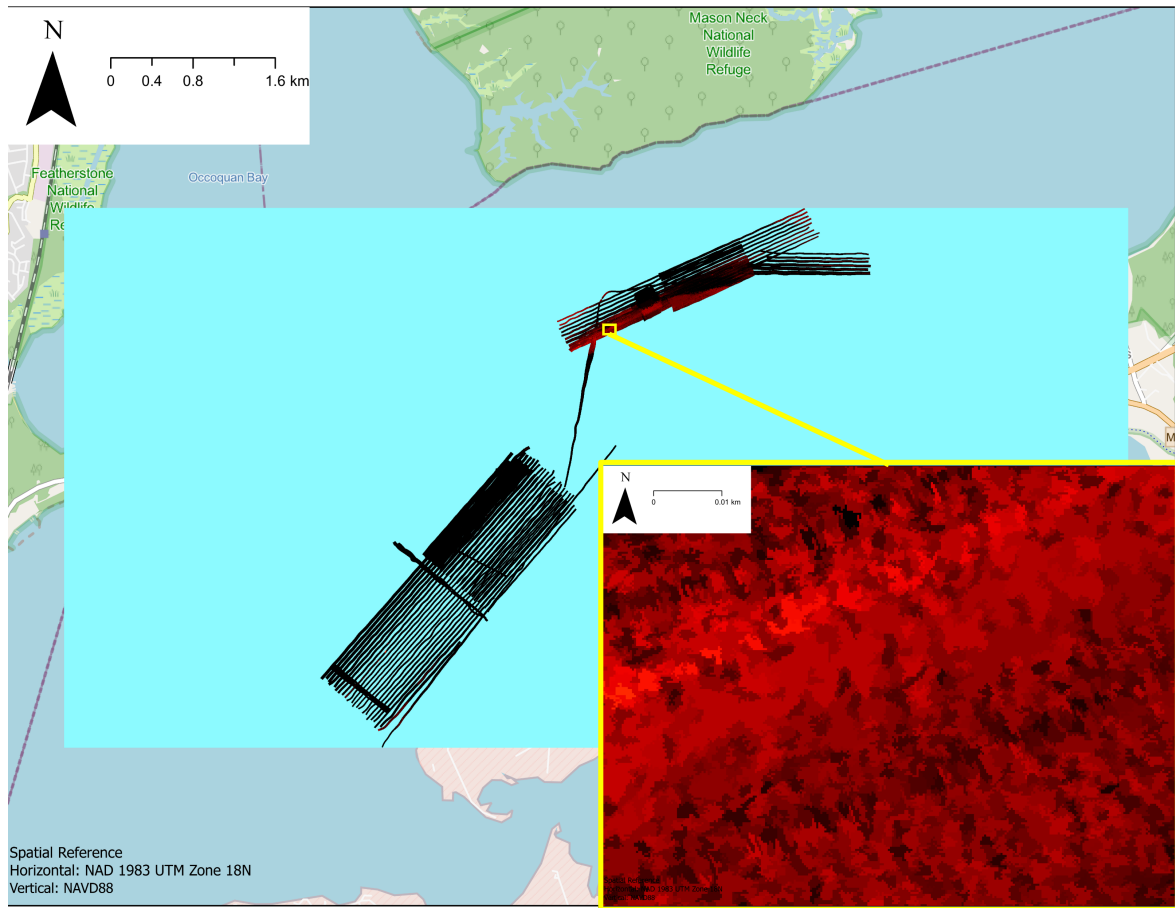


Figure 4.3: Results of segmentation tool. Area with no backscatter value (NaN) is set to cyan.

classified as low bearing capacity. Location of the misclassification are highlighted in figure 4.5. In figure 4.7 confusion matrix of the classifier results are shown along with precision, accuracy, and recall metrics of the final classifier.

When initially dividing the drop penetrometer points into two classes (see figure 3.13), the average QSBC of the 'high' class was 20.4 kPa, whereas the average QSBC of the 'low' class was 14.5 kPa. Comparing that to the results of the classifier (see table 4.1, 'Classifier' column), the average QSBC of drops that were classified as 'high' were 21.8 kPa, and the average QSBC of drops classified as 'low' were 15.4 kPa. Classification errors being from the initially 'high' labelled class to the classifier deeming

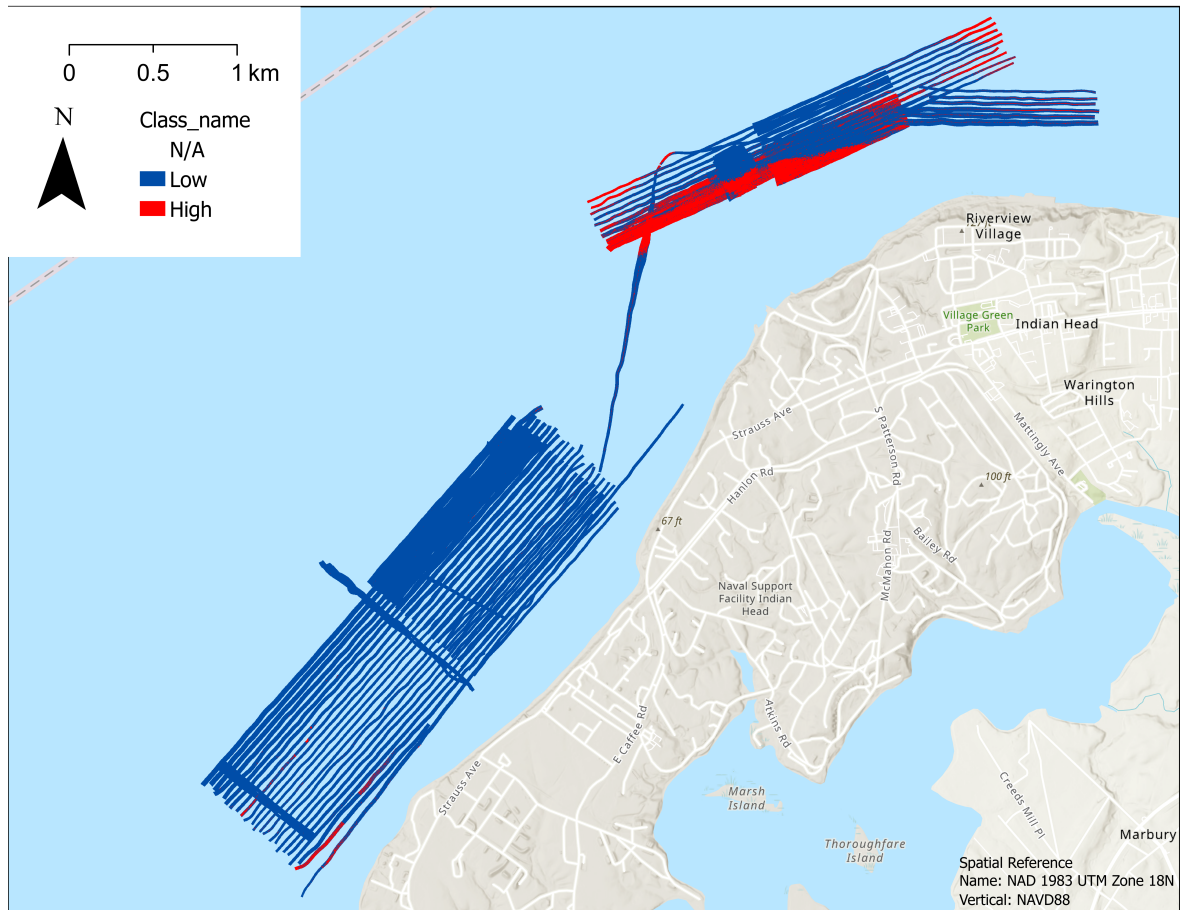


Figure 4.4: Final map product from classification through GIS. Note that NaN class is transparent both in the legend and in the map. Average QSBC for Low: 15.4 kPa, average QSBC for High: 21.8 kPa

those areas 'low' caused this shift in average QSBC of the 'low' class.

Imperfections in the sonar data input can be seen in the classified data, which becomes more noticeable when zoomed in like figure 4.8. In files with no overlap between the lines, the nadir signal is visible as a stripe of 'high' surrounded by 'low'. This effect is nonexistent near the channel where there is adequate overlap and post-processing corrections are more accurately calculated. This highlights the need for high quality data collection, since even with post-processing efforts residual noise from the sonar can show up in the final result.

Drop #	Penetrometer	Classifier
F1	High	Low
F2	High	Low
F3	Low	Low
F4	Low	Low
F5	Low	Low
F6	Low	Low
F7	Low	Low
F8	Low	Low
F9	Low	Low
F10	High	High
F11	High	High
F12	High	Low
F13	Low	Low
F14	Low	Low
F15	Low	Low
F16	High	Low
F17	Low	Low
F18	Low	Low

Table 4.1: Comparison between drop penetrometer results and the final GIS classifier of each drop location. Locations with classification mismatch (all Type I errors) are highlighted in gray.

Comparing the results of the classifier described here to other classifiers, this classifier performed on par with other classifiers. [Lucieer \(2008\)](#) looked at 1 km^2 area 4 km offshore from Perth, Australia to identify reefs. Accuracy of this classifier reported overall accuracy of 0.818 for a two class classification system. [Hamill et al. \(2018\)](#) classified approximately 1 km^2 on the Colorado river using a recreational grade side scan sonar with average precision of 0.66 and average recall of 0.66 with sand/-gravel/boulder classification. The lower precision could be attributed to the lower quality sonar system and the "opportunistic sampling" collection method used. [Qin et al. \(2021\)](#) applied deep learning techniques when training the classifier. Three class (reef/mud/sand wave) classifier was used to train a neural network and achieved 3.5% error rate. While there is sediment textural difference between all the classifiers, the all-mud bearing capacity classifier described in this thesis shows approximately similar

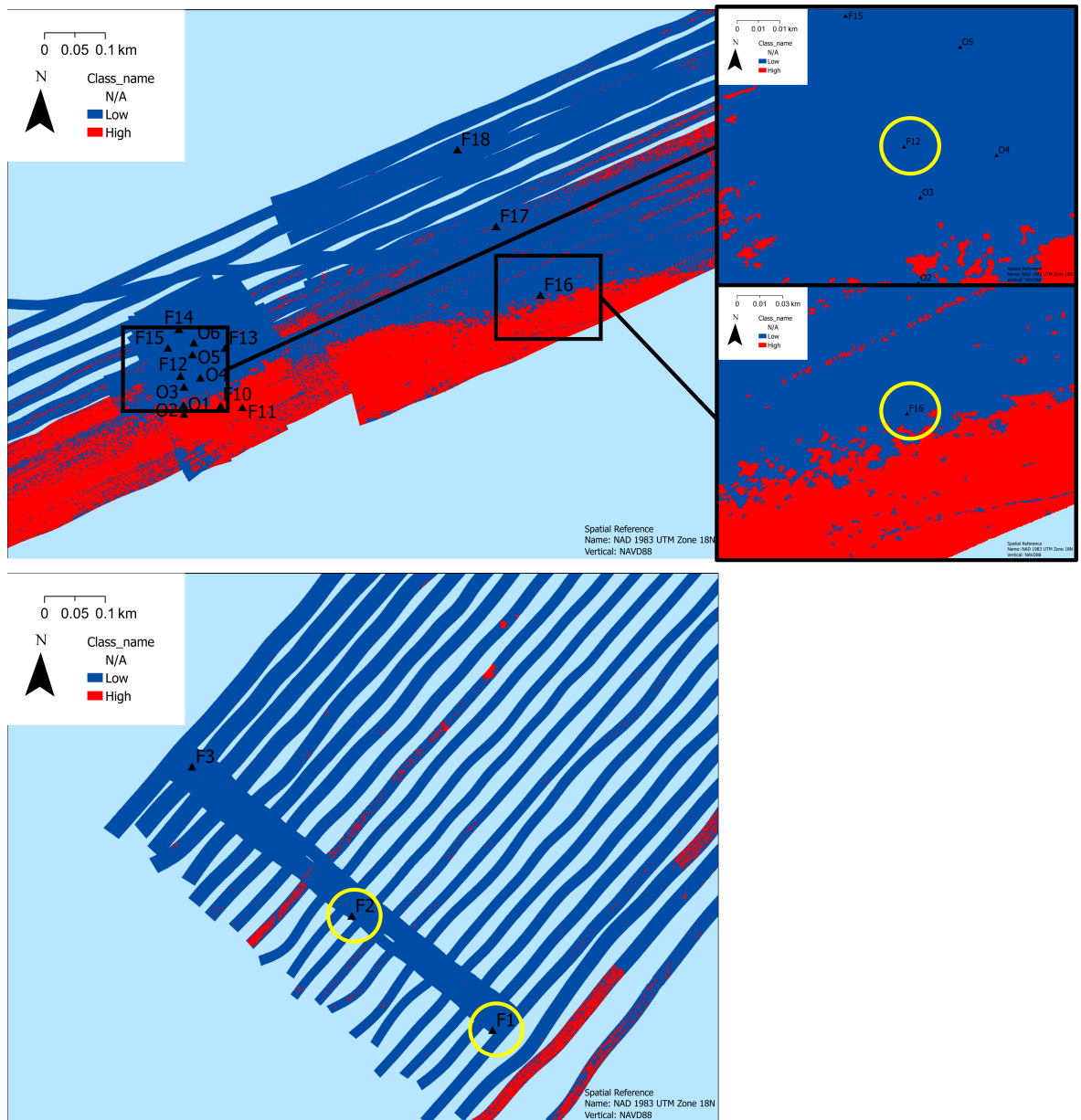


Figure 4.5: Zoomed in images of misclassified points which are circled in yellow.

precision and accuracy (0.75 and 0.78, respectively).

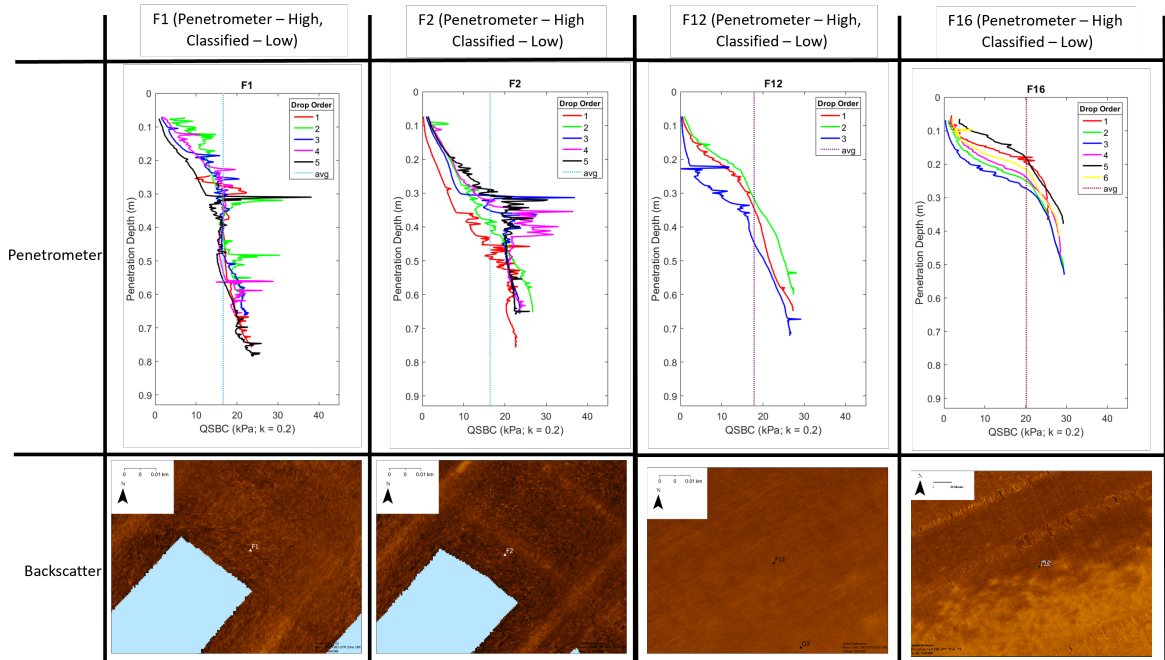


Figure 4.6: Table showing the drop penetrometer profile and sonar backscatter snippet of only the misclassified points.

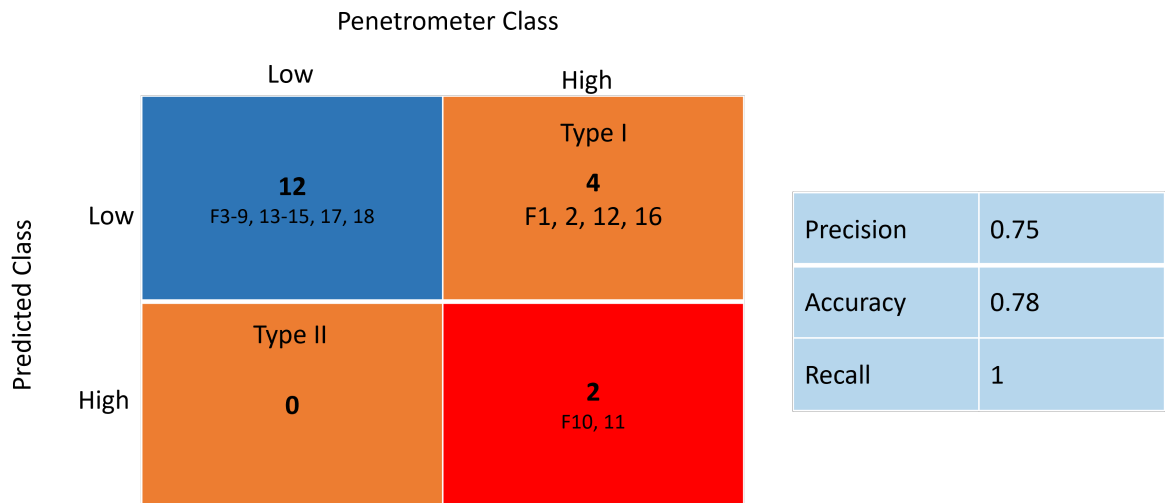


Figure 4.7: Left: Confusion matrix of True class (penetrometer result) and Predicted class (classifier result). 4 out of 18 were misclassified with all errors being Type I. Right: Calculated precision, accuracy, and recall of the classifier.

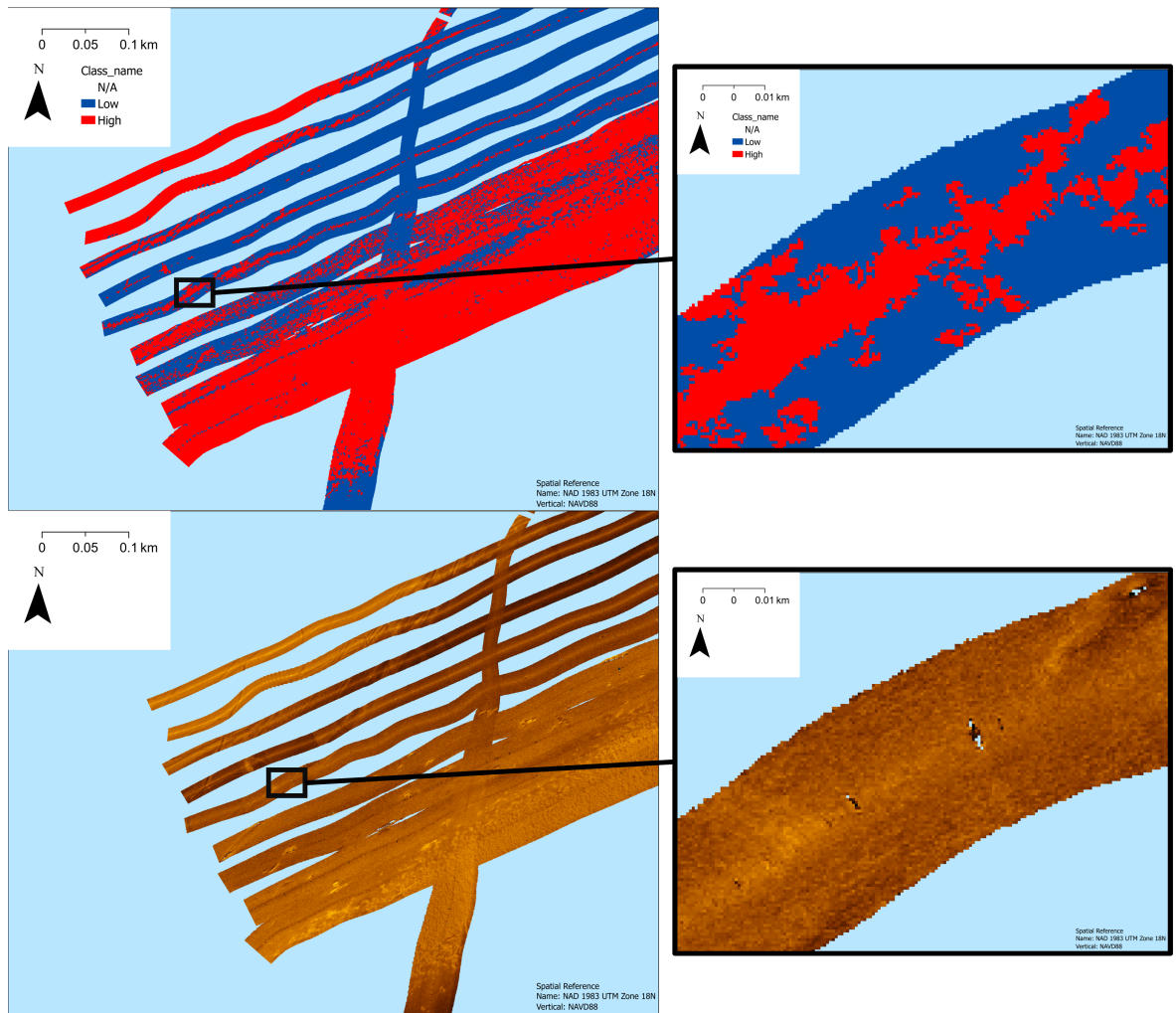


Figure 4.8: Zoomed in image from figures 4.4 and 2.9 which highlights residual nadir effects from the initial sonar data.

Chapter 5

SYNTHESIS AND FUTURE WORK

Surface backscatter can be related to shallow sub-surface properties of the sediment. While it is possible to train a bearing capacity classifier for an area with relatively small difference in backscatter intensity, the quality of the survey must be high to achieve good agreement. With a survey that is not dialed in specifically for backscatter analysis, the classifier cannot perform to its full potential. A good backscatter survey will include getting overlapping coverage so that nadir effects can be removed over the entire survey area, having consistent acquisition settings throughout the survey, and most importantly an equipment calibration day. Backscatter acquisition settings need to be adjusted based on how the collected data looks on the site. Having time built in to calibrate at a new location can optimize collection quality and can also serve as initial scouting for the area.

Looking closer at the classification results, the points that are misclassified tend to be on the transition between the two classes. One way to improve precision would be to do multiple drop penetrometer surveys. For example, the first survey would include getting backscatter coverage and penetrometer drops on the widest range of backscatter intensity. The classifier needs to be trained with the data from the first survey. The second survey should be to address any issues in the backscatter mosaic and to get more penetrometer data in the transition zone to fine tune the classifier specifically in this zone. A histogram of backscatter intensity like figure 2.13 can be used to easily identify the gaps in penetrometer data, and can be used to produce a map of where those data gaps are like figure 2.14 to assist in operation planning.

For UXO management, the application of this classifier can inform management personnel on whether or not the munition will be exposed on the surface. Backscatter and drop penetrometer data from near the managed UXO site should be collected for similar sediment quality and used to train a bearing capacity classifier. The classifier can then be applied to a sonar survey done inside the management zone to minimize contact with the bed therefore reducing risk in data collection. For incorporating the classifier into a UXO mobility prediction model, utilizing a simplified, linear fit profile of QSBC should also be considered. Figures 3.19, 3.20 show good agreement of burial prediction between the simplified and observed profiles.

Concepts and methods described in this thesis could be expanded in various directions. The classification accuracy could be improved. Getting a more dense drop penetrometer coverage and allowing for more even number of training samples between classes could improve accuracy, and analyzing what the most optimal amount of drop penetrometer data would be useful in furthering the method. Applying the classifier to an archived survey data set would be difficult but interesting. In a hydrologically stable area with available survey data, take geophysical samples and attempt to train a classifier. Testing this drop penetrometer retrofit concept in a variety of environmental conditions would be interesting as well and not just in calm environments. The classifier has been developed for UXO burial and mobility models but bearing capacity is important also in other applications such as underwater construction and habitat restoration. Working with an interested party (wind farm, offshore construction, etc) to test out the classifier in a commercial setting could offer insights into where the classifier shines and fails.

Bibliography

- J. T. Anderson, D. Van Holliday, R. Kloser, D. G. Reid, and Y. Simard. Acoustic seabed classification: Current practice and future directions. *ICES Journal of Marine Science*, 65(6):1004–1011, September 2008. ISSN 1095-9289, 1054-3139. doi: 10.1093/icesjms/fsn061.
- S. Blott. GRADISTAT. Kenneth Pye Associates Ltd., 2010.
- C. Brown, J. Beaudoin, M. Brissette, and V. Gazzola. Multispectral Multibeam Echo Sounder Backscatter as a Tool for Improved Seafloor Characterization. *Geosciences*, 9(3):126, March 2019. ISSN 2076-3263. doi: 10.3390/geosciences9030126.
- C. J. Brown and P. Blondel. Developments in the application of multibeam sonar backscatter for seafloor habitat mapping. *Applied Acoustics*, 70(10):1242–1247, October 2009. ISSN 0003682X. doi: 10.1016/j.apacoust.2008.08.004.
- Chesapeake_Technology. SONARWIZ 7.11 User Manual - Time Varying Gain (TVG) Control, 2023.
- A. E. Draut, G. C. Kineke, D. W. Velasco, M. A. Allison, and R. J. Prime. Influence of the Atchafalaya River on recent evolution of the chenier-plain inner continental shelf, northern Gulf of Mexico. *Continental Shelf Research*, 25(1):91–112, January 2005. ISSN 02784343. doi: 10.1016/j.csr.2004.09.002.
- A. Dutkiewicz, R. D. Müller, S. O’Callaghan, and H. Jónasson. Census of seafloor sediments in the world’s ocean. *Geology*, 43(9):795–798, September 2015. ISSN 0091-7613, 1943-2682. doi: 10.1130/G36883.1.

- K. R. Dyer. *Coastal and Estuarine Sediment Dynamics*. JohnWiley & Sons Ltd., Great Britain, 1986. ISBN 0-471-90876-2.
- ESRI. Segmentation—ArcGIS Pro — Documentation. <https://pro.arcgis.com/en/pro-app/3.1/help/analysis/image-analyst/segmentation.htm>, 2023.
- C. Fischenich. Stability Thresholds for Stream Restoration Materials. Technical Note TN-EMRRP-SR-29, ERDC, 2001.
- R. L. Folk. *Petrology of Sedimentary Rocks*. Hemphill Publishing Co., Austin, TX, 1974.
- L. Fonseca and L. Mayer. Remote estimation of surficial seafloor properties through the application Angular Range Analysis to multibeam sonar data. *Marine Geophysical Researches*, 28(2):119–126, July 2007. ISSN 0025-3235, 1573-0581. doi: 10.1007/s11001-007-9019-4.
- L. E. Fonseca, L. A. Mayer, and B. J. Kraft. Seafloor Characterization Through the Application of AVO Analysis to Multibeam Sonar Data. In *University of Bath Boundary Influences in High Frequency Shallow Water Acoustics*, page 11, Bath, UK, September 2005. Center for Coastal and Ocean Mapping.
- X. Guo, Z. Liu, J. Zheng, Q. Luo, and X. Liu. Bearing capacity factors of T-bar from surficial to stable penetration into deep-sea sediments. *Soil Dynamics and Earthquake Engineering*, 165:107671, February 2023. ISSN 02677261. doi: 10.1016/j.soildyn.2022.107671.
- J. R. Gutsche. Spatial Variability and Control on the Distribution of Microbialites: Case Study from Pavillion Lake, British Columbia, Canada. Master’s thesis, University of Delaware, 2011.
- D. Hamill, D. Buscombe, and J. M. Wheaton. Alluvial substrate mapping by automated texture segmentation of recreational-grade side scan sonar imagery. *PLOS*

- ONE*, 13(3):e0194373, March 2018. ISSN 1932-6203. doi: 10.1371/journal.pone.0194373.
- A. Hettler and G. Gudehus. Influence of the foundation width on the bearing capacity factor. *Soils and Foundations*, 28(4):81–92, December 1988. ISSN 0038-0806. doi: 10.3208/sandf1972.28.4_81.
- F. Hjulström. *Studies of the Morphological Activity of Rivers as Illustrated by the River Fyris, Bulletin*. Doctorate Dissertation, The Geological institution of the University of Upsala, Uppsala, 1935.
- S. Hoy and K. Kissinger. Multibeam Calibration: Conducting a Patch Test NOAA Ship Okeanos Explorer, February 2010, 2010.
- J. E. Hughes Clarke, L. A. Mayer, and D. E. Wells. Shallow-water imaging multibeam sonars: A new tool for investigating seafloor processes in the coastal zone and on the continental shelf. *Marine Geophysical Researches*, 18(6):607–629, December 1996. ISSN 0025-3235, 1573-0581. doi: 10.1007/BF00313877.
- Hypack. Patch Testing. <https://slideplayer.com/slide/1596461/>, 2013.
- M. R. Jensen, V. Zania, and B. M. Lehane. The effects of sand grading on the bearing capacity of surface foundations. In *European Conference on Physical Modelling in Geotechnics*, pages 17–24, Luleå, Sweden, 2020.
- B. M. Keller. Imaging the Twilight Zone: The Morphology and Distribution of Mesophotic Zone Features, a Case Study from Bonaire, Dutch Caribbean. Master’s thesis, University of Delaware, 2011.
- R. Leach. Engineering Properties of Wetland Soils, WRP Technical Note SG-RS-1.2, May 1994.
- D. W. Lewis and D. McConchie. *Analytical Sedimentology*. Springer US, Boston, MA, 1994. ISBN 978-1-4613-6131-2. doi: 10.1007/978-1-4615-2636-0.

- V. L. Lucieer. Object-oriented classification of sidescan sonar data for mapping benthic marine habitats. *International Journal of Remote Sensing*, 29(3):905–921, February 2008. ISSN 0143-1161, 1366-5901. doi: 10.1080/01431160701311309.
- X. Lurton, G. Lamarche, C. Brown, V. Lucieer, G. Rice, A. C. G. Schimel, and T. Weber. Backscatter measurements by seafloor-mapping sonars; Guidelines and Recommendations. Technical report, 2015.
- J Marulli and J Mallarach. A GIS methodology for assessing ecological connectivity: Application to the Barcelona Metropolitan Area. *Landscape and Urban Planning*, 71(2-4):243–262, March 2005. ISSN 01692046. doi: 10.1016/S0169-2046(04)00079-9.
- R. J. Mitchell and J. A. Hull. Stability and Bearing Capacity of Bottom Sediments. In *Coastal Engineering 1974*, pages 1252–1273, Copenhagen, Denmark, June 1974. American Society of Civil Engineers. ISBN 978-0-87262-113-8 978-0-7844-7962-9. doi: 10.1061/9780872621138.076.
- NOAA. How does backscatter help us understand the sea floor? <https://oceanservice.noaa.gov/facts/backscatter.html>, October 2023.
- I. M. Parnum, A. N. Gavrilov, and P. J. W. Siwabessy. Analysis of Multibeam Sonar Data for the Purposes of Seafloor Classification. In *Underwater Acoustic Measurements: Technologies & Results, 2nd International Conference and Exhibition*, page 9, June 2007.
- C. A. Pilditch, C. W. Emerson, and J. Grant. Effect of scallop shells and sediment grain size on phytoplankton flux to the bed. *Continental Shelf Research*, 17(15): 1869–1885, December 1997. ISSN 02784343. doi: 10.1016/S0278-4343(97)00050-2.
- J. Plachý, V. Weiss, and L. Bartuška. Problems with Approximate Bearing Capacity of Gravel Soils. *IOP Conference Series: Earth and Environmental Science*, 44:022022, October 2016. ISSN 1755-1307, 1755-1315. doi: 10.1088/1755-1315/44/2/022022.

- X. Qin, X. Luo, Z. Wu, and Jihong Shang. Optimizing the Sediment Classification of Small Side-Scan Sonar Images Based on Deep Learning. *IEEE Access*, 9:29416–29428, 2021. ISSN 2169-3536. doi: 10.1109/ACCESS.2021.3052206.
- N. A. Raineault, A. C. Trembanis, and D. C. Miller. Mapping Benthic Habitats in Delaware Bay and the Coastal Atlantic: Acoustic Techniques Provide Greater Coverage and High Resolution in Complex, Shallow-Water Environments. *Estuaries and Coasts*, 35(2):682–699, March 2011. ISSN 1559-2723, 1559-2731. doi: 10.1007/s12237-011-9457-8.
- C. Sahin, I. Safak, A. Sheremet, and A. J. Mehta. Observations on cohesive bed reworking by waves: Atchafalaya Shelf, Louisiana: Cohesive Bed Reworking by Waves. *Journal of Geophysical Research: Oceans*, 117(C9):n/a–n/a, September 2012. ISSN 01480227. doi: 10.1029/2011JC007821.
- B. B. Salem. Application of GIS to biodiversity monitoring. *Journal of Arid Environments*, 54(1):91–114, May 2003. ISSN 01401963. doi: 10.1006/jare.2001.0887.
- A. C. G. Schimel, J. Beaudoin, I. M. Parnum, T. Le Bas, V. Schmidt, G. Keith, and D. Ierodiaconou. Multibeam sonar backscatter data processing. *Marine Geophysical Research*, 39(1-2):121–137, June 2018. ISSN 0025-3235, 1573-0581. doi: 10.1007/s11001-018-9341-z.
- T. Shields. Clearing the Channel to Alexandria. *The Washington Post*, pages <https://www.washingtonpost.com/archive/local/1999/11/28/clearing-the-channel-to-alexandria/a7ad1beb-960a-4702-9337-c5ff75fc3b03/>, November 1999.
- S. Sonti. Application of Geographic Information System (GIS) in Forest Management. *Journal of Geography & Natural Disasters*, 05(03), 2015. ISSN 21670587. doi: 10.4172/2167-0587.1000145.

- N. Stark, G. Coco, K. R. Bryan, and A. Kopf. In-Situ Geotechnical Characterization of Mixed-Grain-Size Bedforms Using A Dynamic Penetrometer. *Journal of Sedimentary Research*, 82(7):540–544, July 2012. ISSN 1527-1404. doi: 10.2110/jsr.2012.45.
- N. Stark, B. Radosavljevic, B. Quinn, and H. Lantuit. Application of portable free-fall penetrometer for geotechnical investigation of Arctic nearshore zone. *Canadian Geotechnical Journal*, 54(1):31–46, January 2017. ISSN 0008-3674, 1208-6010. doi: 10.1139/cgj-2016-0087.
- M. P. Strager, J. J. Fletcher, J. M. Strager, C. B. Yuill, R. N. Eli, J. T. Petty, and S. J. Lamont. Watershed analysis with GIS: The watershed characterization and modeling system software application. *Computers & Geosciences*, 36(7):970–976, July 2010. ISSN 00983004. doi: 10.1016/j.cageo.2010.01.003.
- W. Thompson, R. Fleming, S. Creem-Regehr, and J. K. Stefanucci. *Visual Perception from a Computer Graphics Perspective*. CRC Press, April 2016. ISBN 978-1-4398-6549-1.
- P. Traykovski and T. Austin. Continuous Monitoring of Mobility, Burial and Re-exposure of Underwater Munitions in Energetic Near-Shore Environments. Final Report, Woods Hole Oceanographic Institute, 266 Woods Hole Road Woods Hole, MA 02543, August 2016.
- A. C. Trembanis and C. DuVal. Unexploded Ordnance Characterization and Detection in Muddy Estuarine Environments. Final MR-2730, University of Delaware, June 2020.
- A. C. Trembanis and C. DuVal. Further Examining the Role of Cohesive Sediments in Munitions Mobility through Additional Infield Deployment of Smart Munitions and Application of a SERDP-developed Penetrometer. Final MR20-1480, University of Delaware, June 2021.

- A. C. Trembanis and J. R. Gutsche. Spatial distribution and characteristics of microbialites through the use of sonar techniques-geoacoustic investigations at Pavilion Lake (Canada). *Atti della Società Toscana di Scienze Naturali Residente in Pisa Memorie*, B(126):47–60, 2019. ISSN 0365-7450. doi: 10.2424/ASTSN.M.2019.04.
- A. C. Trembanis, A. L. Forrest, B. M. Keller, and M. R. Patterson. Mesophotic Coral Ecosystems: A Geoacoustically Derived Proxy for Habitat and Relative Diversity for the Leeward Shelf of Bonaire, Dutch Caribbean. *Frontiers in Marine Science*, 4, March 2017. ISSN 2296-7745. doi: 10.3389/fmars.2017.00051.
- P. J. Valent, R. H. Bennett, and W. A. Dunlap. Dynamic Soil-Structure Interaction Behavior on the Seafloor. Final NORDA Report 227, Naval Ocean Research and Development Activity, Stennis Space Center, Mississippi, August 1988.
- H. Van Rein, C. J. Brown, R. Quinn, J. Breen, and D. Schoeman. An evaluation of acoustic seabed classification techniques for marine biotope monitoring over broad-scales (>1 km²) and meso-scales (10 m²–1 km²). *Estuarine, Coastal and Shelf Science*, 93(4):336–349, July 2011. ISSN 02727714. doi: 10.1016/j.ecss.2011.04.011.
- J. V. Wilson, S. A. Jenkins, J. Wasyl, A. DeVisser, and B. Sugiyama. Predicting the Mobility and Burial of Underwater Unexploded Ordnance (UXO) using the UXO Mobility Model. Field Test Report, PMRF Barking Sands, Kauai, Hawaii, May 2008.
- X. Yang, W. Chen, G. Gartner, L. Meng, and M. P. Peterson, editors. *Remote Sensing and Geospatial Technologies for Coastal Ecosystem Assessment and Management*. Lecture Notes in Geoinformation and Cartography. Springer Berlin Heidelberg, Berlin, Heidelberg, 2009. ISBN 978-3-540-88182-7 978-3-540-88183-4. doi: 10.1007/978-3-540-88183-4.
- X. Yu, J. Zhai, B. Zou, Q. Shao, and G. Hou. A Novel Acoustic Sediment Classification Method Based on the K-Mdoids Algorithm Using Multibeam Echosounder

Backscatter Intensity. *Journal of Marine Science and Engineering*, 9(5):508, May 2021. ISSN 2077-1312. doi: 10.3390/jmse9050508.

R. Zakariya, M. A. Abdullah, R. C. Hasan, and I. Khalil. Automatic classification techniques for type of sediment map from multibeam sonar data. *IOP Conference Series: Earth and Environmental Science*, 117:012047, February 2018. ISSN 1755-1307, 1755-1315. doi: 10.1088/1755-1315/117/1/012047.

P. Zhou, G. Chen, M. Wang, J. Chen, and Y. Li. Sediment Classification of Acoustic Backscatter Image Based on Stacked Denoising Autoencoder and Modified Extreme Learning Machine. *Remote Sensing*, 12(22):3762, November 2020. ISSN 2072-4292. doi: 10.3390/rs12223762.

Appendix A

GEOTECHNICAL ANALYSIS RESULTS

October (Grab)			February (Grab, Penetrometer)			February (Grab, Penetrometer)		
Grab #	Lat	Lon	Grab #	Lat	Lon	Grab #	Lat	Lon
O1	38.6070	-77.1863	F1	38.5713	-77.2139	F10	38.6071	-77.1856
O2	38.6071	-77.1863	F2	38.5729	-77.2166	F11	38.6071	-77.1852
O3	38.6074	-77.1863	F3	38.5750	-77.2197	F12	38.6076	-77.1863
O4	38.6075	-77.1860	F4	38.5861	-77.2080	F13	38.6080	-77.1855
O5	38.6079	-77.1861	F5	38.5834	-77.2010	F14	38.6083	-77.1864
O6	38.6081	-77.1861	F6	38.5920	-77.2004	F15	38.6080	-77.1866
O7	38.5926	-77.2014	F7	38.5922	-77.2003	F16	38.6089	-77.1796
O8	38.5923	-77.2010	F8	38.5926	-77.2011	F17	38.6099	-77.1804
O9	38.5919	-77.2007	F9	38.5924	-77.2011	F18	38.6110	-77.1812

Table A.1: Sampling latitude and longitude for sediment grabs and drop penetrometer. Only grab samples were taken in October, while both grab samples and drop penetrometer data were collected in February.

Drop #	1	2	3	4	5	6	7	8	9	10	11	12	13	14	15	16	17	18
R	97	86	108	96	82	116	119	113	113	205	197	133	127	121	118	125	157	120
G	35	30	40	33	27	44	45	42	43	115	107	54	50	47	45	49	73	47
B	0	0	0	0	0	0	0	0	0	0	0	0	0	0	0	0	0	0
Luminosity	42	28	52	42	42	52	75	52	64	131	112	70	70	65	58	75	76	75

Figure A.1: Average RGB values of a 3 m square around sediment sampling points.

	F1	F2	F3	F4	F5	F6	F7	F8	F9
SAMPLE TYPE	Unimodal, Poorly Sorted								
TEXTURAL GROUP:	Standy Mid								
SEDIMENT NAME:	Very Fine Sand								
METHOD									
MOMENTS	40.74	42.07	40.89	40.73	41.18	39.88	41.14	40.73	41.42
MEAN	26.24	27.12	25.80	25.93	26.22	26.22	27.16	32.21	26.01
SKWENESS	4.688	2.542	3.258	3.241	3.676	6.263	4.249	7.458	4.832
KURTOSIS	119.8	61.91	69.18	82.72	186.49	110.8	110.8	153.2	102.7
MEAN	31.30	30.21	31.20	30.21	31.14	28.76	30.50	29.21	31.85
SORTING	2.215	2.592	2.235	2.428	2.246	2.297	2.217	2.261	2.219
SKWENESS	-1.016	-1.201	-1.033	-1.131	-1.032	-1.141	-1.059	-1.097	-1.045
KURTOSIS	3.87	4.451	3.843	4.711	3.778	4.097	4.061	4.061	3.878
MEAN	4.998	5.049	4.998	5.047	4.991	5.120	5.016	4.972	4.972
SORTING	1.374	1.279	1.160	1.279	1.168	1.226	1.324	1.324	1.150
SKWENESS	1.016	1.304	1.033	1.317	1.032	1.144	1.069	1.065	1.045
KURTOSIS	3.87	4.451	3.843	4.714	3.778	4.097	4.064	4.064	3.878
MEAN	34.23	33.31	34.37	33.87	34.54	31.17	33.36	31.60	34.91
SORTING	2.152	2.440	2.165	2.259	2.170	2.421	2.407	2.407	2.152
SKWENESS	-0.245	-0.354	-0.247	-0.286	-0.263	-0.210	-0.280	-0.213	-0.251
KURTOSIS	1.054	1.096	1.047	1.098	1.040	1.105	1.097	1.097	1.043
MEAN	4.860	4.908	4.862	4.884	4.856	5.004	4.906	4.884	4.840
SKWENESS	1.106	1.287	1.115	1.170	1.121	1.276	1.168	1.267	1.105
KURTOSIS	0.245	0.354	0.247	0.286	0.263	0.210	0.280	0.213	0.251
MEAN	1.051	1.056	1.047	1.068	1.040	1.105	1.066	1.067	1.043
WARD METHOD	Very Coarse Silt								
WARD METHOD	Poorly Sorted								
SKWENESS	Very Fine Skewed								
KURTOSIS	Miscellaneous								
MODE (mm)	76.50	76.50	76.50	76.50	76.50	76.50	76.50	76.50	76.50
MODE (phi)	3.716	3.721	3.721	3.721	3.721	3.721	3.721	3.721	3.721
D10 (mm)	8.080	8.004	8.843	8.826	9.894	9.225	9.242	7.527	10.32
D20 (mm)	36.10	37.88	30.22	36.42	36.79	34.79	36.47	35.34	36.85
D60 (mm)	76.08	78.98	70.51	76.65	76.79	76.44	77.40	76.98	77.06
D80 / D10 (mm)	9.406	9.744	7.967	8.683	8.683	8.532	8.532	8.532	8.532
D80 / D20 (mm)	66.09	70.38	66.61	67.83	66.99	68.91	68.91	69.42	66.73
D75 / D25 (mm)	2.831	3.311	2.882	2.911	2.920	3.088	3.051	3.088	2.873
D75 / D50 (mm)	37.79	45.18	38.53	39.20	38.53	39.47	39.47	39.85	38.92
D10 (phi)	3.716	3.662	3.708	3.705	3.703	3.710	3.692	3.699	3.698
D20 (phi)	4.792	4.722	4.787	4.779	4.765	4.845	4.777	4.823	4.762
D60 (phi)	6.645	6.965	6.667	6.824	6.672	7.051	6.742	7.048	6.598
D80 / D10 (phi)	1.788	1.902	1.798	1.842	1.802	1.902	1.826	1.802	1.784
D80 / D20 (phi)	2.929	3.203	2.950	3.119	2.969	3.344	3.051	3.249	2.900
D75 / D25 (phi)	1.503	1.438	1.374	1.382	1.380	1.397	1.397	1.398	1.374
D75 / D50 (phi)	1.503	1.729	1.527	1.537	1.546	1.627	1.611	1.627	1.523
% GRAVEL	0.0%	0.0%	0.0%	0.0%	0.0%	0.0%	0.0%	0.0%	0.0%
% SAND	21.3%	27.4%	22.0%	22.2%	22.3%	21.5%	23.0%	21.9%	22.5%
% SILT	78.7%	72.6%	78.0%	77.7%	77.7%	78.5%	77.0%	78.1%	77.5%
% V COARSE GRAVEL	0.0%	0.0%	0.0%	0.0%	0.0%	0.0%	0.0%	0.0%	0.0%
% COARSE GRAVEL	0.0%	0.0%	0.0%	0.0%	0.0%	0.0%	0.0%	0.0%	0.0%
% MEDIUM GRAVEL	0.0%	0.0%	0.0%	0.0%	0.0%	0.0%	0.0%	0.0%	0.0%
% FINE GRAVEL	0.0%	0.0%	0.0%	0.0%	0.0%	0.0%	0.0%	0.0%	0.0%
% V FINE GRAVEL	0.0%	0.0%	0.0%	0.0%	0.0%	0.0%	0.0%	0.0%	0.0%
% COARSE SAND	0.0%	0.0%	0.0%	0.0%	0.0%	0.0%	0.0%	0.0%	0.0%
% COARSE SAND	0.0%	0.0%	0.0%	0.0%	0.0%	0.0%	0.0%	0.0%	0.0%
% MEDIUM SAND	0.0%	0.0%	0.0%	0.0%	0.0%	0.0%	0.0%	0.0%	0.0%
% FINE SAND	0.0%	0.0%	0.0%	0.0%	0.0%	0.0%	0.0%	0.0%	0.0%
% V FINE SAND	21.2%	27.3%	21.9%	22.2%	22.2%	21.4%	22.9%	21.9%	22.4%
% V COARSE SILT	35.6%	30.7%	32.1%	34.9%	35.4%	34.9%	34.1%	33.5%	35.4%
% COARSE SILT	27.9%	24.1%	27.7%	26.6%	26.8%	26.7%	26.9%	26.3%	27.7%
% MEDIUM SILT	8.0%	8.0%	7.8%	7.4%	7.8%	8.0%	7.9%	8.0%	7.9%
% FINE SILT	4.8%	4.8%	4.8%	4.9%	4.8%	5.4%	5.0%	5.0%	4.7%
% V FINE SILT	2.7%	2.4%	2.4%	2.1%	2.7%	3.5%	2.1%	3.5%	2.5%
% CLAY	0.0%	2.3%	1.8%	1.8%	0.0%	1.3%	0.6%	1.2%	0.6%

Table A.3: Grain size analysis results from February (F1 - F9).

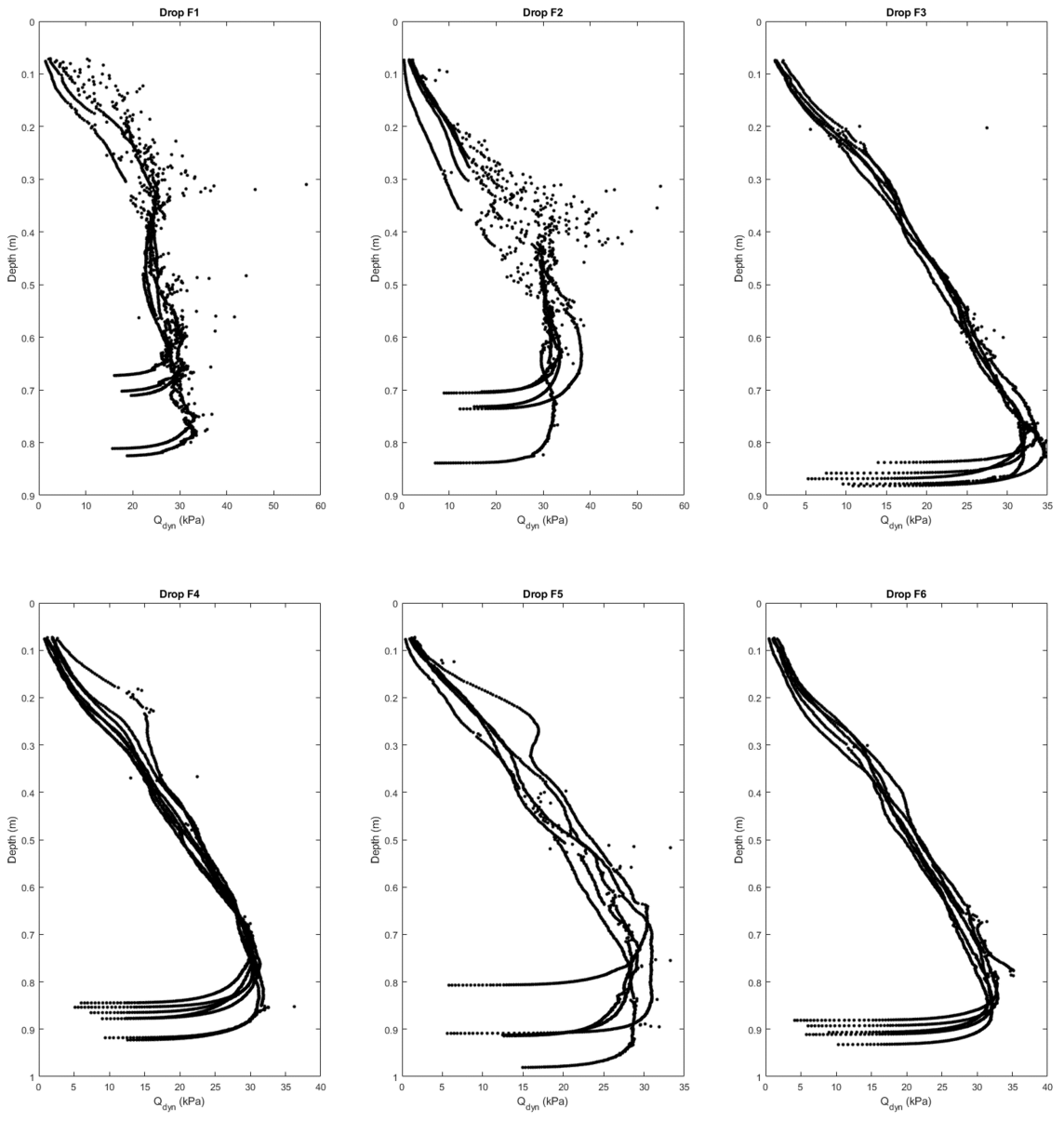


Figure A.2: Penetrometer results F1 - F6.

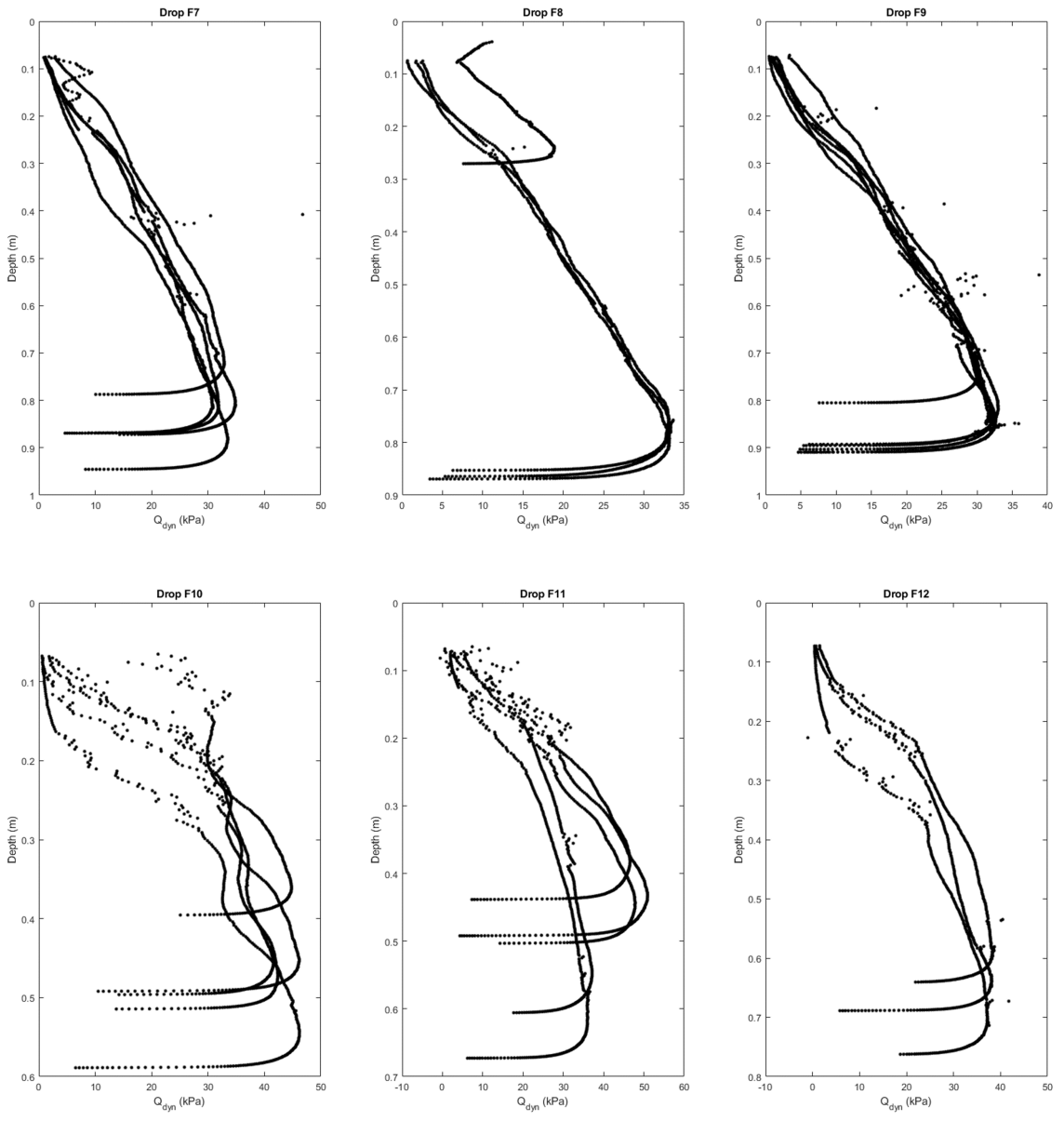


Figure A.3: Penetrometer results F7 - F12.

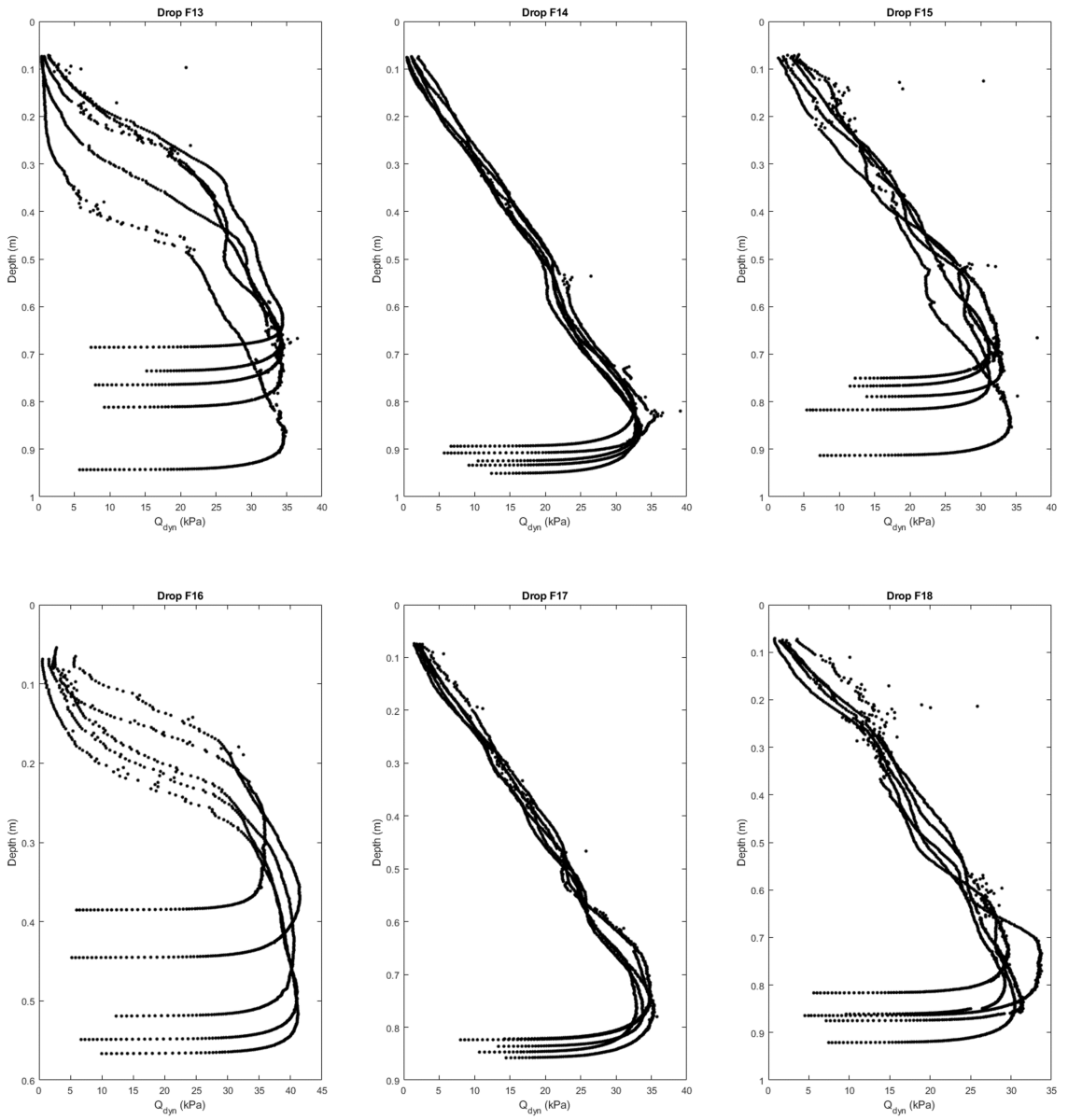


Figure A.4: Penetrometer results F13 - F18.

	Slope	Intercept	R2	Penetrometer class
F1	0.0319	-0.0783	0.71	High
F2	0.0202	0.0902	0.78	High
F3	0.0330	0.0173	0.98	Low
F4	0.0331	0.0293	0.97	Low
F5	0.0345	0.0259	0.93	Low
F6	0.0327	0.0519	0.98	Low
F7	0.0319	0.0308	0.93	Low
F8	0.0315	0.0286	0.99	Low
F9	0.0328	0.0412	0.98	Low
F10	0.0123	0.0322	0.73	High
F11	0.0121	0.0749	0.55	High
F12	0.0195	0.0686	0.87	High
F13	0.0234	0.0972	0.81	Low
F14	0.0335	0.0638	0.99	Low
F15	0.0311	0.0072	0.95	Low
F16	0.0119	0.0499	0.80	High
F17	0.0292	0.0420	0.99	Low
F18	0.0355	0.0003	0.96	Low

Table A.5: Slope and intercept value for the simplified QSBC profile in each location.

Appendix B

DETAILED ANALYSIS STEPS

Sonar Backscatter Processing

1. Raw Data Import:

For Norbit import

- a. Locate all the .s7k files and the CTD sound profile files. In the Import Data menu, choose bathymetry import. Look through file specific options and check that all options look correct. Load in the .s7ks into SonarWiz.
- b. Before any corrections, look through the files and check that the acquisition and project coordinate systems are the same (look at the files with a basemap, confirm general location and depth looks logical).
- c. For files that were bad recordings (mis-click while collecting, mid-line restart, turns, etc.), delete at this stage. Do not waste computing resources on correcting bad files.
- d. Open the SVP import wizard. The SVP wizard is not the most intuitive tool to use and you must import and save the SVP files one at a time.
- e. Open one of the SVP files. Visually confirm that the SVP looks reasonable. Manually input file time and lat/lon which you should be able to get from the CTD itself. This information for some reason is not automatically exported.
- f. Once it looks right, click save. Now the file is saved in a format that SonarWiz will accept. To open the next file, DO NOT PRESS OPEN. YOU MUST CLICK NEW. Repeat the import steps for every SVP file you

have.

- g. The SVPs and bathy line files should show up in your main workspace.

For SSS import

- a. Download all side scan files from the Iver3 internal computer.
- b. In the import menu, choose side scan and look through file specific options for settings. Usually for SSS files you need to select what channels you are importing. For high frequency side scan, channels 1 and 2 are used.
- c. Check coordinate systems and make sure it's all correct.
- d. Delete any turn lines, but you shouldn't have incorrect files if you set the mission up correctly.
- e. You should see the imported files in your main workspace.
- f. The files should be automatically bottom tracked during import. Look through the files in a digitizer view, and manually re-bottom track if there are any fish or large objects in the water column that's disrupting the bottom track.

2. Bathymetry Corrections:

- a. Under the Bathymetry tab, click on Tide + SV manager. Depending on whether time or location had more impact on your sound velocity, choose Closest time or Closest location for auto SV. Change ray trace method to profile. For the Norbit sonar with the Portus pole tide corrections are not needed. Merge.
- b. Under the Bathymetry tab, click on the Patch Test tool. Latency does not need to be patched in most modern MBES systems.
- c. Refer to figure [2.5](#) for which patch test lines to select.
- d. Isolate your roll test lines. Select to patch for Roll. Do an auto correct, with 0.5 step size. You should be seeing a nice U shaped graph (or V). The line should be at the lowest point of the U. The auto correct should give you

a good ballpark value. Change your step size to 0.01 and manually adjust until the two lines feel the best matched. Merge.

e. Repeat c & d for pitch and heading patch lines.

f. You now should have bathymetry that is mostly smooth, without harsh lines where different beams meet. If your data acquisition was horrible, there's not much you can do at this point.

3. Backscatter Corrections:

For Norbit backscatter

a. The bathy adjustments should already be done at this stage for Norbit s7k files. Select a file and right click. Choose 'process backscatter'.

b. Select all the s7k files that you want backscatter for. Click next.

c. Adjust any settings you want to adjust. EGN should be yes, and the EGN table should be built with just the Norbit files. Nadir filter can be yes if there is a strong nadir effect you want to get rid of. AGC should be no. Destripe can be yes if there were a lot of striping in your data due to waves or poor steering. Static gain at this stage should be turned off, it will be adjusted when you intensity match. d. Click finish. The Norbit files should now show up in the sidescan files tab.

For SSS backscatter

a. Import the files as Sidescan files.

b. Select one of the Iver files and open sonar file manager. Select gain settings.

c. Enable EGN, rebuild EGN table. Select all Iver files and calculate a new EGN table, name it something different from the Norbit EGN table.

d. Apply and close. Back in the sonar file manager, select the file you just applied the new Iver EGN table. Click make like selected.

e. In the SSS only section, toggle on EGN. In files to modify, select all Iver files you want the EGN applied to. Click OK to apply the EGN to all Iver

files.

4. Intensity Match

- a. Determine which you want your standard backscatter intensity to be, Norbit or Iver. In this study Iver was set as the standard to match to.
- b. Select any valid Norbit survey lines in the sonar file manager. Open gain settings.
- c. EGN should be turned on from backscatter corrections step. Enable UGC. I prefer editing in TVG mode so turn that toggle on.
- d. All the editing is done in the equation below the two graphs. Only change the last value in the equation, that will change the intensity of all points without changing the logarithmic curve that's been set by the EGN.
- e. Try out different values until it looks like a good match between the two.
- f. For the exports, you will need one with a transparent background for overlaying on other maps and another with a solid color background to easily do classification with. For the solid color background, choose something like green or solid blue to have an easier time classifying.

Grain Size Analysis

1. Sub-Sampling:

- a. Wash and dry overnight the needed number of 500ml wide mouth mason jars.
- b. Pre-label the jars with the grab number. It is up to you to come up with a comprehensive labelling system. It is a good idea to label all the glassware you are using.
- c. Weigh the empty (but labeled) jar. Write it down on an excel sheet.
- d. Tare the scale. Put the 30 g of sediment in the jar. I typically aim for between 25.000g to 25.010g, as close as you can get to 25.000 g. If it's really

annoying more is better than less. Write down the sediment weight on the excel sheet.

e. Repeat steps c and d until you have measured out all the grab samples you have. Make sure and double count that your total number of jars equals the number of samples you got from the field.

2. Sample Preparation for Wet Sieving:

a. Familiarize yourself with all the safety equipment. This is the hazardous part of your analysis.

b. UNDER THE FUME HOOD: Pour hydrogen peroxide into the 500 ml beaker. Take care not to splash any on yourself or in the lab area.

c. Pour a SMALL AMOUNT of hydrogen peroxide in the beaker into the sample mason jar. By small I mean a dollop at most. If you are heavy handed in pouring at this stage, the samples will bubble up and overflow (this means a re-do of that sample and any that are contaminated by the overflow).

d. Swirl the mason jar around to mix in the hydrogen peroxide. You will start to notice bubbles forming. Once all the jars are swirled, close the fume hood.

e. Wait until most of the hydrogen peroxide has reacted. You might notice smoke coming from the beakers. This is normal. Keep an eye out for any bubbles that climb too high up on the mason jar – if you do notice a jar that's looking too close to overflowing, take a clean silicone spatula and mix the sample to pop the bubbles.

f. Add a little more hydrogen peroxide once you cannot see more bubbles forming in the jars.

g. Continue adding hydrogen peroxide to the samples. You will notice that the hydrogen peroxide will leave water in the jar as it reacts with organic matter. This will eventually dilute the hydrogen peroxide if it's left in the

jar. Put the jars in the oven as needed to expedite evaporation, but you CANNOT let it dry out completely in the oven. You have mud samples, and baked mud is a brick. MONITOR THE WATER LEVEL IN THE JARS.

h. At some point you will notice that the stickiness of the bubbles is gone, and while there are still bubbles coming up, they do not form large bubbles at the top. You can now increase the amount of hydrogen peroxide added at each step to a hefty splash.

i. Repeat adding hydrogen peroxide and evaporating the water until there is no more reaction when hydrogen peroxide is added (no bubbling).

3. Wet Sieving:

a. Set up your sieve, funnel, and cylinder like figure 3.5 (right).

b. Label a cylinder and a large beaker with the sample name

c. Fill up the sample jar halfway with DI water

d. Close the sample jar, and shake vigorously. There should be no sediment stuck to the bottom of the jar. Some may be baked onto the side of the jar since hydrogen peroxide produces enough heat to bake mud. You can ignore this side-bake, it's impossible to get off.

e. Dump the contents of the sample jar into the sieve.

f. Rinse the empty jar and the lid with DI water from the squirt bottle into the sieve. Rinse until the water is completely clear coming out from the jar.

g. Using the squirt bottle, rinse the sediment in the sieve. Move the sieve around if you need to, but MAKE SURE TO CATCH ALL THE WATER WITH THE FUNNEL. Keep rinsing until the water coming from the bottom of the sieve runs clear.

h. Rinse the bottom of the sieve (don't turn it over, just lift and squirt) into the funnel. Set sieve on a table. Rinse the funnel as well. You should not exceed 980ml in total rinse water.

i. What's left on the sieve is your sand fraction, and what's in the cylinder

is your mud fraction.

- j. Remove the cylinder and place the beaker under the funnel.
- k. Place the sieve upside down in the funnel and rinse the sand on the sieve into the beaker. Amount of water used is not important here, as long as the beaker does not overflow.
- l. Repeat for any number of samples you would like to analyze.

4. Dry Sieving:

- a. Put the beaker with sand and water into the oven overnight until fully dry.
- b. Next day, take the beaker out of the oven and place it in the desiccator dome until fully cooled.
- c. Prepare the RO-TAP. For typical mud, you won't need anything above #18 sieve, so I usually set it up with 18 (half height), 25, 35, 45, 60, 80, 120 (half height), 230, and pan (units: μm).
- d. Take one of the sand beakers out of the desiccator and get all the sand into the top sieve. Use a brush if you need to, but make sure to smack the brush into the sieve to get all the particles out from the brush.
- e. Put the stack lid (silver and thin) on. Put the RO-TAP lid (black, thick, and has a cork piece on top) on top of the stack lid.
- f. Set the timer for 13 minutes. The buttons are pretty intuitive, and you can't mess it up so be brave and push all the buttons if you want to.
- g. Put on hearing protection and press start.
- h. While that's sieving, prepare your measuring station. You will need a piece of parchment paper or waxed paper larger than the sieves, 9 small tins with each sieve size labels on them (including pan), and the grain size analysis report paper with the sample name on it.
- i. Work from the top sieve down. Carefully upend the sieve onto the parchment paper and smack the sieve a couple times to get all the sand

out. Weigh your tin. Write down the tin weight on the report. Pour the sand grains on the parchment paper into the tin. DO NOT SPILL ANY GRAINS OUTSIDE THE TIN. Write down the total tin + sediment weight onto the paper.

j. Repeat process until you weighed out everything, including the pan dust.

k. Pour the pan dust into the mud cylinder since it passed through the 63 μm sieve.

5. Pipetting Preparation:

a. You will start with 4 cylinders with varying volumes of muddy water in it (under 980 ml!).

b. Pour DI water into the cylinder until it's somewhat close to 980 ml, but not exceeding it.

c. Weigh out exactly 1.000 g of $(\text{NaPO}_3)_6$ onto a small piece of wax paper. Pour it all into a 1000ml volumetric flask. Add DI water into it exactly to the 1000ml mark. Mix until completely dissolved. This is your deflocculant. You will re-make this solution for every set of 4. For example, DO NOT use day 1's solution in day 2's solution. Every sample should only use a single solution.

d. With the 20 ml pipette, pipette in 20 ml of deflocculant into each of the cylinders.

e. Top up the cylinders with DI water squirt bottle to exactly the 1000ml mark.

f. Prepare the 50ml beakers, lining them up in order on the workspace. They should be marked with a set number and water draw time (20s, 2m, 4m, 8m, 15m, 30m, 2h, 8h, 32h).

g. On the analysis worksheet, write down the sample number and the beaker set number. Weigh each beaker and write it down.

h. Fill a 500ml beaker with DI water and set it to the side. This is your pipette rinse beaker. Change the water as often as you think is necessary.

6. Pipetting:

a. Take the turbulence rod (metal plate at the bottom of a rod with holes in it to produce turbulence) and mix the first cylinder vigorously for 2 minutes. Do not splash any out or get air bubbles in.

b. Start a timer at the end of the 2 minutes. Rinse the turbulence rod with DI water into the cylinder.

c. Take the 20ml pipette and insert until the 20cm mark into the water. The top sharpie mark should sit right at the water surface.

d. Once the timer hits 20s, take a 20ml sample. Pipette into the prepared 50ml beaker.

e. Quickly rinse the inside of the pipette of any remaining grains of mud using the pipette rinse beaker into the same 50ml beaker. You will not have enough time to add deflocculant into this beaker, so set the 20s beaker aside after the pipette rinse.

f. Between 4m and 8m you should have enough time to add deflocculant into all the previous samples. Pipette 20ml of the prepared deflocculant into each 50ml beaker.

g. Repeat steps c - f for 2m, 4m, 8m, and 15m samples. Pipetting timing for multiple samples are shown in table [B.1](#).

h. For 30m to 32h, you will be pipetting at 10cm depth instead of 20cm. This is the bottom mark on the 20ml pipette. The processing steps are otherwise the same.

i. Place 50ml beakers with the sample and deflocculant into the oven to dry overnight.

j. Once completely dry, place samples in the desiccator dome to cool down. Weigh and record total weight to the analysis worksheet.

Time	Sample	action	Time	Sample	action	Time	Sample	action
0:00	1	shake	0:00	1	shake	0:00	1	shake
0:00	1	start	0:00	1	start	0:00	1	start
0:00:20	1	20 second	0:00:20	1	20 second	0:00:20	1	20 second
0:02	1	2 minute	0:02	1	2 minute	0:02	1	2 minute
0:04	1	4 minute	0:04	1	4 minute	0:04	1	4 minute
0:08	1	8 minute	0:08	1	8 minute	0:08	1	8 minute
0:15	1	15 minute	0:15	1	15 minute	0:15	1	15 minute
0:30	1	30 minute	0:30	1	30 minute	0:30	1	30 minute
0:33	2	shake	0:33	2	shake	0:33	2	shake
0:35	2	start	0:35	2	start	0:35	2	start
0:35:20	2	20 second	0:35:20	2	20 second	0:35:20	2	20 second
0:37	2	2 minute	0:37	2	2 minute	0:37	2	2 minute
0:39	2	4 minute	0:39	2	4 minute	0:39	2	4 minute
0:43	2	8 minute	0:43	2	8 minute	0:43	2	8 minute
0:50	2	15 minute	0:50	2	15 minute	0:50	2	15 minute
1:05	2	30 minute	1:05	2	30 minute	1:05	2	30 minute
1:08	3	shake	1:08	3	shake	2:00	1	2 hour
1:10	3	start	1:10	3	start	2:35	2	2 hour
1:10:20	3	20 second	1:10:20	3	20 second	8:00	1	8 hour
1:12	3	2 minute	1:12	3	2 minute	8:35	2	8 hour
1:14	3	4 minute	1:14	3	4 minute	32:00:00	1	32 hour
1:18	3	8 minute	1:18	3	8 minute	32:35:00	2	32 hour
1:25	3	15 minute	1:25	3	15 minute			
1:40	3	30 minute	1:40	3	30 minute			
1:48	4	shake	2:00	1	2 hour			
1:50	4	start	2:35	2	2 hour			
1:50:20	4	20 second	3:10	3	2 hour			
1:52	4	2 minute	8:00	1	8 hour			
1:54	4	4 minute	8:35	2	8 hour			
1:58	4	8 minute	9:10	3	8 hour			
2:00	1	2 hour	32:00:00	1	32 hour			
2:05	4	15 minute	32:35:00	2	32 hour			
2:20	4	30 minute	33:10:00	3	32 hour			
2:35	2	2 hour						
3:10	3	2 hour						
3:50	4	2 hour						
8:00	1	8 hour						
8:35	2	8 hour						
9:10	3	8 hour						
9:50	4	8 hour						
32:00:00	1	32 hour						
32:35:00	2	32 hour						
33:10:00	3	32 hour						
33:50:00	4	32 hour						

Table B.1: Pipetting timing for multiple sample analysis. Left: 4 samples at once. Middle: 3 samples at once. Right: 2 samples at once.

ArcGIS Classification Wizard

- a. Load in the GeoTiff with the distinct background color from SonarWiz.
- b. While the GeoTiff is selected and active, go to the imagery tab. Click classification wizard. If the GeoTiff is not active, the classification wizard will be grayed out.
- c. Configure the wizard to your liking. The settings used in this study is specified in chapter 4, sediment classification.
- d. Click the arrow next to the file button in classification schema. If you don't have a premade classification schema, click default schema. You will be able to edit the schema in the third step of the wizard.
- e. Ignore the optional settings and click next.
- f. Choose your desired spectral and spatial detail. More information on what the two numbers mean is given in chapter 4. Click next.
- g. You will most likely need to set up your own classes in the schema and put in the training samples. Delete all classification segments given in NLCD2011 (the default) and add new classes that fit your needs. Save the schema under a comprehensible name.
- h. Click on the class you want. The shapes above the classes should be activated now. Choose point. Toggle on your point notes on where the geotechnical sampling was done. With that reference in place, place the training sample points as exactly as you can.
- i. Place a good amount of NaN points in the background color area. It should be about the same number of training points as your other classes. This allows you to make the background transparent in the export steps.
- j. Click next. Choose support vector machine for the classifier, and for segment attributes choose color, mean digital number, and standard deviation. Toggling on the standard deviation allows for more 'natural' classification results. This is also where you can experiment to get desired results.

k. Click run and review results. Repeat steps if needed.

Appendix C
MATLAB CODES

1. BlueDrop to CSV - by Dr. Carter DuVal

```
function getBlueDropDataCSV
```

```
% Function to import data from blueDrop portable free-fall penetrometer.  
% Opens data from .mat provided by Nina Stark's group at Virginia Tech.  
% Writes all variables from .mat into a struct.
```

```
%INPUT
```

```
% GUI input to select files .
```

```
%
```

```
%OUTPUT
```

```
% Automatically saves .mat file of imported .csv file
```

```
%
```

```
%Carter DuVal, 2023
```

```
%Naval Research Laboratory
```

```
%Stennis Space Center, MS
```

```
%Carter.DuVal@nrlssc.navy.mil
```

```
%
```

```
%%%%%%%%%%%%%%%%%%%%%%%%%%%%%%%%%%%%%%%%%%%%%%%%%%%%%%%%%
```

```

%GUI to select files
[filename, ~] = uigetfile ('*.csv ',' Select the .CSV files ',...
    'MultiSelect', 'on');

if ischar(filename)
    filename = cellstr(filename);
end

for fileidx = 1:numel(filename)
    disp([' Now reading file ',filename{fileidx}]); %display file name
    BlueDropOut = readtable(filename{fileidx});
    drop = ['D' extractBefore(filename{fileidx}, '.') ]; %grab drop name

    eval(['drop '=BlueDropOut;']);

    %Saves in local directory — this can be altered as necessary.
    save(['drop '.mat'], drop);

    clear BlueDropOut drop
end

```

2. Data parsing and cleanup - by Sun Woo Park

```

%% Preamble
%Code for cleaning up QSBC data produced from
%getBlueDropDataCSV. Written for author's Master's thesis work — May be
%rough

%2023.07.17 by Sun Woo Park (swpark037@gmail.com)
%University of Delaware

```

```

clear all; close all; clc

%% Read in Log file
%Read in log data with drop site name, lat, lon, and file path to each .mat
%file. It helps to make this log file before starting analysis. I'm sure
%there's more efficient ways to do this but the file names are not
%sequential so I'd rather do the manual labor of setting up the log file .

bluedrop_log = readtable("C:\Users\swpar\Desktop\UD\Thesis\
    RAMBLE_20230227_penetrometer\drop_location_filepath.xlsx");

% %% Remove bad drops
% %these were found manually, but you should look at your qdyn max values
% to figure out which files have bad drops in them. Bad drops give you 10^6
% qdyn max numbers and that's just wrong.

% D0F7D(506:end,:) = [];
% D0F07(984:end,:) = [];
% D0F24(1023:end,:) = [];
% D0F31(506:end,:) = [];
% D0F53(443:end,:) = [];
% D0F1B(541:end,:) = [];
% D0F48(1:100,:) = [];
% D0F51(415:end,:) = [];

%% Load in .mat files
%Using the loaded log file, bring in the .mat files with raw data.

```

```
%because bluedrop_log is a table, you need to use curly brackets to read
%things as a cell and transform the cell into characters for matlab to
%read.
```

```
names = bluedrop_log{:,1};
```

```
for index = 1 : length(names)
```

```
    raw.one.(names{index}) = load(char(bluedrop_log{index,4}));
```

```
    raw.two.(names{index}) = load(char(bluedrop_log{index,5}));
```

```
    if isempty(char(bluedrop_log{index,6})) == 0 %checking if there's a third file .
```

```
        raw.three.(names{index}) = load(char(bluedrop_log{index,6}));
```

```
        F{index} = [raw.one.(names{index}).(char(fieldnames(raw.one.(names{
            index}))))); raw.two.(names{index}).(char(fieldnames(raw.two.(names{
            index}))))); raw.three.(names{index}).(char(fieldnames(raw.three.(names
            {index})))));
```

```
    else
```

```
        raw.three.(names{index}) = NaN;
```

```
        F{index} = [raw.one.(names{index}).(char(fieldnames(raw.one.(names{index}
            }))))); raw.two.(names{index}).(char(fieldnames(raw.two.(names{index}
            ))));
```

```
    end %Now all the data should be vertically stacked by location (for me, F1
        to F18).
```

```
% Extracting the values I want from the F struture and saving it in a double
    array format; It's easier for me
```

```

% to plot and use if they are in this form.
depth.(names{index}) = table2array(F{index}(:,12));
qsbc_0_2.(names{index}) = table2array(F{index}(:,14));
qsbc_0_4.(names{index}) = table2array(F{index}(:,15));
qsbc_1_0.(names{index}) = table2array(F{index}(:,16));
qsbc_1_5.(names{index}) = table2array(F{index}(:,17));
qdyn.(names{index}) = table2array(F{index}(:,18));

end

%% Export
% Just so that I am not wasting computing resources re-computing the for
% loop. Continue on to BlueDrop_plot.m with these files.

save('swp_penetrometer_depth.mat', 'depth')
save('swp_qsbc_0_2.mat', 'qsbc_0_2')
save('swp_qsbc_0_4.mat', 'qsbc_0_4')
save('swp_qsbc_1_0.mat', 'qsbc_1_0')
save('swp_qsbc_1_5.mat', 'qsbc_1_5')
save('swp_qdyn.mat', 'qdyn')

```

3. Plotting Data - by Sun Woo Park

```

%% Preamble
%For penetrometer data plotting needs
%This code is the third part in a series of codes to analyze Blue Drop data
%getBlueDropDataCSV.m – BlueDrop_cleanup.m – BlueDrop_plot.m

```

```
%Written for author's Master's thesis work – Rough code to get things done
%and not much more
```

```
%2023.07.17 by Sun Woo Park (swpark037@gmail.com)
%University of Delaware
```

```
clear all; close all; clc
```

```
%% Read in XML files
```

```
%These are the exported files from BlueDrop_cleanup.m
```

```
load('C:\Users\swpar\Desktop\UD\Thesis\RAMBLE_20230227_penetrometer\
    Processed4Plots\swp_penetrometer_depth.mat');
```

```
load('C:\Users\swpar\Desktop\UD\Thesis\RAMBLE_20230227_penetrometer\
    Processed4Plots\swp_qsbc_0.2.mat');
```

```
load('C:\Users\swpar\Desktop\UD\Thesis\RAMBLE_20230227_penetrometer\
    Processed4Plots\swp_qsbc_0.4.mat');
```

```
load('C:\Users\swpar\Desktop\UD\Thesis\RAMBLE_20230227_penetrometer\
    Processed4Plots\swp_qsbc_1.0.mat');
```

```
load('C:\Users\swpar\Desktop\UD\Thesis\RAMBLE_20230227_penetrometer\
    Processed4Plots\swp_qsbc_1.5.mat');
```

```
load('C:\Users\swpar\Desktop\UD\Thesis\RAMBLE_20230227_penetrometer\
    Processed4Plots\swp_qdyn.mat');
```

```
%% Read other data
```

```
grainsize = xlsread('C:\Users\swpar\Desktop\Grainsize_Analysis\
    RAMBLE_FEB_analysis_v1.xlsx');
```

```

d50_microns = grainsize(32,:);
d50_phi = grainsize(39,:);
sand_percent = grainsize(46,:);
mud_percent = grainsize(47,:);

%% Separate out specific data from each location

for ind = 1:18

    max_depth(ind) = max(depth.(subsref(fieldnames(depth),substruct('{}',{ind}))))
        ; %getting max penetration depth at each location
    max_qdyn(ind) = max(qdyn.(subsref(fieldnames(qdyn),substruct('{}',{ind})))));
        %getting max qdyn values at each location, bad drops were already removed.

    % To get an average qdyn, you can't have any NaN values in the matrix.
    rmnan_qdyn.(subsref(fieldnames(depth),substruct('{}',{ind}))) (:,1) = depth.(
        subsref(fieldnames(depth),substruct('{}',{ind})));
    rmnan_qdyn.(subsref(fieldnames(depth),substruct('{}',{ind}))) (:,2) = qdyn.(
        subsref(fieldnames(depth),substruct('{}',{ind}))); %make a new matrix to
        mess around with
    [rows, columns] = find(isnan(rmnan_qdyn.(subsref(fieldnames(depth),substruct
       ('{}',{ind}))))); %find row numbers in the matrix with NaN values in it
    rmnan_qdyn.(subsref(fieldnames(depth),substruct('{}',{ind})))(rows, :) = []; %
        delete those rows.

    avg_qdyn(ind) = mean(rmnan_qdyn.(subsref(fieldnames(qdyn),substruct('{}',{
        ind}))))(:,2));

```

```

% Getting the nearest point to each 10cm interval depth in each location , but
    using
% the NaN–removed values. Messy but it’s quicker to copy paste
% sometimes.
[c_1, row_1] = min(abs(rmnan_qdyn.(subsref(fieldnames(depth),substruct('{}',{
    ind}}))(:,1)–0.1));
ten_cm_qdyn(ind) = rmnan_qdyn.(subsref(fieldnames(rmnan_qdyn),substruct
    ('{}',{ind}})))(row_1,2);
ten_cm_depth(ind) = rmnan_qdyn.(subsref(fieldnames(rmnan_qdyn),substruct
    ('{}',{ind}})))(row_1,1);

[c_2, row_2] = min(abs(rmnan_qdyn.(subsref(fieldnames(depth),substruct('{}',{
    ind}}))(:,1)–0.2));
twenty_cm_qdyn(ind) = rmnan_qdyn.(subsref(fieldnames(rmnan_qdyn),substruct
    ('{}',{ind}})))(row_2,2);
twenty_cm_depth(ind) = rmnan_qdyn.(subsref(fieldnames(rmnan_qdyn),substruct
    ('{}',{ind}})))(row_2,1);

[c_3, row_3] = min(abs(rmnan_qdyn.(subsref(fieldnames(depth),substruct('{}',{
    ind}}))(:,1)–0.3));
thirty_cm_qdyn(ind) = rmnan_qdyn.(subsref(fieldnames(rmnan_qdyn),substruct
    ('{}',{ind}})))(row_3,2);
thirty_cm_depth(ind) = rmnan_qdyn.(subsref(fieldnames(rmnan_qdyn),substruct
    ('{}',{ind}})))(row_3,1);

[c_4, row_4] = min(abs(rmnan_qdyn.(subsref(fieldnames(depth),substruct('{}',{
    ind}}))(:,1)–0.4));

```

```
fourty_cm_qdyn(ind) = rmnan_qdyn.(subsref(fieldnames(rmnan_qdyn),substruct
    ('{}',{ind}))) (row_4,2);
```

```
fourty_cm_depth(ind) = rmnan_qdyn.(subsref(fieldnames(rmnan_qdyn),substruct
    ('{}',{ind}))) (row_4,1);
```

```
[c_5, row_5] = min(abs(rmnan_qdyn.(subsref(fieldnames(depth),substruct('{}',{
    ind}))) (:,1)-0.5));
```

```
fifty_cm_qdyn(ind) = rmnan_qdyn.(subsref(fieldnames(rmnan_qdyn),substruct
    ('{}',{ind}))) (row_5,2);
```

```
fifty_cm_depth(ind) = rmnan_qdyn.(subsref(fieldnames(rmnan_qdyn),substruct
    ('{}',{ind}))) (row_5,1);
```

```
[c_6, row_6] = min(abs(rmnan_qdyn.(subsref(fieldnames(depth),substruct('{}',{
    ind}))) (:,1)-0.6));
```

```
sixty_cm_qdyn(ind) = rmnan_qdyn.(subsref(fieldnames(rmnan_qdyn),substruct
    ('{}',{ind}))) (row_6,2);
```

```
sixty_cm_depth(ind) = rmnan_qdyn.(subsref(fieldnames(rmnan_qdyn),substruct
    ('{}',{ind}))) (row_6,1);
```

```
[c_7, row_7] = min(abs(rmnan_qdyn.(subsref(fieldnames(depth),substruct('{}',{
    ind}))) (:,1)-0.7));
```

```
seventy_cm_qdyn(ind) = rmnan_qdyn.(subsref(fieldnames(rmnan_qdyn),substruct
    ('{}',{ind}))) (row_7,2);
```

```
seventy_cm_depth(ind) = rmnan_qdyn.(subsref(fieldnames(rmnan_qdyn),
    substruct('{}',{ind}))) (row_7,1);
```

```
[c_8, row_8] = min(abs(rmnan_qdyn.(subsref(fieldnames(depth),substruct('{}',{
    ind}))) (:,1)-0.8));
```

```

    eighty_cm_qdyn(ind) = rmnan_qdyn.(subsref(fieldnames(rmnan_qdyn),substruct
        ('{},{ind}')))(row_8,2);
    eighty_cm_depth(ind) = rmnan_qdyn.(subsref(fieldnames(rmnan_qdyn),substruct
        ('{},{ind}')))(row_8,1);
end

```

```

nums = [1:18];

```

```

% %% File export for GIS
% %You only do this once after you're happy with all the numbers
%
% export_matrix = zeros(24,18);
%
% export_matrix(1,:) = 1:18;
% export_matrix(2,:) = ten_cm_depth;
% export_matrix(3,:) = ten_cm_qdyn;
% export_matrix(4,:) = twenty_cm_depth;
% export_matrix(5,:) = twenty_cm_qdyn;
% export_matrix(6,:) = thirty_cm_depth;
% export_matrix(7,:) = thirty_cm_qdyn;
% export_matrix(8,:) = forty_cm_depth;
% export_matrix(9,:) = forty_cm_qdyn;
% export_matrix(10,:) = fifty_cm_depth;
% export_matrix(11,:) = fifty_cm_qdyn;
% export_matrix(12,:) = sixty_cm_depth;
% export_matrix(13,:) = sixty_cm_qdyn;
% export_matrix(14,:) = seventy_cm_depth;
% export_matrix(15,:) = seventy_cm_qdyn;
% export_matrix(16,:) = eighty_cm_depth;

```

```

% export_matrix(17,:) = eighty_cm_qdyn;
%
% export_matrix(18,:) = max_qdyn;
% export_matrix(19,:) = avg_qdyn;
% export_matrix(20,:) = max_depth;
% export_matrix(21,:) = d50_phi;
% export_matrix(22,:) = d50_microns;
% export_matrix(23,:) = sand_percent;
% export_matrix(24,:) = mud_percent;
%
% writematrix(export_matrix,'bluedrop_plot_export.xls')

%% Other Plots
% plot whatever you want. See what works, what doesn't

```

4. Getting the average value of backscatter intensity around grab points - by Sun Woo Park

```

clear variables ; close all ; clc

% For loading in a RGB GeoTIFF of sonar backscatter and calculating the
% average RGB value within a 3m radius of sediment sampling point.
% Plus it will calculate the average value of backscatter intensity value
% of high and low areas

% by Sun Woo Park (swpark037@gmail.com), 2023.10.11
% MATLAB 2023b with Mapping Toolbox.

%% Read image file using readgeoraster

```

```

fname = "C:\SonarWiz-Projects\Actual_thesis\GeoTiff\Actual_thesis_cleaned.tif";
[A,R] = readgeoraster(fname);

A_noalpha = A(:,:,1:3); %mapshow requires only RGB values for plotting – remove
alpha values

[x,y] = worldGrid(R); % Create grid of X,Y values
[lat,lon] = projinv(R.ProjectedCRS,x,y); % Convert grid of X,Y values to latitude/
longitude

%% Plot latitude/longitude min/max on geographic axes to confirm – no need to do
this step multiple times.
[latlim,lonlim] = geoquadline(lat,lon);

figure
geoplot(latlim ([1 2 2 1 1]),lonlim ([1,1,2,2,1]) ,"r","LineWidth",2)
geobasemap satellite
title ("geographic axes")

figure
mapshow(A_noalpha,R)
title ("potomac.tif")

%% Load in sediment sampling location lat lon

grab = readmatrix("C:\Users\swpar\Desktop\UD\Thesis\Grainsize_Analysis\
Ponar_location_FEB.xlsx");
grab_lat = grab(:,2);

```

```

grab_lon = grab(:,3);

%% Find the closest point in the whole geotiff to the sampling point
B = reshape(lat,[],1);
C = reshape(lon,[],1); %making everything in one column since dsearchn didn't like
    it being a full matrix
D = dsearchn([B, C], [grab_lat, grab_lon]);

tiff_point = zeros(18,2);
row_num = zeros(1,18);
col_num = zeros(1,18);

for i = 1:18

    tiff_point(i,:) = [lat(D(i)), lon(D(i))];
    [row_num(i),col_num(i)] = find(lat==tiff_point(i,1)); % Get to the m*n of points
        on the matrix of these grab locations

end

%% Get the roughlyly 3m circle of pixels from the grab location
% From sonarwiz export, I know my pixel is 0.3m per side. 11 pixel square
% with the grab point in the center should be good enough. 3m area since
% the boat length, the distance between the grab and the penetrometer, and
% the GPS accuracy adds about 3m of error to my measurments.

% Call in rgb values using A_noalpha(row_num(1), col_num(1),1). The third

```

```
% value controls the R G B, respectively.
```

```
% get the appx. 3m square around my grab points
```

```
for k = 1:18
```

```
for j = 1:5
```

```
grab_area(j,1,k) = row_num(k)-j;
```

```
grab_area(j+6,1,k) = row_num(k)+j;
```

```
grab_area(j,2,k) = col_num(k)-j;
```

```
grab_area(j+6,2,k) = col_num(k)+j;
```

```
end
```

```
grab_area(6,1,k) = row_num(k);
```

```
grab_area(6,2,k) = col_num(k);
```

```
end
```

```
double_A = im2double(A);
```

```
for m = 1:18
```

```
for l = 1:11
```

```
color_r(l,m) = double_A(grab_area(1,1,m), grab_area(1,2,m), 1);
```

```
color_g(l,m) = double_A(grab_area(1,1,m), grab_area(1,2,m), 2);
```

```
color_b(l,m) = double_A(grab_area(1,1,m), grab_area(1,2,m), 3);
```

```
end
```

```
end
```

```
avg_color = zeros(3,18);
```

```

for n = 1:18
avg_color(1,n) = mean(color_r(:,n));
avg_color(2,n) = mean(color_g(:,n));
avg_color(3,n) = mean(color_b(:,n));
end

avg_rgb = uint8(255*avg_color); %convert back to 0 – 255 rgb color value numbers.

```

5. Making a confusion matrix - by Sun Woo Park

```

clear variables; close all; clc

% For creating a confusion matrix to calculate sediment classifier
% accuracy. Refer to https://www.mathworks.com/help/stats/confusionmat.html
% for additional info on confusion matrix creation in Matlab.

% by Sun Woo Park (swpark037@gmail.com), 2023.11.22
% MATLAB 2023b

%% Making the matrix

g1 = {'Low','Low','Low','Low','Low','Low','Low','Low','Low','Low','High','High','High','
      Low','Low','Low','High','Low','Low'}; % Known groups. Penetrometer results
g2 = {'Low','Low','Low','Low','Low','Low','Low','Low','Low','Low','High','High','High','
      High','Low','Low','Low','High','Low'}; % Predicted groups. Classifier results

[conf,order] = confusionmat(g1,g2,'Order',{'Low','High'});

```

```

confusionchart(conf, order)

%% Calculate accuracy, precision, etc

p = conf(1,1)/(conf(1,1)+conf(1,2)); %precision
a = (conf(1,1)+conf(2,2))/sum(sum(conf)); %accuracy
r = conf(1,1)/(conf(1,1)+conf(2,1)); %recall

6. Displaying CTD casts - by Sun Woo Park

close all; clear variables; clc

%% Preamble
% Simple code for displaying CTD data
% Export all values from the Castaway as matlab data file
% by Sun Woo Park, 2023.11.27

%% Load in data
% Choose the deepest cast in each fieldwork session

Apr = load("C:\Users\swpar\Desktop\UD\Thesis\ctd_mat_data\
  CC1618007_20230424_163309.mat");
Feb = load("C:\Users\swpar\Desktop\UD\Thesis\ctd_mat_data\
  CC1618007_20230228_201636.mat");
Oct = load("C:\Users\swpar\Desktop\UD\Thesis\ctd_mat_data\
  CC1618007_20221011_132647.mat");

%%
figure ()

```

```
plot(Oct.Sound_velocity, Oct.Depth, 'LineWidth',5)
hold on
plot(Feb.Sound_velocity, Feb.Depth, 'LineWidth',5)
plot(Apr.Sound_velocity, Apr.Depth, 'LineWidth',5)
hold off
set(gca, 'YDir','reverse ',' FontSize',15)
legend('Oct', 'Feb', 'Apr', Location='best')
xlabel('Sound Speed (m/s)')
ylabel('Depth (m)')
```